THE IN-LINE VIRTUAL IMPACTOR

A Dissertation

by

SATYANARAYANAN SESHADRI

Submitted to the Office of Graduate Studies of
Texas A&M University
in partial fulfillment of the requirements for the degree of

DOCTOR OF PHILOSOPHY

December 2007

Major Subject: Mechanical Engineering

THE IN-LINE VIRTUAL IMPACTOR

A Dissertation

by

SATYANARAYANAN SESHADRI

Submitted to the Office of Graduate Studies of
Texas A&M University
in partial fulfillment of the requirements for the degree of

DOCTOR OF PHILOSOPHY

Approved by:

Co-Chairs of Committee,	Andrew R. McFarland
	John S. Haglund
Committee Members,	Edward S. Fry
	Yassin A. Hassan
Head of Department,	Dennis L. O'Neal

December 2007

Major Subject: Mechanical Engineering

ABSTRACT

The In-line Virtual Impactor. (December 2007)

Satyanarayanan Seshadri, B.E., University of Madras;

M.S., Texas A&M University

Co-Chairs of Advisory Committee: Dr. Andrew R. McFarland
Dr. John S. Haglund

A circumferential slot In-line Virtual Impactor (IVI) has been designed using Computational Fluid Dynamics (CFD) simulation tools and experimentally characterized using monodispersed liquid aerosols to validate simulation results. The base design, IVI-100, has an application as a pre-separator for sampling inlets, where the device scalps large particles from the aerosol size distribution. The IVI-100 samples air in at 111 L/min and deliver the fine aerosol fraction in a 100 L/min flow and provide a cutpoint particle size of 10 μm, with a pressure drop of 45 Pa.

An inverted dual cone configuration encased inside a tube provides the IVI-100 with a characteristic circumferential slot of width 0.254 mm (0.100 inches) and a slot length of 239 mm (9.42 inches) at the critical zone. The upper cone causes the flow to accelerate to an average throat velocity of 3.15 m/s, while the lower cone directs the major flow toward the exit port and minimizes recirculation zones that could cause flow instabilities in the major flow region. The cutpoint Stokes number is 0.73; however, the cutpoint can be adjusted by changing the geometrical spacing between the acceleration

nozzle exit plane and a flow divider. Good agreement is obtained between numerically predicted and experimentally observed performance.

An aerosol size selective inlet for bioaerosol and other air sampling applications using an upgraded prototype of IVI-100, mounted inside a BSI-100 inlet shell was tested in an aerosol wind tunnel over a speed range of 2 – 24 km/hr. The BSI-IVI-100 inlet has a cutpoint of 11 μm aerodynamic diameter and delivers the fine fraction at 100 L/m. The geometric standard deviation of the fractionation curve is 1.51 and the performance is not affected by wind speeds.

An IVI-350, which is an adaptation of the IVI to be used as a powder fractionator, was designed based on computational simulations, and provides a cutpoint of 3 μm AD, while operating in a total flow rate of 350 L/min. Four Identical IVI -350 units will be operated in parallel to fractionate aerosolized powders in a 1400 L/min flow. An optimized inlet, with a contoured tear-drop shaped insert provides uniform flow to four identical IVI units and prevents powder accumulation in the system entrance.

DEDICATION

To my parents, for their love and unfailing trust in me

ACKNOWLEDGEMENTS

I would like to express my sincere appreciation and gratitude to my advisor, Dr. Andrew R. McFarland, for his guidance and support in the successful completion of my research endeavors at the Aerosol Lab. It is his faith in my ability and work that served as constant encouragement to compete and succeed in all the projects I undertook here. Many thanks are also due to Dr. Peter McIntyre, who supported my project in the initial stages and for the many unique opportunities to work in lead roles in important projects, which are generally rare for graduate students. I would also like to thank Drs. Fry, Haglund and Hassan for serving as my dissertation committee members, for their time and effort.

The Aerosol Lab was a wonderful place to work and study at and part of what makes the lab is the people whom you interact with everyday. I would like to express my strong appreciation and gratitude to my colleagues with whom I have formed bonds that will last a lifetime. I would especially like to thank Dr. Hari, for the many informative discussions and friendly advice we had, Dr. Hu for his sagacious advice and Chinese humor, Mr. Baehl for his help with the wind tunnel experiments, Mr. LaCroix, Dr. King and all who made the lab a desirable place to work. My special thanks are due to Gary Bradley, Charles Cox and Youngjin Seo for their camaraderie and light and hearty times at the lab. Finally, I would like to express my thanks to my friends and family who formed the support system in good times and bad. Many thanks are also due to all the people who had knowingly or unknowingly helped me in any possible way.

This work was supported in part by the Edgewood Chemical Biological Center of the U.S. Army Research, Development, and Engineering Command under Contract DAAD13-03-C-0050. I would like to thank Drs. Edward W. Stuebing and Jerold R. Bottiger of the Army for their support. Additional financial support was provided by the Aerosol Technology Laboratory of the Texas Engineering Experiment Station and by Accelerator Technology Corporation (ATC), College Station, TX under Contract 06-0997.

TABLE OF CONTENTS

Page

CHAPTER Page

CHAPTER Page

LIST OF FIGURES

FIGURE Page

FIGURE Page

FIGURE Page

LIST OF TABLES

CHAPTER I

INTRODUCTION

Microscopically-sized particles are used in a wide variety of fields that includes superconducting wire manufacturing using Powder-In-Tube (PIT), Jin et al., (1987), inhalable pharmaceutical drugs, cosmetics, paints etc... In most of these applications particle sizes in the batch of powders used play a critical role in realizing the desired performance. For example, the penetration of inhaled drugs in the human respiratory tract is highly dependant on particle size. In fact it is one of the methods of achieving targeted drug delivery (Finlay, 2001). These particles are generated using different mechanical and chemical means including milling, Flame Spray Pyrolysis (FSP), etc…These processes typically produce particles having a size distribution that is approximately lognormal (Mäkelä et al., 2004) with a significant tail for the larger sizes. In certain applications, like the PIT processing, it is essential to eliminate, with near 100% efficiency, the larger sizes from the distributions as these particles limit the size to which the PIT filament could be drawn. Similarly in many air sampling studies, it is necessary to be able to separate the particles in the ambient atmosphere in to different size fractions so as to enable an assessment of the effects of the individual size groups on human health and environment.

This dissertation follows the format of *Aerosol Science Technology*.

In this chapter, the various means and methods that have evolved for manipulation and collection of microscopic particles in the form an aerosol are explored. The effects of particle sizes in PIT processing of superconducting wire and tubes and in efficacy of inhaled aerosol drugs are discussed. To conclude this chapter, the goals of this dissertation research are identified.

1.1 Mechanics of Aerosols

An aerosol can be defined as a solid or liquid phase that is suspended in a gaseous medium. The most common aerosol that we see and observe is the visible pollution from diesel trucks, automobiles, smoke stacks, etc… The heath effect of these emissions have been a motivation for studying the aerosol particles. A more detailed review on the history of particle measurement is provided by Chow (1995). Suspended particles are characterized based on a wide variety of parameters such as size, chemical composition, light-scattering and light-absorption properties, hygroscopicity etc. A variety of instruments have been developed to identify the nature and source of these particles by employing any one of these parameters. In this discussion, we will solely characterize the particles based on their size. Collection or extraction of the particles from an aerosol is achieved by the following five mechanisms, which are, inertial impaction, interception, gravitational settling, diffusion and electrostatic precipitation. The dominant mechanism involved is highly dependant on the particle size. A more detailed description on these mechanisms can be found in Hinds (1999). Of particular interest in this study is inertial impaction. As the name suggests, the principle parameter governing this mechanism is particle inertia and a widely-used device that employs this principle

for collection of particles from an air stream is called an impactor. In its typical configuration, an impactor consists of a nozzle directing air at a flat plate. Particle transport characteristics in an inertial impactor has been classified on the basis of a dimensionless parameter called the Stokes number, *Stk*. It is defined as a ratio of the stopping distance of a particle to a characteristic dimension of an obstacle, or,

$$Stk = \frac{\tau U_0}{d_c} \tag{1.1}$$

where τ is the relaxation time of the particle, U_o is the mean free stream velocity and d_c is the characteristic dimension of the obstacle. For $Stk >> 1$, particles will continue in a straight line as the gas turns around the obstacle therefore impacting on the obstacle. For $Stk << 1$, particles will follow the gas streamlines.

Particle penetration through an impactor is normally expressed as a ratio of the total number of particles present in the exhaust to the amount present in the impinging flow stream. Impactors are typically characterized by the cutpoint, which is defined as the particle size for which the penetration is 50%.

1.2 History of Impactors

Inertial impactors were first devised by M.F. Pouchet in 1860 for inhalation studies, air sampling in hospitals and near swamplands (Marple, 2004). The very first impactors were used for quickly obtaining a sample on a glass slide for examination under a microscope for obtaining a correlation between the ambient air and the disease affecting the patient. Since then impactors have evolved into a variety of configuration, however the basic nature of the device has essentially remained unchanged. Impactor

concepts developed until the 1960's involved acceleration of a particle laden flow stream to a high velocity and impacting it normally onto a plate resulting in the collection of particles with a large Stokes number, as governed by Equation 1.1. With the development of 'Virtual Impactors' in the mid 1960's, impactors that use a real plate came to be called as the 'Real or Classical Impactors'.

In a real impactor, size separation is achieved due to the varying inertia acquired by the different sized particles in the accelerating flow field. By manipulating the flow velocity and the nozzle geometry, desired fractionation cutpoint could be achieved. A major draw back of this design is the problem associated with particle bounce and re-entrainment in to the flow stream.

1.3 The Virtual Impactor

The virtual impactor, as a particle classification device, was first developed by Conner (1966) and subsequently by Hounam and Sherwood (1965) as an option to the classical inertial impactors in order to eliminate particle bounce and re-entrainment problems. Figure 1.1 shows a schematic of particle behavior in a virtual impactor. The particle laden air stream is impinged normally upon a slowly pumped near-stagnant void (minor flow), which draws about 10 percent of the total flow entering the device. The remainder of the flow is split equally in a cross flow (major flow), there by setting up the stage for classifying the particles based on their inertia. Since its introduction, the virtual impactor has been investigated by many researchers using theoretical and experimental techniques. Ravenhall et al. (1978) analyzed the performance of a slotted virtual impactor, whose flow fields were obtained by using potential flow theory. They studied

the effects of jet-to-plate spacing and the accelerator-to-receiver width ratios and identified stable operating regions. In a follow up study Ravenhall et al. (1982) extended the theoretical analyses to include the viscous nature of the fluid by numerically solving the Navier Stokes Equations. Hassan et al. (1979) performed a numerical analysis on an axisymmetic virtual impactor while a more detailed theoretical analysis was performed by Marple and Chien (1980). They determined the characteristics of a virtual impactor by numerical solution of the Navier Stokes equation and equations of motion of the particles. They studied the effect of various geometrical parameters like throat length, nozzle to collection probe distance, collection and inlet nozzle design etc. on the collection efficiencies of small and large particles. Influence of nozzle Reynolds number and the minor to total flow ratio on the behavior and collection efficiencies were also presented. They reported significant losses on the internal walls for particle sizes near the cutpoint. While numerical analyses were slowly catching pace, exhaustive experimental evaluations were being performed on round jet virtual impactors. McFarland et al. (1978) evaluated the performance of a dichotomous sampler operated at 14 L/min and having a cut point of 3.8 μm. They reported internal wall losses of the order of 7 percent for a single stage and 10.8 percent for a two stage unit. Loo et al. (1979) used a virtual impactor based sampler for large scale monitoring of airborne particulate matter. Later Loo and Cork, 1988 presented the design details on the development of a high efficiency virtual impactor which operated at 16.7 L/min and had a cutpoint of 2.5 μm. While these studies were mostly on round jet virtual impactors there was a need for high volume sampling that could not be achieved by a single round jet nozzle. A rectangular jet or slot virtual impactor was used to overcome this difficulty.

The virtual impactor could be theoretically scaled to any flow rate by just increasing the length of the nozzle. Masuda (1979) studied the performance of a rectangular slot virtual impactor and also suggested improvements to performance by adding sheath and core flows. It is of interest to note that the coarse particle flow in a virtual impactor is always contaminated by fine particle by an amount proportional to the ratio of the flow drawn through the collection nozzle. In order to minimize that problem, Masuda (1979) and Chen and Yeh (1987) used a central core filtered air in the nozzle of the virtual impactor. Sioutas et al. (1994) developed a high volume low cutpoint rectangular slot virtual impactor that had reported cutpoints of 0.15-0.25 μm, pushing the sampling range of virtual impactors to submicrometer levels. Recently Lee et al. (2003) reported the performance evaluation of a nano particle virtual impactor whose cutpoint ranged from 15 – 60 nm. Haglund and McFarland (2004) and Gotoh and Masuda (2001) observed that in rectangular slot virtual impactors, loss of particles close to the bounding walls or the end loss could be quite significant. Haglund and McFarland (2004) developed a novel bioaerosol concentrator that utilized the principle of joining the ends of the rectangular slot to complete the circle, thus eliminating end losses. It was called the Circumferential Slot Virtual Impactor (CSVI).

Traditionally virtual impactors have been used for concentration of ambient aerosol with the particles of interest being in the minor flow stream. However there are certain applications such as powder-in-tube processing of superconducting wires, where it is of interest to eliminate large particles from a batch of precursor powders. When these powders are processed using a virtual impactor, particles beyond a certain size are transmitted completely to the minor flow stream thereby eliminating all large particles

from the precursor powder. The feasibility of using a virtual impactor for size fractionation of bulk powders in investigated in this study. As a motivation to the study of bulk powder fractionation, the following sections discuss the importance of particle size in preparation of therapeutic drugs for administration as aerosols and in superconductor precursor powder processing where controlling particle size provides marked improvement in wire performance.

1.4 Powder-In-Tube Processing of HTS Conductors

The powder-in-tube method was one of the first techniques for producing High Temperature Superconductors (HTS). It is most commonly employed for manufacture of Bi-2223 conductors (Fu et al., 2003). With the recent discovery of superconductivity of MgB_2 at ~40K and the interest regarding its performance, PIT processing has emerged as the preferred method for fabrication of MgB_2 conductors (Glowacki et al., 2001). Figure 1.2 shows the various steps involved in the process. Silver or silver alloy is used as the tube material for Bi based conductors while copper based metals are employed for the MgB_2 conductor. Typically, the tube is filled with HTS powder, then extruded or drawn to wire about 1-2 mm in diameter. For multifilament conductor, the wire is drawn in a hexagonal shape, cut into shorter lengths, and formed into a stack of 7, 19, 37, 55, 61, 85, or higher numbers of filaments. This stack is then inserted in another tube, and the composite is extruded or drawn to wire. The restacking and redrawing steps are omitted for monofilament wire. For round wire, the final step is heat treatment, but most conductors are made in a flat "tape" format achieved by rolling the wire to an aspect ratio of ~10:1.

Fu et al. (2003) identified that particle size plays a critical role in limiting the ultimate current density in PIT fabricated wires and tubes. For improving the current carrying performance of the conductor, larger number of finer filaments would be necessary. However, the limiting factor in drawing finer filament is the size of particles in the core powders. Typically the powder particles are much harder than the tube/matrix metal. Hence when drawing, as the tube approach the size of the largest particle in the batch, these particles are likely to pierce the tube and hence destroy the filament and the surrounding matrix during heat treatment. Hence it is desirable to remove the larger particle from the precursor powders with near 100 % efficiency prior to packing in the tube for drawing.

1.5 Effect of Particle Size on Its Transport and Deposition in Human Respiratory Tract

Aerosols are commonly used for administration of therapeutic drugs to the lungs for treatment of millions of peoples with variety of diseases such as asthma, Chronic Obstructive Pulmonary Disease (COPD), and other lung diseases that are characterized by obstruction of airways and shortness of breath. There are several important parameters to be considered while choosing the aerosol route as the delivery mechanism for a new drug. The key of which is the particle size of the Inhaled Pharmaceutical Aerosol (IPA) as it governs the region in the respiratory tract where the particles deposit. Figure 1.3 broadly identifies the effect of particle size on the deposition of aerosol particles in the human respiratory tract. It has been observed that if the particle sizes are

too large, they are lost in the mouth and throat regions, while extremely small particles tend to be exhaled after inhalation.

The geometry of the respiratory tract is highly complex and variable from person to person. However, a variety of simplified models have been developed to model airflow and particle deposition in the respiratory tract (Finlay, 2001). Sedimentation, impaction and diffusion are the primary mechanisms that cause deposition of inhaled particles in the lung. Prediction of particle deposition in lungs has been carried out by approximating the airways as circular tubes, oriented in different fashions (Tsuda et al., 1994). Stahlhofen (1980) presented extensive experimental data on regional deposition of aerosol particles in human respiratory tract and has aided in the development and validation of empirical model for particle deposition. His studies showed that the peak particle deposition was near 6 μm in the tracheo-bronchial region and near 3 μm for the alveolar region. Based on these studies, a rule-of- thumb that the IPA must be in the 1 – 5 μm size range to reach the lung has been proposed (Finlay et al., 1997). Thus a powder processing device capable of effectively stripping large particles out of bulk powder at relatively large mass throughputs would aid in the development of a variety of IPA's in a cost effective manner.

1.6 Scope of This Dissertation Research

The main objective of this dissertation research was to develop an efficient and cost effective method for size classification and pre-separation of microscopic particles in an air stream. Computational Fluid Dynamics (CFD) techniques were employed to develop the initial design and for optimization of a new fractionator, the Inline Virtual Impactor (IVI). The IVI was used as a pre-separator in Bell Shaped Inlet, BSI-100, for sampling ambient air. A systematic analysis on the penetration performance and the effect of various geometrical parameters on the performance of the IVI was carried out numerically and key results were experimentally verified to validate numerical predictions.

For bulk powder processing applications, a modified version of the IVI, operating in a 0.0058 m^3/s (350 L/min) flowrate with a cutpoint of 3 μm AD, was developed. Finally, details on the conceptual design for the separation system in a powder processing pilot plant are presented. The main components of the pilot plant include a jet milling system for size reduction of raw feed powder, the IVI system and particulate collection system. The IVI system contains four IVI units that will process 0.024 m^3/s (50 CFM) flow in parallel. In order to distribute the flow evenly in to these units, a special inlet configuration was designed and the details of which will be presented in this discussion

CHAPTER II

CFD METHODS

Computers have been used to routinely solve fluid flow problems since the early 1980's. But these were typically fairly simple problems due to the limited computing power and the complex nature of algorithms required for generalizing the solution methods. Recent developments in solution methods together with ever increasing computing power have made the solution of complex problems less machine and labor intensive and more affordable. CFD provides a cost effective alternative to scale model testing and helps in understanding complex flow phenomena, which was hitherto not possible through experimental methods.

2.1 CFD Methods Using ANSYS CFX

ANSYS CFX™ (Ver. 10.0, Canonsburg, PA) was developed to solve the equations governing the fluid motion using the finite volume method (ANSYS, 2005). In this method, the region under investigation is divided into many control volumes, and the governing equations are discretized and solved for each control volume. CFX uses a coupled algebraic multi-grid solver that solves the hydrodynamic system of equations across all grid nodes. Thus we obtain an approximate result for each of the variables solved at specific points throughout the domain, which in turn presents us an insight in to the nature of the flow in the domain.

CFX™ was used for modeling the performance of the IVI. Initial geometric design and optimization studies were performed using 2D simulations; however, once the appropriate combination of parameters was determined, a 3D simulation was performed on the final design to ensure that the 2D predictions were representative of the fluid flow and particle physics in the IVI. The following sections briefly describe the equations of fluid motion that are solved, and the meshing strategy for performing 2D and 3D simulations.

2.2 Flow Field and Particle Tracking

Fluid-particle transport in the IVI was modeled with an Eulerian-Lagrangian framework. The bulk fluid (continuous phase) flow field was solved using the Eulerian approach and then the particle trajectories were calculated using Lagrangian tracking, with the assumption that the particles neither influence the flow field nor each other. Hari et al. (2005) determined that tracking of 500 particles of each size was sufficient to ensure the independence of the obtained results from the number of particles included in tracking. In this study, 1000 particles of each size were tracked to determine the fractionation characteristics of the IVI. Each particle was tracked from the injection point to its final destination (either a flow boundary or an internal wall). Particles contacting an internal wall were considered to adhere to the wall. Penetration (major-flow transmission efficiency) for each size was obtained as the ratio of the number of particles in the major flow exit to the number of particles that were originally injected at the inlet boundary.

2.3 Modeling Approaches

A fluid flow with more than one phase present is generally termed as multiphase flow. Of special interest in this study is the gas-solid two phase flows where the gaseous fluid is modeled as the continuous phase and the particles are modeled as the dispersed phase. A classification of dispersed two phase flows with regards to the importance of interaction mechanism is discussed by Elghobashi (1994) Two phase flows can be classified as dilute and dense flows and the choice of fluid coupling model used in the CFD studies are based the volume fraction of the dispersed phase. The volume fraction of the particles in a unit volume of gas is expressed as

$$\alpha_p = \frac{\sum_i N_i V_{pi}}{V} \tag{2.1}$$

Here N_i is the number of particles in the size fraction i, having particle volume $V_{pi} = \frac{\pi}{6} D_{pi}$, where D_{pi} is the particle diameter. A two phase system is regarded as dilute (two-way coupling) up to $\alpha_p = 10^{-3}$. The influence of particle phase on the fluid is neglected for $\alpha_p < 10^{-6}$ (one-way coupling). The flow through the IVI is modeled as a gas-solid two phase flow with one-way coupling.

2.4 Governing Equations

Balance of momentum in a linearly viscous fluid flow is represented in its most general form as:

$$\nabla \bullet \mathbf{T} + \rho \mathbf{b} = \rho \frac{d\mathbf{v}}{dt} \tag{2.2}$$

Here '**b'** is the body forces, ρ is the fluid density, **v** is the fluid velocity, **T** is the Cauchy stress tensor and **D** is the symmetric part of the velocity gradient given by

$$\mathbf{T} = -p\mathbf{I} + 2\mu\mathbf{D} \tag{2.3}$$

$$\mathbf{D} = \frac{1}{2}\left[\frac{\partial \mathbf{v}}{\partial \mathbf{x}} + \left(\frac{\partial \mathbf{v}}{\partial \mathbf{x}}\right)^{T}\right] \tag{2.4}$$

For incompressible fluid flow, Equation 2.2 can be represented by

$$\frac{\partial \mathbf{v}}{\partial t} = -\frac{1}{\rho}\frac{\partial p}{\partial \mathbf{x}} + \mu\Delta\mathbf{v} + \mathbf{b} \tag{2.5}$$

where μ is the molecular viscosity and p is the thermodynamic pressure.

Equation 2.5 is obtained by utilizing the balance of mass (mass conservation) equation for an incompressible fluid, which is given by Equation 2.6

$$\nabla \bullet \mathbf{v} = 0 \tag{2.6}$$

Neglecting the body forces and expressing the conservation of mass and momentum equations in the component form, Equation 2.5 becomes

$$\rho\frac{\partial u_i}{\partial t} + \rho u_j\frac{\partial u_i}{\partial x_j} = -\frac{\partial p}{\partial x_i} + \frac{\partial t_{ij}}{\partial x_j} \tag{2.7}$$

Here $t_{ij} = 2\mu D_{ij}$

2.5 Geometry and Meshing

ICEMCFD™ (Ver. 10.0, ANSYS, Cannonsburg, PA) is a multipurpose mesh generation tool from ANSYS. It has the capacity to parametrically create grids from geometry in multi-block structured, unstructured hexahedral, tetrahedral, hybrid grids consisting of hexahedral, tetrahedral, pyramidal and prismatic cells.

Figure 2.1 shows the geometry used in the simulations along with the boundary conditions. As the flow in the IVI can be considered to be axi-symmetric, a computational model representative of the IVI geometry was created by revolving the 2D profile by an angle of 3 to 5º about the central axis (Figure 2.2), as suggested in the CFX user manual (ANSYS, 2005). A block structured body fitted mesh was generated over the entire domain and is shown in Figure 2.3. Mass flow rate inlet boundary conditions were prescribed at both the inlet and outlet flow ports. Symmetric boundary condition was assigned to the axis and the surfaces in the θ direction. All the other surfaces were treated as no-slip walls.

Full domain 3D simulations were performed on a hybrid mesh generated from the inner flow paths that was modeled as a solid volume using Autodesk Inventor™ 8.0, and exported as an IGES file. Typically the mesh, shown in Figure 2.4a, consisted of over 2 million tetrahedral elements with the near wall regions being resolved using three layers of prismatic cells. Use of prismatic elements (Figure 2.4b) provides better control of the size of cells for better resolution of near wall features. In case of turbulent flows, the first cell size of the prismatic elements is determined based on the y^+ requirements of the turbulence model used. For low Reynolds number turbulence model like the *k-ω* model a y^+ of 2 is chosen. The size of the first cell is then calculated using Equation 2.8

$$y = Ly^+ \sqrt{80}\,\mathrm{Re}_L^{-13/14} \tag{2.8}$$

Here, L is the characteristic length, Re_L is the Reynolds number based on the characteristic length and the throat velocity 'U'.

CHAPTER III

EXPERIMENTAL METHODS

This chapter outlines the experimental methodology employed for the characterization of aerosol sampling devices. The procedure for generation of monodisperse test aerosols, aerosolization of Arizona Road Dust (ARD), bench-top or standalone testing of aerosol separation devices and wind tunnel evaluation of sampling inlets are described. Further, the operation of various devices that are utilized in these tests are briefly examined and finally the uncertainty in data obtained is evaluated using the "Kline McCilntock" method.

3.1 Generation of Monodisperse Liquid Particles

Liquid test aerosols, for sizes larger than about 3 μm AD are generated with a vibrating orifice aerosol generator (VOAG, Model 3450, TSI Inc., St. Paul, MN). A combination of 9% oleic acid and 1% sodium fluorescein salt (uranine) is dissolved in 90% ethanol to create a liquid master solution. After droplets are formed by the aerosol generator, the volatile ethanol evaporates leaving a residual non-volatile particle consisting of oleic acid and green fluorescent tracer. The desired particle size is obtained by diluting the master solution with ethanol, while maintaining other VOAG parameters constant. The volume of master solution required for a given volume of diluent is estimated using Equation 3.1, (Berglund and Liu, 1973).

$$D_p = \left(\frac{6QC_{vol}}{\pi f} \right)^{\frac{1}{3}} \tag{3.1}$$

where,

$$C_{vol} = \frac{x_{nv} V_{ms}}{V_{ms} + V_{dil}}$$

Here:

D_p = particle diameter

Q = liquid volume flow rate

C_{vol}= volume fraction non-volatile material

f = frequency of applied signal

x_{nv} = non-volatile volume fraction of master solution

V_{ms} = volume of master solution

V_{dil} = volume of diluting solution

Typical operating parameters of the VOAG for generating particles in the 3 – 17 μm range include a syringe pump ram speed of 0.00052 cm/s (governs the liquid flowrate) and a vibration frequency range of 40 to 90 kHz.

The consistency of the aerosol being generated by the VOAG was monitored with an Aerodynamic Particle Sizer (APS, Model 3310, TSI Inc, Shoreview, MN); however, the true size of the aerosol particles was determined microscopically as the liquid droplets are known to distort when accelerated in the APS measurement section (Chen et al., 1990). To determine the mean droplet size, the particles were impacted onto a glass slide coated with an oil-phobic agent (NYEBAR, Type Q, 2.0%, NYE Lubricants Inc., New Bedford, MA). The diameters of these particles were then measured using an optical microscope (Nikon Eclipse E600, Nikon Instruments Inc. Melville, NY). The

Aerodynamic Size (AD) of the droplets was calculated from the microscopically-measured size, adjusted for flattening of the droplets on a microscope slide according to the method described by Olan-Figueroa et al. (1982) but with a flattening factor of 1.29, (Thien, 2006).

3.2 Generation of Test Dust Using a Fluidized Bed Dust Generator

Fluidized beds are used to de-agglomerate and aerosolize dry dust. In these experiments, a fluidized bed was used for dispersion of ARD for characterization of IVI performance under dust loadings. The fluidized bed consists of a fluidizing medium and the dust to be dispersed. The fluidized bed arrangement is schematically shown in Figure 3.1. For dispersing dust uniformly, a weighed quantity of ARD was mixed with the bed medium (1000 μm glass beads) and loaded into the apparatus and fluidized using 10 L/min of clean dry air. The glass beads remain suspended in the chamber while the dust particles were elutriated out of the bed. It is important that the flowrate through the fluidized bed is maintained such that the terminal settling velocities of the particles are small as compared to their elutriation velocity while the reverse should be true for the bed material. Dispersion characteristics of a similar fluidized bed generator is described in detail by Willeke et al. (1974).

Prameters that govern the output rate from the fluidized bed aerosol generator are the ratio of glass bead mass to powder mass and the elutriation flowrate. For the dust feeder used here, the range of permissible elutriation flowrates were from 9 to 30 L/min. A mixture containing 20 g of ARD and 100 g of glass beads were loaded into the bed and the elutriation flowrate was set at 10 L/min. The observed output rate was 1.6 mg/L.

When the flowrate was 13 L/min, the output rate was 2.9 mg/L. It was observed that the condition of the interiors of the IVI was dusty after 10 minutes of sampling with the higher mass loading. Hence, 1.6 mg/L loading rate was used for all characterization tests. The uniformity of the output from the generator was verified by obtaining multiple reference samples before and after sampling with IVI. Figure 3.2 shows the dust output over a 10 minute sampling interval. Pre-weighed membrane filters were used to collect 2 reference samples before and after sampling with IVI. Mass of ARD collected on the reference filters was compared to ensure uniformity. The sample filter from the IVI major flow exhaust was analyzed only when the mass collected on the reference filters were comparable to each other.

3.3 Fluorometric Analysis

Turner Quantech Digital Filter Fluorometers (Model FM109515, Quantech Barnstead International, Dubuque, IA) were utilized for measurement of the mass concentration of fluorescent tracer in liquid solutions of particulate matter removed from the collection filters. The fluorometer is designed to perform quantitative fluorescence measurements on various fluorescent materials like fluorescein, rhodamine etc. A quartz-halogen lamp is used to provide excitation energy and the emission light is detected using a low noise, high gain photomultiplier tube. The above model operated in a wavelength range of 340 – 650 nm and the dye specific excitation and emission wavelengths are obtained using optical filters (Barnstead-Thermolyne, 1999).

The fluorometer provides concentration measurements in the form of Fluorescent Intensity Unit (FIU), which is directly proportional to the mass of the aerosol present in

the sample filters. The filters were placed in a solution containing a mixture of 50% isopropyl alcohol and 50% distilled water (v/v) for at least four hours before analysis. It should be ensured that the Fluorescent Intensity Unit (FIU) reading falls within the linear region of the curve that relates the mass concentration of fluorescein to the FIU. Figure 3.2 shows a sample calibration curve at a gain level of 13.

3.4 Coulter Counter Analysis

The particle size distributions of dry test powders were analyzed with a Multisizer™ 3 Coulter Counter (Beckmann Coulter, Inc., Fullerton, CA). Using Electrical Sensing Zone Method, also known as ESZ[1], the Coulter counter provides number, volume, mass and surface area size distributions in one measurement, with an overall sizing range of 0.4 μm to 1,200 μm. Its response is unaffected by particle color, shape, composition, density, or refractive index.

Particle size measurement is accomplished by measuring the momentary increase in impedance across the orifice or the "sensing zone" as the particles, suspended in a weak electrolyte solution (e.g., Isoton II, part no. 8546719, Beckmann Coulter, Inc., Fullerton, CA), passes through them. Two electrodes, are placed one on either side of the orifice, and a voltage applied across the orifice creates a sensing zone. This change in impedance across the sensing zone due to a particle produces a pulse that is digitally processed in real time. The Coulter Principle states that the pulse is directly proportional to the tri-dimensional volume of the particle that produced it. Analyzing these pulses

[1] Technology defined by the International Standard ISO 13319 (ISO 13319:2000: Determination of particle size distributions -- Electrical sensing zone method).

enables a size distribution to be acquired and displayed in volume (μm^3) and diameter (μm). In addition, a metering device is used to draw a known volume of the particle suspension through the orifice; a count of the number of pulses can then yield the number concentration of particles in the sample (Beckmann-Coulter, 2001)

The samples to be analyzed were initially collected on a membrane filter (DTTP14250, Millipore, Billerica, MA) and they were soaked in Isoton and vigorously shaken to loosen the particles adhering to the filter paper. Then the suspension was placed in a sonic bath for about an hour to de-agglomerate any clumps that may have formed during sampling. Later, a 500 μL aliquot of a well stirred sample was introduced in to 120 mL of fresh Isoton solution and sample cup was placed in the sample stand, and the suspension was gently stirred to prevent sedimentation of large particles. Standard testing procedure for calibration and sample measurement as provided in the Multisizer 3 user manual was adopted for all analyses. A 100 μm orifice rated for measuring particles from 2 – 60 μm was used in all analyses. Particle size data was exported to spreadsheet (MS Excel) using OEM software (AccuComp, Beckman Coulter, Inc, Fullerton, CA).

3.5 Bench-Top Testing

A schematic of the test setup is shown in Figure 3.4. Aerosol, generated with a vibrating orifice aerosol generator (Section 3.1) was passed through a flow duct where the aerosol is sampled through the aerosol classification device (IVI, in this study) being characterized. Transmission efficiency of the IVI can be expressed as the ratio of particle

collection rate at the major flow exhaust to the rate of particle transport into the IVI at the inlet. The major flow transmission efficiency is expressed as

$$\eta_{maj} = \frac{\text{Particle transport rate from major flow exhaust port}}{\text{Particle transport rate into IVI inlet}} \tag{3.2}$$

Aerosol sampling filters (Type A/D glass fiber, Pall Corp., East Hills, NY) are used to collect aerosol particles from flow exhausts. Reference samples, used to provide information for the denominator in Equation 3.2, are acquired by replacing the IVI in the setup of Figure 3.4 with a filter sampler. For a given set of experimental conditions, the reference filter and IVI were alternated to obtain at least three replicate samples. Fluorometric analysis for obtaining the aerosol concentration in the test and reference filters is described in Section 3.3. For selected tests, wall losses were obtained by opening the IVI unit and extracting the deposited particles using a cotton swab moistened with isopropyl alcohol similar to the method described by Loo and Jaklevic (1974) and analyzing the swabs fluorometrically.

Equation (3.2) can be written as

$$\eta_{maj} = \left[\frac{FIU_s}{FIU_{ref}}\right] \cdot \left[\frac{V_s}{V_{ref}}\right] \cdot \left[\frac{Q_{ref}}{Q_s}\right] \cdot \left[\frac{t_{ref}}{t_s}\right] \tag{3.3}$$

where

subscripts "*s* and *ref*" denote sample and reference values respectively

FIU = raw fluorometer reading in fluorescence intensity units

V = volume of solvent used to soak a filter

Q = volumetric air flow rate

t = test duration

It may be necessary to dilute the extracted fluorescein samples in order to have the FIU readings in the linear range at a given gain level. A 50% (v/v), mixture of pure isopropyl and distilled water was used for diluting the samples. The dilution ratio is given by,

$$d = \frac{V_s}{V_s + V_d} \tag{3.4}$$

where V_s is the sample volume and V_d is the dilution volume. The dilution level required for a given sample was determined by trial and error. The uncertainty involved in the estimation of major flow transmission efficiency using the bench top is described in Section 3.7

3.6 Wind Tunnel Evaluation

The BSI-IVI inlet was tested in an aerosol wind tunnel facility to characterize the penetration under simulated field sampling conditions. Monodisperse liquid aerosols with particles ranging in size from 3.2 to 17.0 µm AD generated with a VOAG, as described in Section 3.1, were used to evaluate the unit at wind speeds of 2, 8 and 24 km/h. Once the desired size of the test aerosol was achieved, particles were sent through a Kr-85 charge neutralizer, which sits above the orifice, to neutralize charges that may have been acquired by the droplets. The test aerosol was drawn into a 0.86 m (34") diameter wind tunnel where it passed through an Air Blender (Blender Products, Denver, CO), which creates counter-rotating vortices that mix the aerosol across the cross section. At a distance of 5.7 duct diameters downstream of the Air Blender, the aerosol passed through a set of flow straightners remove flow swirl. Figures 3.5 shows a schematic of the wind tunnel test setup.

A fan and motor arrangement with a speed controller was used to deliver air through the wind tunnel. The air was re-circulated, HEPA filtered and sent back to the intake of the fan. The centrifugal fan (Model No. 200 BSW CL 3 ARR 1, IAP, Inc., Phillips, WI) has a capacity of 10,000 cfm (4.72 m^3/s) at 3 kPa static pressure. The motor (Marathon Electric) is rated at 29.8 kW (40 hp) at 3600 rpm. A variable frequency drive (Model VLT 6042, Danfoss-Graham, Milwaukee, WI), was used to control the motor, is rated at 29.8 kW (40 hp) and 460 volts. The three test wind speeds of 2, 8, and 24 km/h (0.55, 2.22, and 6.67 m/s) were obtained by varying the controller frequency. Wind speed at the test section was measured with a thermal anemometer (Model 8355, TSI Inc., Shoreview, MN).

The wind tunnel test section is just downstream of the duct exit plane, i.e., in the free jet issuing from the tunnel. Reference samples were obtained by simultaneously collecting aerosol with two isokinentic probes that were placed along side the BSI-IVI inlet and from the major flow exhaust stream from the IVI. The samples were collected on glass fiber filters (Type A/E glass fiber, Pall Corp., East Hills, NY). For a given particle size and wind speed, the aerosol penetration through the inlet, P, was then calculated from:

$$P = \frac{c_{inlet}}{c_{iso}} \tag{3.5}$$

where c_{inlet} = aerosol concentration of the sample aerosol calculated from the material collected on the major flow exhaust filter

c_{iso} = average aerosol concentration in the wind tunnel calculate using two isokinetic probes

Relative concentrations of aerosol in the test and reference samples were obtained by eluting the fluorescein dye with a 50/50 (v/v) of isopropyl alcohol and distilled water for at least four hours and the analyzing solutions with fluorometer.

3.7 Uncertainty Analysis

Experimental data is subject to various sources of errors, which can be categorized as bias/systematic errors, precision/random errors and errors due to defects in the experimental arrangements. Systematic errors tend to affect all data readings and its effects could be minimized by identifying the sources of errors and applying suitable corrective actions. Precision errors on the other hand occur due to random fluctuations in the various instrument readings. These errors generally propagate and contribute to uncertainty in the measured data. The Kline and McClintock (1953) method attempts to quantify the uncertainty in the data in single sample experiments, thus providing an idea on the error bounds of the final result. Uncertainty estimates on the aerosol penetration through the IVI system, also referred to as the major flow transmission efficiency in the standalone testing, and on Stokes number are provided in this discussion.

For the Kline-McClintock method, the uncertainty associated with a parameter R is given by

$$w_R = \sqrt{\sum_{i=1}^{n}\left(\frac{\partial R}{\partial x_i} w_i\right)^2} \tag{3.6}$$

where

w_R = the calculated uncertainty in the result R

x_i = independent variable with an associated uncertainty

w_i = the estimated uncertainty in the variable x_i

n = number of independent variables with an associated uncertainty in the parameter R

Aerosol penetration through the inlet and Stokes number can be expressed in terms of their fundamental measured quantities as follows:

$$P = \left[\frac{FIU_s}{FIU_{ref}}\right] \cdot \left[\frac{V_s}{V_{ref}}\right] \cdot \left[\frac{Q_{ref}}{Q_s}\right] \cdot \left[\frac{t_{ref}}{t_s}\right] \tag{3.7}$$

$$Stk = \frac{C_c \cdot \rho_p \cdot d_p{}^2 \cdot U}{9 \cdot \mu \cdot W} \tag{3.8}$$

where

subscripts "*s* and *ref*" denote sample and reference values respectively

P = inlet penetration

FIU = raw fluorometer reading in fluorescence intensity units

V = volume of total solvent used to soak filters

Q = volumetric air flow rate

t = test duration

Stk = Stokes number

C_c = Cunningham slip correction factor

d_p = diameter of the test particle

ρ_p = density of the test particle

U = throat velocity

μ = viscosity of air

W = throat width, used as the characteristic dimension

The total uncertainty in inlet penetration can be estimated by incorporating individual uncertainties in the measurable quantities *FIU*, *V*, and *Q*, which represent the raw fluorometer readings, solvent volume used for soaking filters, and the total volumetric flow rates respectively. Thus the relative uncertainty in inlet penetration is given as:

$$\frac{w_P}{P} = \sqrt{\sum \left(\frac{a_i w_{x_i}}{x_i} \right)^2} \tag{3.9}$$

or,

$$\frac{w_p}{P} = \sqrt{\left(\frac{w_{FIU_s}}{FIU_s} \right)^2 + \left(\frac{-w_{FIU_{ref}}}{FIU_{ref}} \right)^2 + \left(\frac{w_{V_s}}{V_s} \right)^2 + \left(\frac{-w_{V_{ref}}}{V_{ref}} \right)^2 + \left(\frac{-w_{Q_s}}{Q_s} \right)^2 + \left(\frac{w_{Q_{ref}}}{Q_{ref}} \right)^2 + \left(\frac{w_{t_{ref}}}{t_{ref}} \right)^2 + \left(\frac{-w_{t_{ref}}}{t_s} \right)^2} \tag{3.10}$$

Here a_i is the exponent of each variable x_i and the uncertainties of various parameters used in Equation 3.7 are:

- Fluorometer reading (*FIU*): 0.6% (0.1% non-linearity error, 0.6% measurement error)
- Error in volume of liquid used to soak filters (*V)*: 0.14% (0.1% each for isopropyl and water dispenser)
- Error in flow measurement (*Q*): 2% for TSI Inc. Mass flowmeters and 5% for Dwyer Inc. rotameters.
- Error in time measurement (*t*): ±1 sec (0.16%) for 10 minute duration tests

In addition to the above uncertainty values, there is also an uncertainty in the rate of aerosol generation, which was estimated to be approximately 3% for liquid aerosols generated using a VOAG.

Based on the above analysis, the uncertainty in the data obtained during standalone tests can be estimated as 4.2%. For wind tunnel experiments, rotameters were

used for flow control and reference and sample were obtained simultaneously. Hence the uncertainty in data from windtunnel experiments was estimated at 7.7%

The uncertainty in the calculated Stokes number is given in general form by

$$w_{Stk} = \sqrt{\sum \left(\frac{\partial Stk}{\partial x_i} w_{x_i} \right)^2} \tag{3.11}$$

The Stokes number could be represented in terms of the volumetric flow rate (Q) as

$$Stk = \frac{C_c \cdot \rho_p \cdot d_p{}^2 \cdot Q}{9 \cdot \mu \cdot \pi \cdot D \cdot W^2} \tag{3.12}$$

The measured variables which contribute to the total uncertainty are the particle diameter, d_p; flow rate, Q; base diameter of the top cone, D; and, the throat width, W. One other source of systematic error in stokes number calculation is the assumption of $C_c = 1$, which is not accurate when the particle sizes approachs the mean free path of the gas. Table 3.1 tabulates the error in C_c, when the following empirical correlation from Hinds (1999), was used for its estimation

$$C_c = 1 + \frac{\lambda}{d_p} \left(2.34 + 1.05 \exp(-0.39 \frac{d_p}{\lambda} \right) \tag{3.13}$$

The relative uncertainty in calculating the Stokes number for a given particle size may be expressed as

$$\frac{w_{Stk}}{Stk} = \sqrt{\left(\frac{w_{\rho_p}}{\rho_p} \right)^2 + \left(\frac{w_\mu}{\mu} \right)^2 + 4\left(\left(\frac{w_{d_f}}{d_f} \right)^2 + \left(\frac{w_f}{f} \right)^2 \right) + \left(\frac{w_Q}{Q} \right)^2 + 4\left(\frac{w_W}{W} \right)^2 + \left(\frac{w_D}{D} \right)^2} \tag{3.14}$$

Here the uncertainties of various parameters used in Equation 3.12.

- Particle density (ρ_p): 2%
- Viscosity of air (μ): 0.2%

- Error in flow measurement: 2% for TSI Inc. Mass flowmeters and 5% for Dwyer Inc. rotameters.
- Uncertainty in throat width (W): 5%
- Uncertainty in cone diameter (D): 0.07%
- Uncertainty in particle size measure on a glass slide (d_f): 2%
- Uncertainty in flattening factor (f): 0.775% or ±0.01 non-dimensional units

Based on the above analysis, the average uncertainty in the calculated Stokes numbers of 10 μm AD aerosol particles were 11.2% and 12.1% for standalone and wind tunnel tests, respectively.

3.8 Quality Assurance

3.8.1 Quality of Test Aerosol

The quality of the test particles was given suitable consideration in terms of its sizing, monodisperse nature, and uniformity of concentration at the test section. A calibrated optical microscope was used for sizing test particles that are impacted on microscopic slides coated with an oil-phobic fluorocarbon surfactant (NYEBAR, Type Q, 2.0%, NYE Lubricants Inc., New Bedford, MA). The microscope was calibrated using a stage micrometer before particle size measurements. It was ensured that particles chosen for measurement lie on the periphery of the impacted sample to avoid measurement of doublets. Several particles are measured before taking an average size reading.

The monodisperse nature of the generated particles arriving at the test section was verified using an APS before the start of sampling and subsequently throughout the duration of each test. A sampling run was suspended if any satellite particles were observed during the test and the samples were discarded. The test was continued after proper adjustments are made to the VOAG and the monodisperse nature of particles was verified.

A uniform concentration of aerosol in the wind tunnel near the test section is critical for acquiring accurate performance data. Two isokinetic nozzles are run as references simultaneously with the sampling inlet. An average reading from the two nozzles was used as the reference reading in order to reduce effects of variation in particle concentration across the test plane. Test durations were sufficiently long to ensure that the fluorescein collected on the filters was at least one order of magnitude greater than the background fluorescein level. All data points presented in this study are represented as the average of at least three test runs for a given operating condition.

3.8.2 Flow and Velocity Measurement

All rotameters and flow measuring equipment were calibrated and checked for leaks prior to testing. A thermal anemometer (VelociCal, Model No. 8355, TSI Inc., Shoreview, MN) was used for conducting wind tunnel velocity measurements. Rotameters (Dwyer Instruments, Michigan City, IN) were used for monitoring flow rates and were calibrated using a Laminar Flow Element (LFE, Model 10-5-400A, CME Division of Aerospace Control Products, Inc. Davenport, IA 52806) for accuracy. The arrangement used for calibration of the rotameters is shown in Figure 3.6, and calibration graphs are presented in Figure 3.7. The flow measurement and control apparatus for the

isokinetic probes is shown in Figure 3.8. Readings obtained from the rotameters during an experiment were corrected for the pressure drop through the system as follows.

$$Q_{actual} = Q_{read} \times \sqrt{\frac{p_a - \Delta p}{p_a}} \tag{3.15}$$

Where Q_{actual} is the actual volumetric flow rate, Q_{read} is the observed volumetric flow rate, p_a is the atmospheric barometric pressure, and Δp is the pressure drop in the system. While testing inlets, the filter media causes a significant pressure drop to occur in the system. In order to overcome the pressure drop, the flow must be compensated to ensure that the flow rate upstream of the filter being pulled through the inlet is the true flow. The system pressure drop was measured using Magnehelic differential pressure gauges (Dwyer Instruments, Michigan City, IN).

3.8.3 Fluorometric Analysis

The fluorescein concentrations resulting from extraction of samples from filters were quantified fluorometrically. Many factors influence the fluorometric analyses including wavelength and intensity of primary light, and the transmission characteristic of the excitation and emission filters that are used in the instrument. Kesavan et al. (2001) observed that the stability of the fluorescent material can be disturbed by small changes in the environment, such as the pH, ionic state of the molecule, nature of the solvent, viscosity, temperature, etc. The optimum excitation and emission wavelengths were found to be 492 nm and 516 nm. The fluorescent solution is also strongly pH dependent, but for values above 9, the intensity is both maximized and constant. Use of the NB490 and SC515 filters and adding one drop of 1N NaOH for every 5 mL of liquid sample satisfies the quality issues for the fluorometric analysis. Confirmation of linearity

in the fluorometer measurements was done by diluting the sample so that it has half the fluorescein concentration. The reading for the diluted sample should be approximately half that of the initial FIU reading.

CHAPTER IV

THE IN-LINE VIRTUAL IMPACTOR

This chapter presents the development of the In-line Virtual Impactor (IVI). The following sections provide a brief introduction in to the history of pre-separators in air sampling inlets followed by the description of the IVI prototype. Finally a detailed discussion on the performance characterization of the prototype is presented.

4.1 Introduction

A typical near-real-time bioaerosol detection system consists of a size selective inlet, a concentrator or collector (e.g., virtual impactor or cyclone), and some form of analyzer. The particle fractionation capability of the inlet is designed to exclude large particles that could foul the internal elements of the sampler or that might confound the detector, for example, it is generally desirable to strip large pollen particles from an aerosol that is to be analyzed for fluorescence characteristics. The majority of large particle fractionators are inertial separation devices with the simplest being the classical inertial impactor. As an example, McFarland et al. (1984) developed an 1100 L/min all-weather PM-10 sampler inlet that scalped large particles from the distribution prior to collection with a filter. To minimize the problem of solid particle carryover, the impaction surface was coated with a layer of high viscosity oil; however, the use of an oiled surface may not provide adequate large particle retention if the concentration of

large particles is very high, as might be the case for some bioaerosol sampling scenarios. Particle trap impactors have been developed to reduce solid particle carryover by collecting the heavier particles in a cup or well instead of a flat plate (Biswas and Flagan, 1988 and Kim et al., 2002).

Virtual impactors were developed as an alternative to classical impactors by Conner (1966) to eliminate solid particle carryover. Subsequently, Peterson, 1975 and Dzubay and Stevens (1975) designed a dichotomous sampler, which worked on the principle of virtual impaction, to characterize ambient aerosols. But, the fractionation characteristic curve of the virtual impactor is not as steep as the real impactor. Further, virtual impactor geometry is complex and its performance is critical to misalignments (Loo and Cork, 1988). Hence, the majority of large particle fractionators used in inlets is still some form of a real impactor, Chow (1995); however, Romay et al. (2002) have developed a circular jet virtual impactor pre-separator for bioaerosol sampling.

A circumferential-slot virtual impactor has certain inherent advantages relative to a circular jet virtual impactor in that a long narrow slot can be easily fabricated and, provided the flow is stable, aerosol fractionation can be achieved with a low expenditure of pressure, Haglund and McFarland (2004). In the following sections, the design, development, and characterization of a dual-cone circumferential-slot Inline Virtual Impactor (IVI) is presented. CFD techniques were used at the design stage as an optimization tool to determine the appropriate combination of the critical geometrical parameters for the IVI. The IVI has sharp separation characteristics similar to those of a real impactor, while it also eliminates particle bounce.

4.2 Prototype Description

The Dual Cone IVI inlet is shown schematically in Figure 4.1. A flow rate of 111 L/min is air drawn into the IVI where it is accelerated in the nozzle formed by the gap between the waistline of the top cone and the tube wall. As the accelerated jet issues from the nozzle, it is split into two parts, the major flow comprised of ninety percent of the total flow and minor the flow comprised of the remaining 10%. The major flow, which contains the aerosol fine fraction, is transported into the region between the inverted lower cone and the flow divider. The second cone is used to minimize the presence of recirculation zones in the major flow region and hence ensure flow stability. The apex angles of the top and bottom cones are 60 and 90 degrees respectively.

As the aerosol enters the critical zone, larger particles are concentrated into the minor flow stream while the smaller aerosol particles, which are the particles of interest, are transported with the major flow. As the particles in the minor flow are not of any consequence when the IVI is operated as a pre-separator, they were not characterized in the current study. However, the use of an IVI as a large-particle concentrator could be accomplished by making minor modifications to the current geometry that would facilitate extraction of particles in the minor flow channel.

With reference to Figure 4.1, alignment spacers are used to position the cones and to maintain the alignment of the cones with respect to the flow divider. Proper alignment of the critical zone is achieved by accurate positioning of the cones relative to the flow divider through the use of alignment spacers. The concentricity of the whole inner assembly with the outer casing is achieved by mating the flow divider concentrically with the minor flow channel. Herein, it is demonstrated that the presence

of three alignment spacers in the flow field does not significantly affect the performance of the IVI.

The IVI prototype described here is indented to be used as a pre-separator for bioaerosol sampling inlets. Characterization of an inlet system with an IVI pre-separator and BSI-100 inlet is presented in Chapter V. Initial design and characterization are presented on pre-separators for bioaerosol sampling devices operating at 100 L/min. However, the device can be scaled to accommodate other flow rates and cutpoints. Modification made to the geometry to operate the inlet system at 300 and 400 L/min are discussed later in this chapter. Finally the development of a modified version of the IVI operating at a flow rate of 350 L/min and a cutpoint of 3 μm AD is presented in Chapter VI. This device is intended to be used as a size fractionator in a powder processing pilot plant

4.3 Numerical Modeling

Figure 2.1 shows the geometry used in our simulations along with the boundary conditions. The general methodology adopted for performing numerical simulations using CFX is described in Chapter II. Two dimensional simulations were used as quick tool for performing parametric study and design optimizations while a full three dimensional domain simulation on the optimized design was used for verification of 2D results.

Two-dimensional simulation results showing velocity contours in the IVI and velocity vectors in the critical zone are shown in Figure 4.2. Velocity vectors in the minor flow region near the critical zone show the presence of a small recirculation

bubble. Although it was not possible to completely eliminate the recirculation because the accelerated flow impinges into a relatively static void, it was minimized by adjusting the geometry.

Examples of particle trajectories computed for 2D geometry are shown in Figure 4.3. Figure 4.3a shows the behavior of 1 μm aerodynamic diameter (AD) aerosol particles, which are well below the cutpoint size of 10 μm AD, and consequently follow the flow stream lines. In contrast, Figure 4.3c shows the trajectories of 25 μm AD particles, which are well above the cutpoint size. They deviate from the flow streamlines in the critical zone and are inertially driven into the minor flow region. Trajectories of cutpoint size (10 μm AD) particles are shown in Figure 4.3b where one-half of the particles enter the major flow region. Particles of this size are prone to impacting on the flow divider radius. However, by observing the particle trajectories and performing suitable modifications to the critical zone geometry it is possible to reduce the wall losses for the desired cutpoint size.

4.4 Performance Characterization

The IVI was experimentally tested to characterize the major-flow transmission efficiency for a range of monodisperse liquid aerosol particle sizes from 4.0 to 15.0 μm AD. Detailed description of the experimental methodology used for characterization of the IVI is presented in Chapter III.

4.4.1 Transmission Efficiency

The major-flow transmission efficiency curves, η_{maj}, obtained for the IVI at an inlet flow rate of 111 L/min and a major flow rate of 100 L/min, are shown in Figure 6. Here, η_{maj} is plotted as a function of Stokes number, *Stk*. The cutpoint Stokes number (Stk_{50}) and cutpoint particle size (D_{50}) are based on conditions where 50% of the total number of particles injected into the IVI is conveyed out with the major flow.

Another parameter that influences the performance of the IVI is the distance between the acceleration nozzle exit plane and the tip of the separator that divides the major and minor flow streams, which distance is identified as *S* in Figure 4.1. The effect of the aspect ratio, *S*/*W*, where *W* is the slot width, was investigated both numerically and experimentally for *S*/*W* values of 1.03, 1.35, and 1.75.

As shown in Figure 4.4, the numerically predicted Stk_{50} value of the IVI is 0.73 when the *S/W* ratio is 1.75. The results of the experimental tests verify this prediction. At an inlet flow rate of 111 L/min, the particle aerodynamic diameter corresponding to these conditions is 10.0 μm AD. Also, Figure 4.4 shows the cutpoint Stokes number to decrease with decreasing values of the *S/W* ratio. This would allow users some flexibility in adjusting the cutpoint for an application where the flow rate is specified.

4.4.2 Slope of the Fractionation Curve

The steepness of the transmission efficiency curve can be represented by the geometric standard deviation, s_g, of the efficiency values, which for discretized data is (McFarland et al., 1984):

$$\ln^2 s_g = \frac{1}{n}\sum_{i=1}^{n}(\ln Stk_i - \ln Stk_{50})^2 \qquad (4.1)$$

where: n = number of intervals. The geometric standard deviation was calculated by dividing the efficiency curve into several equal transmission efficiency increments and assuming Stk_i to be the Stokes number corresponding to the interval midpoint. Major flow transmission efficiencies ranging from 5 to 80 % were utilized in calculating the steepness as the major flow transmission efficiency is asymptotic to 90 %. For 7 equally spaced intervals, Equation 4.1 yields a value of 1.51 for s_g. By comparison, Haglund and McFarland (2004) presented minor flow efficiency results for slot virtual impactors with traditional geometries, and the steepness of their curve, calculated from Equation 3, was 2.1.

The steepness of a major flow fractionation curve can also be estimated from:

$$\hat{s}_g = \sqrt{\frac{D_{16}}{D_{84}}} \tag{4.2}$$

where: D_{16} = particle size associated with a transmission efficiency of 16% and D_{84} = size associated with a transmission efficiency of 84%. The steepness parameter, $\hat{s}_g$, would be the geometric standard deviation if the fractionation curve were a log-normal function. Using Equation 4.2, the steepness of the IVI fractionation curve is 1.60, whereas the steepness of the fractionation curve of Haglund and McFarland (2004) is 2.05. The fractionation curve of a classical real impactor, Lee (2001), has a steepness of 1.4 when calculated with Equation 4.2. This indicates that the performance characteristics of the IVI are steeper than the slot virtual impactor and comparable to that of a real slot impactor.

Estimation of major flow transmission efficiency and steepness of the fractionation curves was generally carried out under the assumption that the test particles

were monodisperse in nature. However Haglund (2003) had noted that the particles generated using the VOAG is not strictly monodisperse. Figure 4.4 shows the calculated transmission efficiency curve modeled using Equation 4.3. The size distribution of three representative test particles is also seen in Figure 4.4. The parameters 'Stk_{50}' and 'b' in Equation 4.3 are 0.73 and 2.5 respectively when the test aerosols are treated as monodispersed.

$$\eta_{maj} = \frac{(1-f)}{1+\left(\frac{Stk}{Stk_{50}}\right)^{b}} \tag{4.3}$$

where f is the minor flow fraction.

Accounting for the polydisperse nature of the test aerosols yielded a Stk_{50} of 0.7 and b of 3. It can be noted that the cutpoint of the device is not significantly affected by the monodisperse assumption. However, the steepness of the transmission efficiency curve as estimated using Equation 4.2 changes to 1.45 from 1.60. Figure 4.5 presents the transmission efficiency curves for both cases.

4.4.3 Effect of Throat Reynolds Number

The IVI was scaled up to be operated at 350 L/min of major flow, which resulted in a throat Reynolds number, *Re*, of 1729 as compared with the value of 545 for the flow rate of 100 L/min through the major flow , where:

$$Re = \frac{\rho_f U w}{\mu} \tag{4.4}$$

Here ρ_f is the density of the carrier fluid (air). The numerically predicted value of Stk_{50} was 0.80 for the higher Reynolds number, which is slightly higher than the value of 0.73 associated with the Reynolds number of 545. This effect of Reynolds number on the

value of Stk_{50} is due to the differences in the flow field and velocity profiles at the different Reynolds numbers.

4.4.4 Internal Wall Losses

The transmission efficiency curves presented in Figure 4.6 take into account the internal wall losses. Figure 4.7 shows the experimental and predicted wall loss characteristics as a function of Stokes number. Losses at the cutpoint Stokes numbers are about 30%, and are predicted to peak at about 60%. While the presence of wall losses tends to shift the cutpoint to lower Stokes number values, wall losses do not interfere with the operation of the IVI as a pre-separator, where only the fine fraction is of interest. Indeed, tests have been conducted with aerosolized dry Arizona Fine Road Dust (ISO 12103 – 1, A2 Fine test Dust, Powder Technology Inc., MN), which has a mass median diameter of about 10 μm. More details on these tests are provided in section 6.2. While the liquid droplets show wall losses of almost 30% near the cutpoint, the dry dust exhibits solid particle carryover and is transported away from the critical zone.

The prediction of wall losses also partially explains why the cutpoint tends to shift to lower values while using smaller *S/W* ratios. In those cases, the particles that travel close to the tube wall get collected on the flow divider. With larger *S/W* ratios, these particles will be transported by the major flow.

4.4.5 Pressure Loss

The experimentally measured pressure drop across the IVI inlet for the flow rate of 111 L/min and the *S/*W value of 1.75 was 45 Pa (0.18-inches of water). The corresponding numerical prediction is 46.1 Pa.

4.4.6 Effect of Alignment Spacers on Major Flow Transmission Efficiency

During the experimental evaluation of the IVI, particles deposition on the alignment spacers in the major flow channel was quantified to determine the impact of those losses on the performance of the device. For particles near the cutpoint size, only about 0.01% of the incoming aerosol was collected on the spacers. Particle deposition was also insignificant for particles beyond the cutpoint size as few of these particles are carried with the major flow. Thus it can be assumed that the presence of the alignment spacers does not significantly influence the collection efficiency. The transmission efficiency curve generated using numerical simulation (presented in Figure 4.6) was obtained from a 3D model that included the spacers in the domain. Figure 4.8 illustrates the effect of the alignment spacers on the flow field in the annular plane located underneath the spacers toward the major flow exit. It can be seen that the disturbance is localized and does not affect the global flow.

4.4.7 Minor Flow Collection Efficiency

Figure 4.9 presents the computed minor flow transmission efficiency curve for S/W ratio of 1.75. The curve contains data for particle size up to 50 μm. In case of heavier particles, their inertia causes them to impact on the casing and thus contributing to the drop in the efficiency curve. A small percentage of the particles that enter the minor flow region gets entrained in the recirculation region and is lost on the walls of the flow divider. Thus, for use of the IVI as a coarse particles concentrator, modifications in the geometry are necessary for minimizing wall losses.

4.4.8 Effect of Minor Flow Ratio on Major Flow Transmission Efficiency

Virtual impactors are conventionally operated at a 9:1 major to minor flow ratio. IVI is also designed to operate using the same flow split. However, it may be of interest to evaluate the performance variation at different flow splits as it would allow the user to vary the cutpoints with out the need to change any hardware. Figure 4.10 presents a comparison of major flow transmission efficiencies for 4:1 (20 % minor flow), 9:1 (10 % minor flow) and 19:1 (5% minor flow) major to minor flow ratios respectively. With increasing minor flow percentage, the cutpoint shifts to lower particle sizes as, one would expect, as the percentage of smaller particles inherently present in the minor flow increases. However, one observes that for particles beyond the cutpoint, the transmission efficiency curves tend to approach each other, as for particles in this range, the inertial effects are dominant. When just 5 % of the flow is extracted through the minor flow, heavier particles loose their momentum and tend to move back to the strong major flow. This results in heavy wall losses on the flow divider.

4.4.9 Effect of Top Cone Angle and Profile

The effect of the apex angle of the top cone on the fractionation efficiency curve was studies using CFD methods. The three different apex angles that were considered were the base case (30 degrees), 45 degree and 60 degree included half angle. Figure 4.11 shows a schematic of the domain with the angles marked. Figure 4.12 presents the results of numerical simulations that were performed on a 2D axi-symmetric geometry using CFX 10.0. Figure 4.13 shows the trajectories of 15 μm particles for the 3 different cone angles. It was observed that the use of a larger angle led to better aerodynamic focusing at the throat which led to better collection efficiency for larger particles in the

minor flow. Better focusing of particles along the tube wall is evident as the cone angle increases. However, there was not much benefit to be derived from this change with regards to the major flow. Also, in an effort to minimize the cross trajectory losses for large particles, a top cone with an elliptical profile was considered. Figure 4.14 shows the schematic of the simulation domain and velocity vectors in the elliptical cone system. Figure 4.15 provides the transmission efficiency in the major and minor flow and also the wall losses with reference to the Stokes number. The throat dimension was the same in all test cases. From numerical simulation results, it was concluded that there was no significant benefit in terms of reduction in wall losses with the use of an elliptical inlet cone. Hence the base case with an included half angle of 30 degrees was retained in the prototype.

4.4.10 Effect of *D/W* Ratio

It was earlier seen that the *S/W* ratio can have significant influence on the transmission efficiency curve. In the same line, the effect of *D/W* ratio on the fractionation efficiency was studied using 2D numerical simulations. The parameters, *S*, *D* and *W* were previously identified in Figure 4.1. Figure 4.16 shows the major flow transmission efficiency for various *D/W* ratios and it could be seen that the performance is not dependent on the *D/W* ratio. The base case was *D/W* = 1. It could also be hypothesized from this study that the performance of the IVI is relatively tolerant to concentric misalignment.

4.4.11 Comparison Between 2D and 3D Numerical Simulations

Initial optimization studies on the IVI design were performed on a 2D domain as shown in Figure 2.1. It is important that the cutpoint predicted by 2D and 3D simulations match in order to rely on the 2D results for adjusting the geometry. Figure 4.17 shows the comparison between the major flow transmission efficiency curve obtained using 2D and 3 D simulation for S/W = 1.75. The cutpoint predicted by both simulations in this case was 0.73. There are minor deviations which are likely due to the manner in which a 2D axi-symmetric simulation is performed in CFX. When revolving the 2D profile along the axis, the profile is displaced by a small 'δ' in order to avoid singularity along the axis, while in 3D the entire domain is simulated and no such displacement is necessary.

4.5 IVI Scale-Up to 300 and 400 L/min

In this section, the scaling up of IVI units for operation at a major flow output rate of 300 and 400 L/min are discussed. IVI with 300 L/min major flow output is referred to as IVI-300 and with 400 L/min output as IVI-400. A similar naming convention is used elsewhere, where the number following "IVI" represents the major flowrate through the device. Based on the initial IVI prototype design, an upgraded version, IVI-100, was manufactured by TSI Inc, St. Paul, MN. Figure 4.18 shows the schematic and a photograph of the upgraded prototype and its performance is shown in Figure 4.19. Based on this characterization curve, the throat width of IVI-100 was increased to maintain the same stokes number for a 11 μm particle when the major flowrate was 400 L/min. It was intended to modify an existing IVI-100 prototype to operate at 400 L/min. However, there was not enough material on the outer casing to accommodate the

increased throat width. Hence the maximum possible throat width that could be obtained without major modifications to the existing prototype was chosen. The following are the details on the numerical simulation for IVI-400

Simulation details

Average throat velocity: 6 m/s

Throat width: 0.18”

S/W ratio: 1.75

Throat Re number: 1800

Average Inlet velocity: 1.4 m/s

Inlet Re: 7590

Velocity at Major flow exhaust: 13.1 m/s

Exhaust Re: 21879

A low Reynolds number Turbulence model (k-ω) was used in the calculation of flow field. A y^+ value of 2 was used for the simulations. The major flow transmission efficiency curve obtained using 2D and 3D numerical simulations are plotted in Figure 4.20, which also contains the efficiency characterization using standalone testing setup. A cutpoint of 10.0 μm AD was obtained from the standalone tests for the IVI-400. IVI-100 was modified to operate at 400 L/min with the intentions of combining it with a BSI-100 inlet to have a BSI-IVI 400 inlet system with a cutpoint greater than 10 μm. However, due to the inherent losses present in the BSI inlet, the combined system failed to achieve the desired cutpoint even after increasing the S/W ratio to 2. It was then decided to operate the current system at 300 L/min and a redesigned version of the IVI-

400 (IVI-400-V2) was developed for use in the 400 L/min inlet system. The details on characterization of the BSI-IVI inlet systems are presented in Chapter V.

IVI-400-V2 (version 2) was initiated to eliminate the need for a 1" to 2" transition and also to accommodate higher flow rates (>400 L/MIN). Based on numerical simulations, IVI-400-V2 has a cutpoint of 12.5 μm AD and when combined with the BSI100 inlet, it is expected to provide cutpoint in the 11 – 11.5 μm range. Figure 4.21 shows the flow characteristics and particle behavior in a 2D domain of IVI-400-V2 and the major flow transmission efficiency curve is presented in Figure 4.22. Based on the geometry shown in Figure 4.21, a new prototype has been developed, a 3D rendering of which is shown in Figure 4.23. Detailed performance characterization of the device is presented elsewhere (Baehl, 2007).

4.6 Summary and Conclusions

A dual-cone circumferential-slot in-line virtual impactor (IVI) has been designed and tested using both numerical and experimental techniques. 2D simulations were initially used to design and optimize the geometry and the predicted cutpoints are in good agreement with the full domain 3D simulations.

The IVI is designed for a cutpoint of 10 μm AD at a major flow rate of 100 L/min. Experimental evaluation of the IVI prototype shows that the cutpoint value is 10 μm when the aspect ratio *S/W* is 1.75, and the experimentally observed performance is in good agreement with numerical predictions. An interesting feature of the IVI is the ability to vary cutpoint by varying the *S/W* ratio through adjustment of the alignment spacer height. Further, the simple construction could allow the device to be used for

multiple flow rates by using different cone sizes to modify the slot width, enabling maintenance of a constant Stk_{50} value. The throat Reynolds number is seen to have a slight effect on the Stk_{50} value. Throat Reynolds number of 545 yields a Stk_{50} value of 0.73 while it is slightly higher at 0.80 when the Reynolds number is 1729.

Wall losses of about 30% are observed near the cutpoint size, however, those losses are essentially associated with the coarse fraction (minor flow), and do not have a significant impact on the desired aerosol fraction (the fine fraction). With dry dusts there is no buildup of deposits even with severe exposure (145 mg of particulate matter with a mass median particle size of about 10 µm AD).

Operation of the IVI at 4:1 and 19:1 major to minor flow ratio, in addition to the conventional 9:1 ratio shows that the Stk_{50} decreases as the minor flow percentage increases. However, the behavior of larger particles (sizes beyond the cutpoint) shows relatively minor variation with different flow ratios as compared to the smaller particles (sizes smaller than the cutpoint).

In addition, the apex angle and the profile and of the top cone does not have any significant effect on the performance of the IVI as a pre-separator.

CHAPTER V

BIOAEROSOL SAMPLING INLETS WITH IN-LINE VIRTUAL IMPACTOR PRE-SEPARATOR

This chapter details the characterization of a combination of a BSI ambient air sampling inlet housing, where BSI represents a Bell-Shaped Inlet (Nene, 2006), and an IVI. The BSI/IVI is used as a size selective inlet for bioaerosols and and other air sampling applications. First, a brief introduction on the development of high volume air sampling methods is presented followed by a discussion on the establishment of the PM standards for air quality monitoring. Finally, the characterization of BSI-IVI inlet systems in an aerosol wind tunnel is presented where the inlets are tested at three different wind speeds, 2, 8 and 24 km/hr, to establish the independence of inlet performance on wind speed.

5.1 Introduction

High volume (hi-vol) samplers were first developed in the late 1940s to sample airborne particles for radioactivity after detonation testing of nuclear weapons. Initial hi-vol sampler designs consisted of a flat filter mounted in a box type frame with a peaked roof cover placed over the top to prevent dust from falling in, (Robson and Foster, 1962). This method of sampling was used extensively from the late 1950's – 80's to

quantify Total Suspended Particulate (TSP) matter in urban ambient environments (Chow, 1995). TSP formed the first basis for compliance with the National Ambient Air Quality Standards (NAAQS) in the U.S. (Clean Air Act, 1970, 42 U.S.C.A. §§7401) and was used extensively until regulatory changes greatly reduced their role (U.S. EPA Federal Register, 1987b). The standard method for sampling was based on the design of the sampling device rather than its performance. Characterization efforts in the 1970's showed that the hi-vols had a 50% cutpoint ranging from 30 to 50 μm (Wedding et al., 1977, McFarland et al., 1980). It was found that the opening underneath the hi-vol's peaked roof allowed dust to be blown into the sampler contributing to a bias in the measured mass concentrations (Bruckman and Rubino, 1976). Further, use of the term 'particulate matter' to describe any airborne pollutants without reference to its physical or chemical nature needed an overhaul as the standards in the Clean Air Act of 1970 were based on health effects. In the late 1970's a 'performance' standard instead of a 'design standard' was proposed (Chow, 1995). With a performance standard, any sampler design could be used for a reference sampler provided it could meet the criteria stipulated in the standard. In addition, a PM_{10} standard for suspended particles was promulgated in 1987 (U.S. EPA Federal Register, 1987a). The term PM_{10} is intended to represent the mass concentration of particles with sizes that pass through a fractionator with a prescribed fractionation curve. The PM_{10} fractionation curve supposedly mimics that of the extra-thoracic region of the human lung system. Criteria that went in the establishment of PM_{10} standard included inhalation properties, measurement methods and health effects of inhaled aerosols. Purdue (1988) presents the details the PM_{10} performance standard and its implementation.

The first reference samplers for the new PM_{10} standards were modified from existing hi-vols and introducing a size selective inlet (SSI) instead of a peaked roof. McFarland et al. (1984) presented the characterization of a size selective inlet based on inertial impactors for the hi-vol sampler while Wedding et al. (1985) presented a cyclone-type inlet for the hi-vol. To prevent large-particle carryover, the fractionators were provided with grease or oil coated collection surfaces. However, as noted before in Chapter IV, the use of grease or oil coated surfaces may not provide adequate particle wetting if the concentration of large particles is high, and over time the collection of fibrous particles on the surfaces cause collection of smaller particles by the mechanism of filtration (Gutfinger and Friedlander, 1985). In contrast, use of a virtual impactor should preclude large particle carryover; however, an early attempt to use a virtual impactor pre-separator in inlets (Dzubay and Stevens, 1975) resulted in poor performance (McFarland et al., 1980). Recently, MSP Inc. (Shoreview, MN) introduced a circular-jet virtual impactor for use as a large particle fractionator in inlets.

Chapter IV presents the initial development of a circumferential-slot in-line virtual impactor (IVI) intended for use as a pre-separator in bioaerosol sampling inlets. The following sections present the characterization of a bioaerosol sampling inlet with an IVI pre-separator, which is designed for a major flow rate of 100 L/min and provides a cutpoint of 11 μm AD. Preliminary results on evaluation of BSI-IVI inlets for 300 and 400 L/min are also given. Detailed evaluation of these inlets will be presented by Baehl (2007).

5.2 Inlet Description

A schematic of the combined inlet and pre-separator is shown in Figure 5.1. The system consists of a circumferential side entrance Bell Shaped Inlet (BSI), which is patterned after a design of McFarland et al., 1977. An insect screen and the IVI are internal to the BSI. During operation, air is aspirated into the inlet, and then directed downward towards the insect screen and IVI. Here the particulate laden air is bifurcated into major and minor flows. The major flow rate is 100 L/min, which is 90 % of the incoming flow and transports the fine aerosol fraction, while the minor flow rate is 11 L/min and carries the larger particles that are deflected from the bending streamlines together with the fines originally associated with the 11 L/min flow rate. The 90% to 10% flow split between the major and the minor flows was maintained for all cases. Thus the 400 L/min system operates at 400 L/min major flow and 44 L/min minor flow, and similarly, the 300 L/min system has major and minor flows of 300 and 33 L/min respectively.

5.3 Performance Characterization

The BSI-IVI inlet was tested in an aerosol wind tunnel facility to characterize the penetration under simulated field sampling conditions. Monodisperse liquid aerosols with particles ranging in size from 3.3 to 17.0 μm AD generated with a VOAG, as described in Section 3.1, were used to evaluate the unit at wind speeds of 2, 8 and 24 km/h. A detailed description of the windtunnel testing arrangement is provided in Section 3.6. Penetration through the inlet was calculated using Equation 3.4 from the mass of aerosol in the filter samples obtained from the isokinetic nozzles and major flow

exhaust of the IVI. Aerosol mass concentration in the liquid used to extract the analytical tracer from a filter sample was analyzed fluorometrically (Section 3.3).

5.3.1 BSI-IVI 100 System

The results of wind tunnel evaluation of the inlet with liquid aerosols are presented in Figure 5.2. For each particle size in the range of 3.3 to 17.0 μm AD, tests were conducted at the wind speeds of 2, 8 and 24 km/hr. With reference to Figure 5.2, there is not much of variability in penetration efficiency with wind speed. The cutpoint is 11 μm AD as determined from interpolation of the penetration efficiency curves.

5.3.2 BSI-IVI 300 and 400 L/min Systems

Figure 5.3 shows the performance curves of the BSI-IVI system with an IVI-400 operated at a 400 L/min major flow rate. It can be seen from Figure 5.3 that the BSI-IVI system in the current configuration yielded a cutpoint of 8.5 μm AD while a value of 11 μm was the design goal. The initial IVI-400 design had an S/W ratio of 1.75, which was increased to 2, but the cutpoint particle size of the inlet system was still only 9.8 μm AD. Thus, a revised design, the IVI 400-V2, was generated to provide a cutpoint of 11 μm AD when combined with the BSI-100 inlet. This units has a cutpoint of 11.2 μm AD (Baehl, 2007).

The previous BSI-IVI-400 system with S/W = 2 (BSI-IVI-400-2) was tested at 300 L/min sampling flow rate and it was observed that a 11 μm cutpoint was achieved with this configuration (Figure 5.4). Table 5.1 presents the performance characteristics of the various BSI-IVI inlet systems.

5.4 Summary and Conclusions

The in-line virtual impactor has been incorporated into a bell shaped inlet and tested for penetration characteristics with liquid aerosols at wind speeds ranging from 2 – 24 km/hr. The combined BSI-IVI system has an experimentally observed cutpoint of 11 μm at 100 L/min major flow rate. When the IVI was tested without the inlet in a static system, the experimentally observed cutpoint was 11 μm AD. A modified IVI with a BSI-100 inlet yielded a cutpoint of 11 μm at 300 L/min while delivering aerosol with a 10 μm cutpoint at 400 L/min. In static testing of the modified prototype, the observed cutpoint was 12 μm AD. A BSI-IVI-400 L/min inlet has been designed with the new IVI-400-V2 prototype, which had a cutpoint of 12.5 μm AD in numerical simulations.

The use of IVI as a pre-separator in aerosol inlets offers maintenance free operation even under severe loading condition, while also eliminating any bias in aerosol measurements due to particle re-entrainment.

CHAPTER VI

POWDER PROCESSING USING IN-LINE VIRTUAL IMPACTORS

Development and use of the IVI for powder processing applications are explored in this chapter. Performance characteristics of an IVI unit used to separate ARD is analyzed and further a conceptual design for a high throughput powder processing system using four identical units for processing 1400 L/min flow is presented. CFD modeling for a specialized inlet utilized for distributing the flow evenly to the IVI units are also discussed.

6.1 Introduction

Virtual impactor as a size fractionator is an attractive alternative to rotating flow-based approaches (e.g., cyclones) for stripping a batch of powder of particles larger than a certain threshold. In a previous study (Seshadri et al., 2005) the use of linear slot virtual impactor for processing Arizona Road Dust (ISO 12103-1, A2 Fine Test Dust) was demonstrated and the limits to the total mass loading were established based on the catastrophic failure at the acceleration nozzle due to clogging. In a follow up study, investigation on the use of virtual impactor as a high volume fractionator for superconducting powders in Powder-in-Tube (PIT) processing was performed to verify achievement of a necessary “zero defect” attribute. The “zero defect” condition here refers to an absence of coarse particles in the product, which is the fine fraction or major

flow. A Linear Slot Virtual impactor (LSVI) was used for separation of powder samples, which had been supplied by various vendors. The separation characteristics were determined by analyzing the size distribution of particles collected in the major flow filter and an initial reference sample using a Coulter counter. The results show that there are no particles beyond 1.5 times the 90 percent threshold diameter in the collected fines. Figure 6.1 presents a sample characterization curve for MgH_2 powder. It is seen that there are no coarse particles beyond 8 μm in the major flow stream. The process parameters were fixed to limit the fraction of particles larger than 5 μm to less than 10%. It can be seen that there is a significant amount of larger particles in the initial sample that could potentially clog the acceleration nozzle by impacting of the internal walls due to the crossing trajectories. For comparison, Figure 6.2 shows the clogging of an LSVI acceleration nozzle by tin powder. Thus it was realized that the use of LSVI is limited to small mass loadings. In order to process significant quantities of powders, a large array of such impactors would have been necessary. As an alternative to the LSVI, the IVI's that were initially developed to strip large particles in aerosol sampling application could be used for fine powder fractionation as well. The following section presents a discussion on the performance of the IVI with ARD.

6.2 IVI 100 ARD Performance

Arizona Road Dust (ARD, Powder Technology Inc. Burnsville, MN) is commonly used for testing filtration devices, particularly in the automotive and heavy equipment industries. In this study A2 fine test dust with a nominal size distribution in the range 0 – 80 μm was fed into the IVI using a fluidized bed dust generator (Section

3.2). Figure 6.3 shows the cumulative and the differential volumetric distribution of ARD as provided by the manufacturer.

The size distribution of ARD after separation in the IVI can be calculated from the particle size distribution, shown in Figure 6.3, and the major flow transmission efficiency curve of the impactor used for processing ARD. Figure 6.4 presents a comparison between the feed powder and the processed powder. Curve 1 in Figure 6.4 shows the calculated cumulative volume distribution of ARD while Curve 2 shows the experimentally obtained volume distribution at the major flow exhaust, sized using a Coulter counter. Particles smaller than 2 μm were not considered for analysis as the 100 μm orifice used in the Coulter counter measures particles in the size range 2 – 60 μm.

6.3 Superconductor Powder Processing Requirements

For powder-in-tube fabrication of superconducting wires and tapes, it is generally desirable to have finer particles as it leads to finer strands in the final product. Table 6.1 provides the details on the upper threshold on the particle size for a variety of superconducting powders from various manufacturers. On an average, the density of the product particles varies from 2 g/cm^3 to 8 g/cm^3 and the cutpoint requirements vary from 1 to 5 μm in physical size. For estimation of mass throughput of particles below a certain threshold the following procedure is adopted.

For a particle of size d_p, the corresponding mass fraction of that particle is estimated using the known size distribution as follows.

If m is the dust loading rate in mg/L, then the mass fraction ΔG_p in mg/L is given by

$$\Delta G_p = \chi \times m \times (1 - f) \tag{6.1}$$

where, χ is the percentage by mass or volume of particles of size d_p in the feed powder and f is the minor flow fraction, typically 0.1. Thus the total mass of particles (G, in mg) of size d_p, collected after processing is given by

$$G = Q \times \Delta G_p \times \eta \tag{6.2}$$

where, Q is the sampling flow rate through the major flow and η is the major flow transmission efficiency for particle of size d_p obtained from the characteristic fractionation curve of the IVI. Thus the total mass of particles below the threshold size d_p is

$$M = \int_0^{d_p} G \, \mathrm{d}d_p \tag{6.3}$$

6.4 IVI System Design

One of design criteria for the powder fractionation system is that it needs to able to process powder at 0.024 m^3/s (50 cfm, 1416 L/min) flow rate. The proposed IVI system design consists of 4 identical IVI units, each of which operates in a 350 L/min inlet flow and designed to have a cutpoint of 3 μm AD. The aerosol coming in to the IVI system is distributed evenly into the independent IVI units using a specially designed inlet nozzle, which eliminates powder accumulation in the manifold, Figure 6.5.

6.4.1 IVI-350 Prototype – CFD Studies

The IVI-350 prototype developed for this application was initially designed with the aid of 2D numerical simulations using CFX. Figure 6.5 shows the geometry and the

velocity contours in the 2D domain and the fractionation efficiency curve for this design is presented in Figure 6.6. The cutpoint of the device is 3 μm AD with zero penetration for any particle beyond 5 μm AD. A 3D model of the geometry is shown in Figure 6.7.

6.4.2 Inlet to Accommodate Four Parallel IVI-350 Units – CFD Studies

For obtaining a good fractionation performance, it is necessary that the particle laden flow when entering the device be as uniform as possible. A specially designed inlet manifold is used to distribute the flow evenly to the IVI units. The inlet consists of a 102 mm x 254 mm (4" x 10") reducer, where the four IVI units are arranged symmetrically on a 254 mm (10") disc and mounted on to the inlet. A contoured insert is placed inside the inlet to gradually displace the flow which becomes nearly uniform when entering the IVI units. Figure 6.9 shows the base case of the inlet and the insert which was further optimized to obtain a more uniform velocity distribution across the four exit planes. From Figure 6.10, it can be observed that the velocity profile at the exit planes, which are the inlet planes to the IVI, is highly skewed towards the inside. To alleviate this problem, the size of the insert was increased to displace the flow to the outer periphery of the reducer, which will later help to distribute the flow more uniformly at the exit planes. Figure 6.11 shows the computational model of the optimized inlet manifold while the velocity distribution and velocity profiles across the exit plane are shown in Figures 6.12 and 6.13. A 3D model view of the complete IVI separation system that will be incorporated in a powder processing pilot plant is shown in Figure 6.14.

6.5 Summary and Conclusions

Fractionation performance of the IVI with Arizona Fine Test Dust demonstrated the ability of the system to operate under heavy dust loading conditions with no large particle carryover. Coulter counter analysis of dust sample collected from the major flow filter is in very good agreement with the calculated size distribution obtained from the manufacturer provided size distribution data for ARD.

Further, a new IVI prototype, IVI-350, was developed using CFD for use as a powder fractionator for processing superconductor precursor powders. The IVI-350 has a cutpoint of 3.0 μm AD, in a 350 L/min flow. The IVI separation system consists of four identical IVI-350 units and a specially designed inlet manifold that was modeled and optimized using CFD.

CHAPTER VII

CONCLUSION

In this study, CFD (ANSYS CFX) was employed to model a virtual impactor concept for separating the smaller particle fraction from an incoming aerosol stream. CFD was used as a design tool to model various prototypes of the In-line Virtual Impactor (IVI) and arrive at an optimized design that was experimentally investigated using monodispersed liquid aerosol particles. There is good agreement between the numerically predicted and experimentally observed performance. The initial IVI design was a prototype that delivers fine aerosol fraction in a 100 L/min flow with a 10 μm AD cutpoint. Numerical studies were performed on the sensitivities of the various geometrical parameters and it was found that only the *S/W* ratio affected the performance significantly. Indeed, the variation of cutpoint based on S/W ratio provides an option for the end user to vary to the cutpoint to a certain extent based on their need. An upgraded version of the IVI 100 was integrated in to the BSI inlet to form the BSI-IVI-100 system with a 11 μm AD cutpoint for use in bioaerosol sampling applications. The BSI-IVI inlet system is one of the first working prototype of a dichotomous sampler based inlet to have been developed in the last three decades. The IVI concept is scalable in terms of flowrate and cutpoint. This had been successfully demonstrated in the development of IVI based inlet systems for 300 and 400 L/min flow rates and in development of IVI-350. The IVI-350 is a 3 μm cutpoint device, operating at an incoming flow rate of 350 L/min, for use as a powder

fractionator. It has been designed to preclude any large particle from a batch of powders with near 100 percent efficiency.

REFERENCES

ANSYS (2005). CFX Release 10: User Manual, Canonsburg, PA.

Baehl, M. M. (2007). Ambient Aerosol Sampling Inlets for Flowrates of 100 and 400 L/min, M.S. Thesis, Department of Mechanical Engineering, Texas A&M University, College Station, TX.

Barnstead-Thermolyne (1999). Turner® Quantech™ Digital Filter Fluorometer Operation Manual, Dubuque, IA.

Beckmann-Coulter (2001). Multisizer 3 User Manual, Fullerton, CA.

Berglund, R. N. and Liu, B. Y. H. (1973). Generation of Monodisperse Aerosol Standards. *Environ. Sci. Tech.* 7:147-153.

Biswas, P. and Flagan, R. C. (1988). The Particle Trap Impactor. *J. Aerosol Sci.* 19:113-121.

Bruckman, L. and Rubino, R. A. (1976). High Volume Sampling: Errors Incurred During Passive Deposition Exposure Periods. *J. Air Pollut. Control Assoc.* 26:881-883.

Chen, B. T., Cheng, Y. S. and Yeh, H. C. (1990). A Study of Density Effect and Droplet Deformation in the Tsi Aerodynamic Particle Sizer. *Aerosol Sci. Techol.* 12:278-285.

Chen, B. T. and Yeh, H. C. (1987). An Improved Virtual Impactor: Design and Performance. *J. Aerosol Sci.* 18:203-214.

Chow, J. (1995). Measurement Methods to Determine Compliance with Ambient Air Quality Standards for Suspended Particles. *J. Air & Waste Manage. Assoc.* 45:320-382.

Conner, W. D. (1966). An Inertial-Type Particle Separator for Collecting Large Samples. *J. Air Pollut. Control Assoc.* 16:35-38.

Dzubay, T. G. and Stevens, R. K. (1975). Ambient Air Analysis with Dichotomous Sampler and X-ray Fluorescence. *Environ. Sci. Technol.* 9:663-668.

Elghobashi, S. (1994). On Predicting Particle-Laden Turbulent Flows. *Appl. Sci. Res.* 52:309-329.

Finlay, W. H., Stapleton, K. W. and Zuberbuhler, P. (1997). Fine Particle Fraction as a Measure of Mass Depositing in the Lung During Inhalation of Nearly Isotonic Nebulized Aerosols. *J. Aerosol Sci.* 28:1301-1309.

Finlay, W. H. (2001). *The Mechanics of Inhaled Pharmaceutical Aerosols,* 1st ed., Academic Press, San Diego.

Fu, X. K., Gupta, A., McIntyre, P. M. and Phares, D. J. (2003). New Size Sorting Technology for Superconducting Powders. *IEEE Trans. Appl. Superconductivity* 13:3494-3497.

Glowacki, B. A., Majoros, M., Vickers, M., Evetts, J. E., Shi, Y. and McDougall, I. (2001). Superconductivity of Powder-in-tube MgB_2 Wires. *Supercond. Sci.Technol.* 14:193-199.

Gotoh, K. and Masuda, H. (2001). Development of Annular-type Virtual Impactor. *Powder Technol.* 118:68-78.

Gutfinger, C. and Friedlander, S. K. (1985). Enhanced Deposition of Suspended Particles to Fibrous Surfaces from Turbulent Gas Streams. *Aerosol Sci. Technol.* 4:1-10.

Haglund, J. S. (2003). Two Linear Slot Virtual Impactors for Bioaerosol Sampling, PhD. Dissertation, Department of Mechanical Engineering, Texas A&M University, College Station, TX.

Haglund, J. S. and McFarland, A. R. (2004). A Circumferential Slot Virtual Impactor. *Aerosol Sci. Techol.* 38:664-674.

Hari, S., Hassan, Y.A. and McFarland, A.R. (2005). Computational Fluid Dynamics Simulation of a Rectangular Slit Real Impactor's Performance. *Nuclear Eng. Des*. 235:1045-1028.

Hassan, Y. A., Jones, B. G. and Yule, T. J. (1979). An Analytical Study of Virtual Impactor Aerosol Separators. *Trans. Am. Nuclear Soc.* 33:182-184.

Hinds, W. C. (1999). *Aerosol Technology,* 2nd ed., John Wiley and Sons, Inc., New York.

Hounam, R. F. and Sherwood, R. J. (1965). The Cascade Centripeter: A Device for Determining the Concentration and Size Distribution of Aerosols. *Amer. Ind. Hyg. Assoc. J.* 2:122-131.

Jin, S., Sherwood, R. C., Dover, R. B. v., Tiefel, T. H. and D. W. Johnson, Jr. (1987). High T[sub C] Superconductors---Composite Wire Fabrication. *Appl. Phys. Lett.* 51:203-204.

Kesavan, J., Doherty, R. W., Wise, D. G. and McFarland, A. R. (2001). *Factors That Affect Fluorescein Analysis*. Edgewood Chemical Biological Center, U.S. Army Soldier and Biological Chemical Command Edgewood, MD. ECBC-TR-208.

Kim, H. T., Han, Y. T., Kim, Y. J., Lee, K. W. and Chun, K. J. (2002). Design and Test of 2.5 μm Cutoff Size Inlet Based on a Particle Cup Impactor Configuration. *Aerosol Sci. Techol.* 36:136-144.

Kline, S. J. and McClintock, F. A. (1953). Describing Uncertainties in Single-Sample Experiments. *Mechanical Eng.* 75:3-8.

Lee, P., Chen, D.-R. and pui, D. Y. H. (2003). Experimental Study of a Nanoparticle Virtual Impactor. *J. Nanoparticle Res.* 5:269-280.

Lee, S. A. (2001). A Slit Impactor Utilizing a Transpirated Impaction Surface for Collection of Bioaerosols, M.S. Thesis, Department of Mechanical Engineering, Texas A&M University, College Station, TX.

Loo, B. W. and Jaklevic, J. M. (1974). *An Evaluation of the ERC Virtual Impactor*. Lawrence Berkeley Lab Report: LBL - 2468.

Loo, B. W., Adachi, R. S., Cork, C. P., Goulding, F. S., Jaklevic, J. M., Landis, D. A. and Searles, W. L. (1979). *A Second Generation Dichotomous Sampler for Large-Scale Monitoring of Airborne Particulate Matter*. Lawrence Berkeley Lab Report: LBL - 8725.

Loo, B. W. and Cork, C. P. (1988). Development of High efficiency Virtual Impactors. *Aerosol Sci. Techol.* 9:167-176.

Mäkelä, J. M., Keskinen, H., Forsblom, T. and Keskinen, J. (2004). Generation of Metal and Metal Oxide Nanoparticles by Liquid Flame Spray Process. *J. Materials Sci.* 39:2783-2788.

Marple, V. A. (2004). History of Impactors - The first 110 years. *Aerosol Sci. Technol.* 38:247-292.

Marple, V. A. and Chien, C. M. (1980). Virtual Impactors: A Theoretical Study. *Environ. Sci. Techol.* 14:976-985.

McFarland, A. R., Wedding, J. B. and Cermak, J. E. (1977). Wind Tunnel Evaluation of a Modified Andersen Impactor and an All-weather Sampler Inlet. *Atmos. Environ.* 11:535-542.

McFarland, A. R., Ortiz, C. A. and Bertch., R. W. (1978). Particle Collection Characteristics of a Single-Stage Dichotomous Sampler. *Environ. Sci. Techol.* 12:679-682.

McFarland, A. R., Ortiz, C. A. and Rodes, C. E. (1980). Characterization of sampling systems. in *Technical Basis for Size Specific Particulate Standard*, Air Pollution Control Assoc., Pittsburgh, PA.

McFarland, A. R., Ortiz, C. A. and Russel W. Bertch, J. (1984). A 10 μm Cutpoint Size Selective Inlet for Hi-Vol Samplers. *J. Air Pollut. Control Assoc.* 34:544-547.

Masuda, H. (1979). An Improved Virtual Impactor for Particle Classification and Generation of Test Aerosols with Narrow Size Distributions. *J. Aerosol Sci.* 10:275-287.

Nene, R. R. (2006). Design of Bioaerosol Sampling Inlets, M.S. Thesis, Department of Mechanical Engineering, Texas A&M University, College Station, TX.

Olan-Figueroa, E., McFarland, A. R. and Ortiz, C. A. (1982). Flattening Coefficients for DOP and Oleic Acid Droplets Deposited on Treated Glass Slides. *Amer. Ind. Hyg. Assoc. J.* 43:628-639.

Patton, J. S. and Byron, P. R. (2007). Inhaling Medicines: Delivering Drugs to the Body Through the Lungs. *Nat. Rev. Drug. Discov.* 6:67-74.

Peterson, C. M. (1975). Aerosol Concentrator and Classifier. U. S. Patent 3,901,798, filed November 21, 1973, and issued August 26, 1975

Purdue, L. J. (1988). EPA PM-10 Methodology Requirements, in *PM-10: Implementation of Standards*, C. V. Mathai and D. H. Stonefield, eds., Air Pollution Control Assoc., Pittsburgh, PA.

Ravenhall, D. G., Forney, L. J. and Hubbard, A. L. (1982). Theory and Observation of a Two-Dimensional Virtual Impactor. *J. Colloidal Intetrface Sci.* 85:508-520.

Ravenhall, D. G., Forney, L. J. and Jazayeri, M. (1978). Aerosol Sizing with a Slotted Virtual Impactor. *J. Colloidal Intetrface Sci.* 65:108-117.

Robson, C. D. and Foster, K. E. (1962). Evaluation of Air Particulate Sampling Equipment. *Amer. Ind. Hyg. Assoc. J.* 23:404-411.

Romay, F. J., Roberts, D. L., Marple, V. A., Liu, B. Y. H. and Olson, B. (2002). A High Performance Aerosol Concentrator for Bioaerosol Agent Detection. *Aerosol Sci. Tech* 36:217-226.

Seshadri, S., Phares, D. J., Kim, T., Kihm, K. D., Smith, D. D. and McIntyre, P. M. (2005). Performance of a Slit Virtual Impactor Operated at High Particle Mass Loading. *J. Aerosol Sci.* 36:541-547.

Sioutas, C., Koutrakis, P. and Burton, R. M. (1994). Development of a Low Cutpoint Slit Virtual Impactor for Sampling Ambient Fine Particles. *J. Aerosol Sci.* 25:1321-1330.

Stahlhofen, W. (1980). Experimental-Determination of the Regional Deposition of Aerosol-Particles in the Human Respiratory-Tract. *Amer. Ind. Hyg. Assoc. J.* 41:385-398.

Thien, B. F. (2006). Flattening Factors for Oleic Acid Droplets Impacted on a Glass Slide, Personal communications. Aerosol Technology Laboratory, Department of Mechanical Engineering, Texas A&M University, College Station, TX.

Tsuda, A., Butler, J. P. and Fredberg, J. J. (1994). Effects of Alveolated Duct Structure on Aerosol Kinetics. 2. Gravitational Sedimentation and Inertial Impaction. *J. Applied Physiology* 76:2510-2516.

U.S. EPA Federal Register (1987a). Reference Method for Determination of Particle Matter as PM-10 in the Atmosphere. 40 CFR Part 50. *Federal Register* 52:24664.

U.S. EPA Federal Register (1987b). Revisions to the National Ambient Air Quality Standards for Particulate Matter, 40 CFR Part 50. *Federal Register* 52:24634.

Wedding, J. B., McFarland, A. R. and Cermak, J. E. (1977). Large Particle Collection Characteristics of Ambient Aerosol Samplers. *Environ. Sci. Techol.* 11:387-390.

Wedding, J. B. and Weigand, M. A. (1985). The Wedding Ambient Aerosol Sampling Inlet (D_{50} = 10 μm) for the High-Volume Sampler. *Atmos. Environ.* 19:535-538.

Willeke, K., Lo, C. S. K. and Whitby, K. T. (1974). Dispersion Characteristics of a Fluidized Bed. *J. Aerosol Sci.* 5:449-455.

APPENDIX A

TABLES AND FIGURES

Table 3.1. Error in assumed value of C_c for various particle sizes

Particle Size (AD) µm	C_c		Error %
	Calculated	Assumed	
3	1.04602	1	4.40
5	1.02761	1	2.69
7	1.01972	1	1.93
10	1.01381	1	1.36
12	1.01151	1	1.14
15	1.00920	1	0.91
20	1.00690	1	0.69

Table 5.1. BSI-IVI inlet performance characteristics

	100 L/min	300 L/min	400 L/min
Cutpoint (μm)	11	11	10
Throat Width (W) inches	0.10	0.18	0.18
S/W	1.75	2.00	2.00

Table 6.1. Separation threshold requirements for various sample powders

No.	Material	Vendor	Specific Gravity	50% Cutpoint, µm physical size	50% Cutpoint, µm AD	90% Threshold, µm physical size	90% Threshold, µm AD
1	MgH_2	Ohio State	1.74	1.94	2.55	**5.00**	**6.59**
1a	MgH_2	Ohio State	1.74	3.87	5.11	**10.00**	**13.18**
2	MgB_2	U. Wisc	1.00	0.47	0.47	**1**	**1**
3	Mg	Hypertech Research	1.74	1.94	2.55	**5.00**	**6.59**
4	Sn	Supra-magnetics	7.28	0.85	2.30	**2.20**	**5.94**
5	Cu_5Sn_4	Supra-magnetics	8.93	0.85	2.55	**2.20**	**6.57**

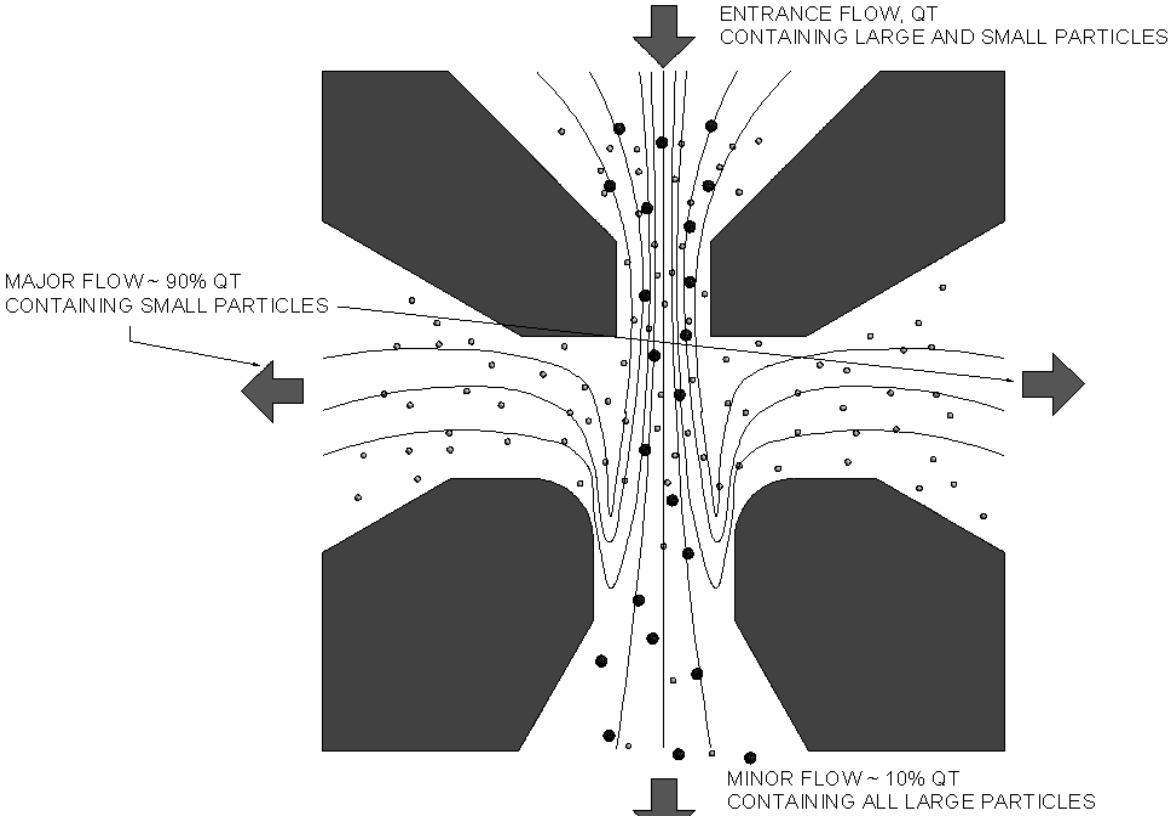

Figure1.1. Schematic of particle separation in a virtual impactor

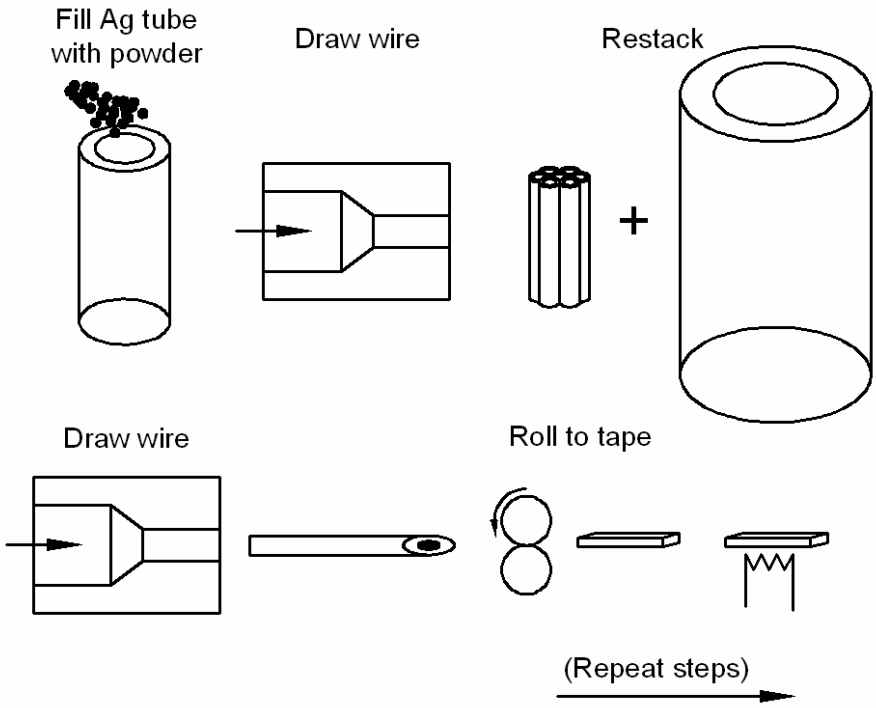

Figure 1.2. PIT fabrication of Bi-2223 tapes and wires

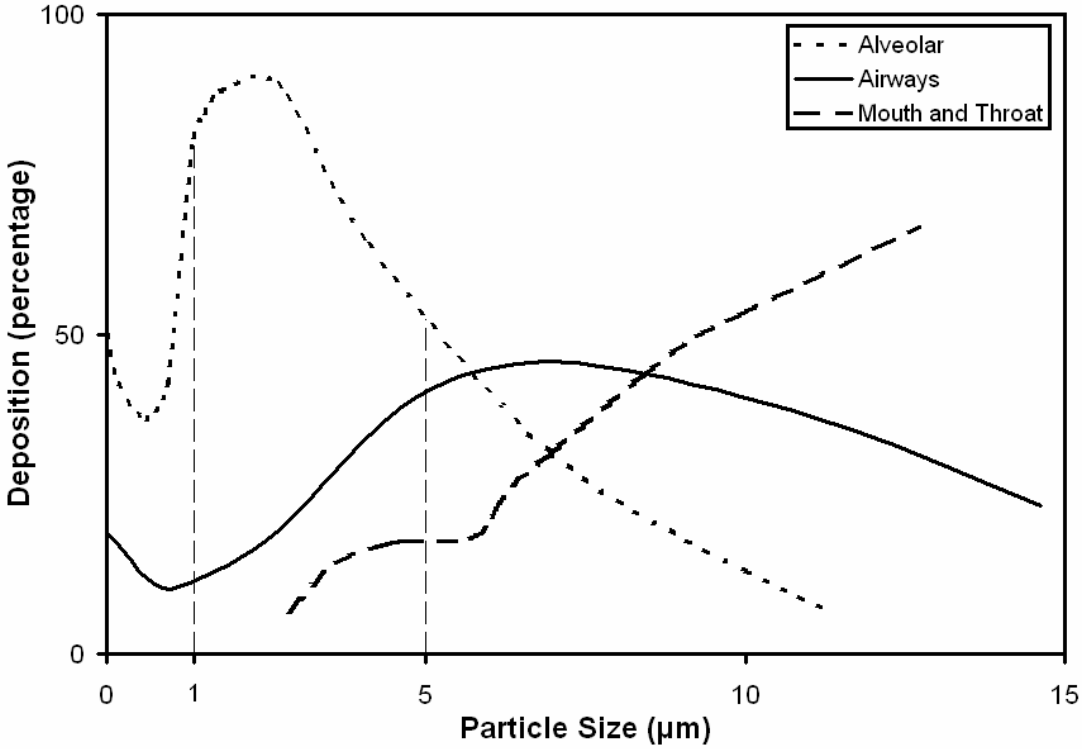

Figure 1.3. Effect of particle size on the deposition of aerosol particles in the human respiratory tract (Patton and Byron, 2007)

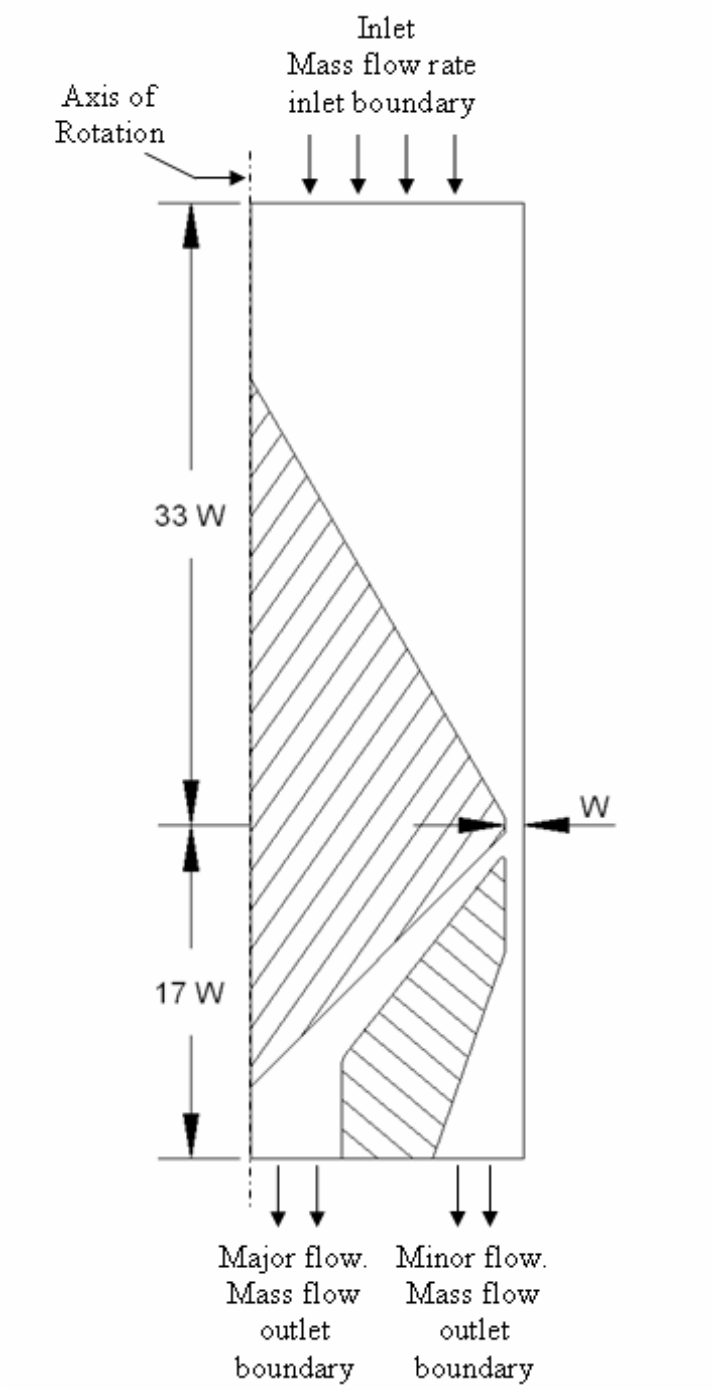

Figure 2.1. Schematic of the 2D domain used in numerical simulations

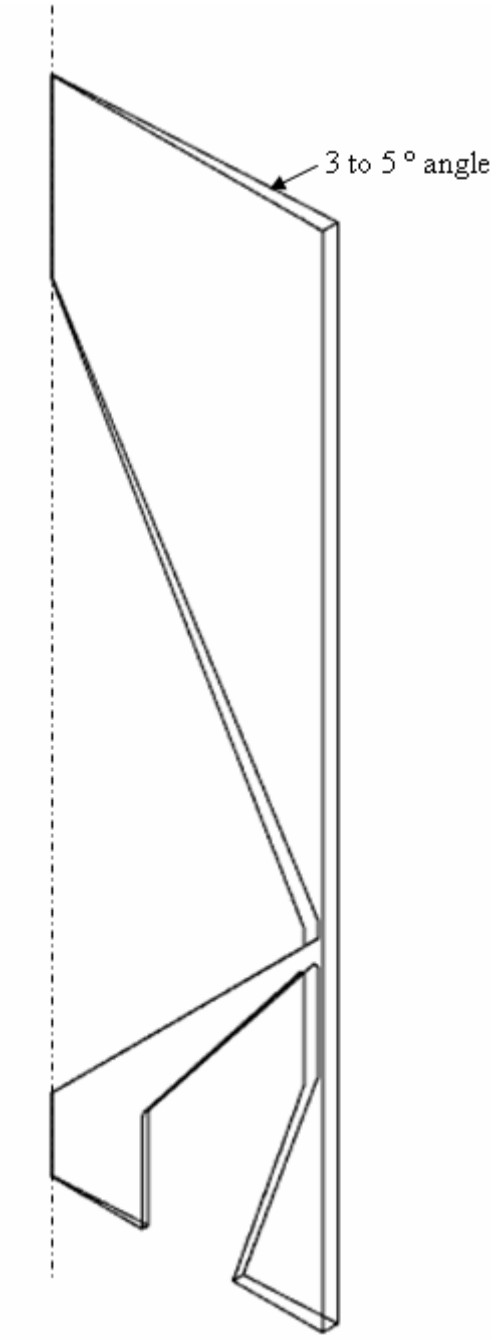

Figure 2.2. Two dimensional domain used for axi-symmetric simulations in CFX

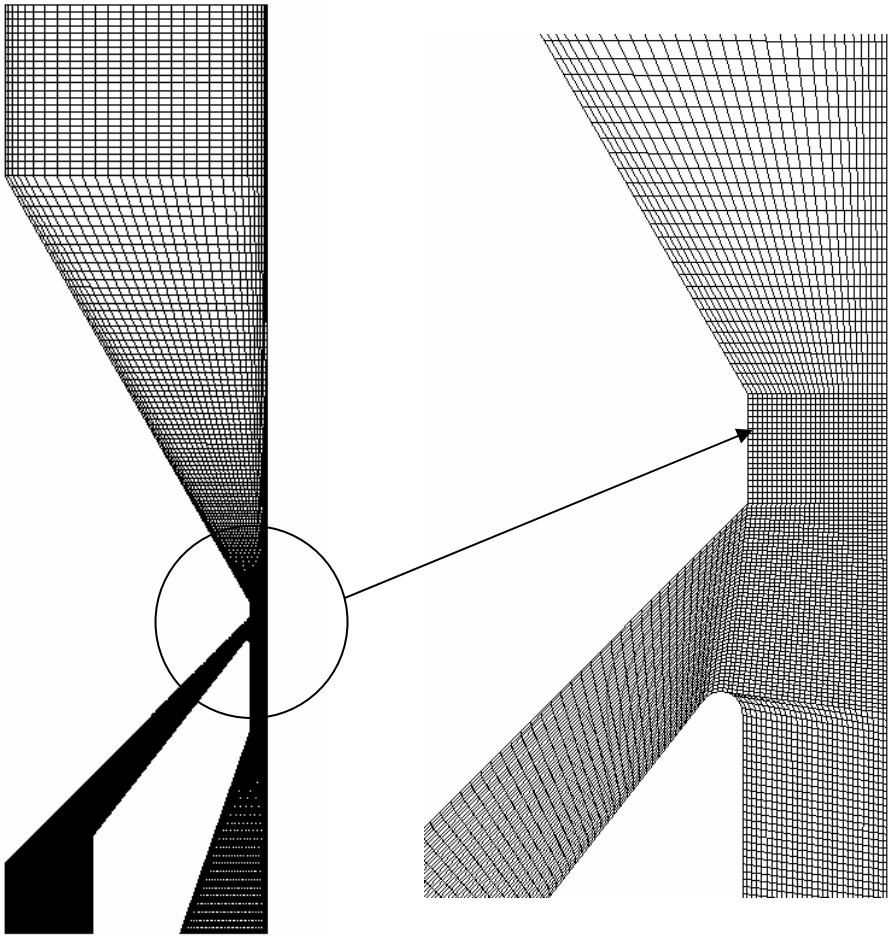

Figure 2.3. Computational mesh used in 2D simulations

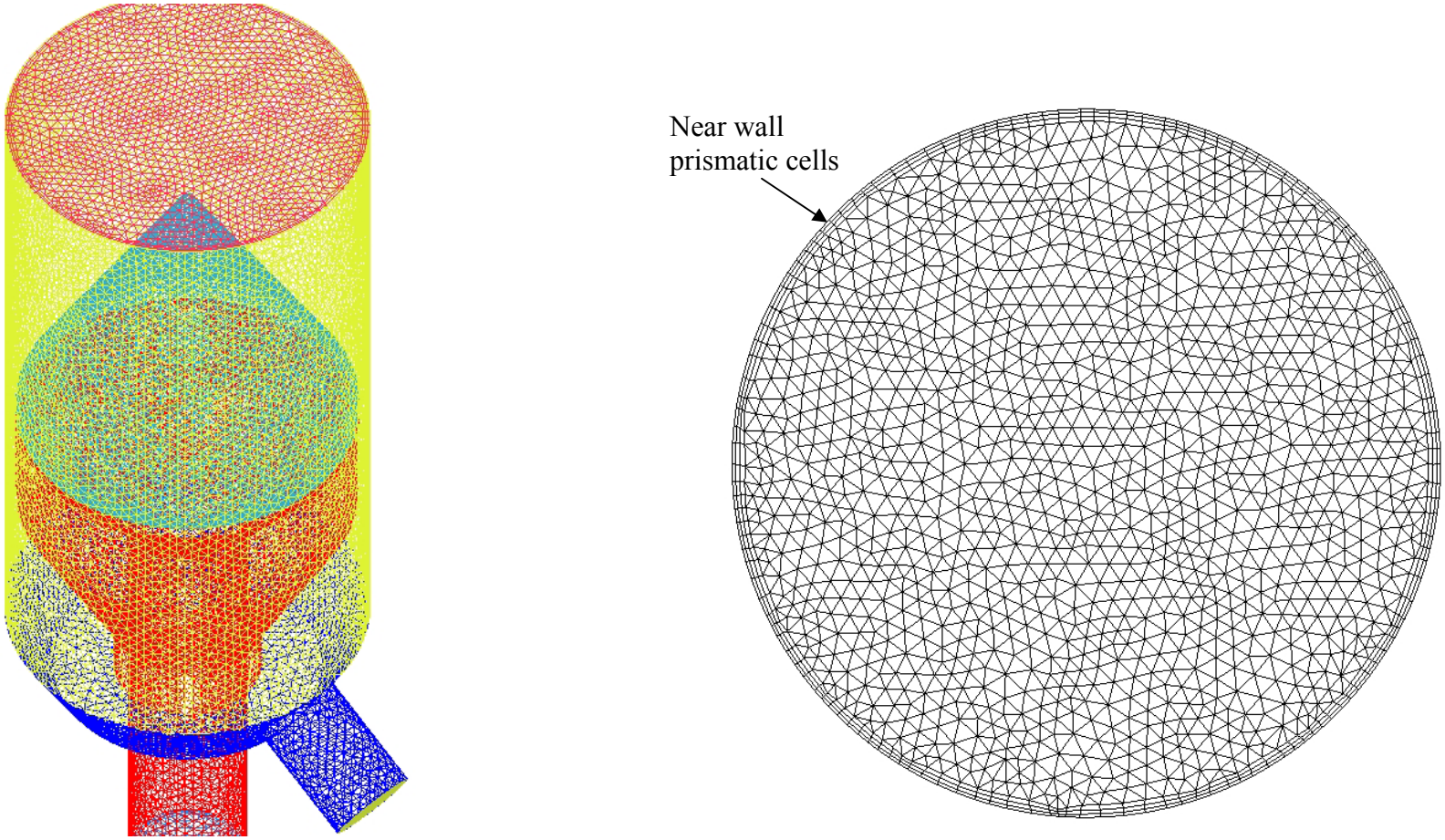

(a) (b)

Figure 2.4. (a) Hybrid tetrahedral and prismatic element mesh on a 3D model of the IVI-100 prototype (b) Prismatic elements

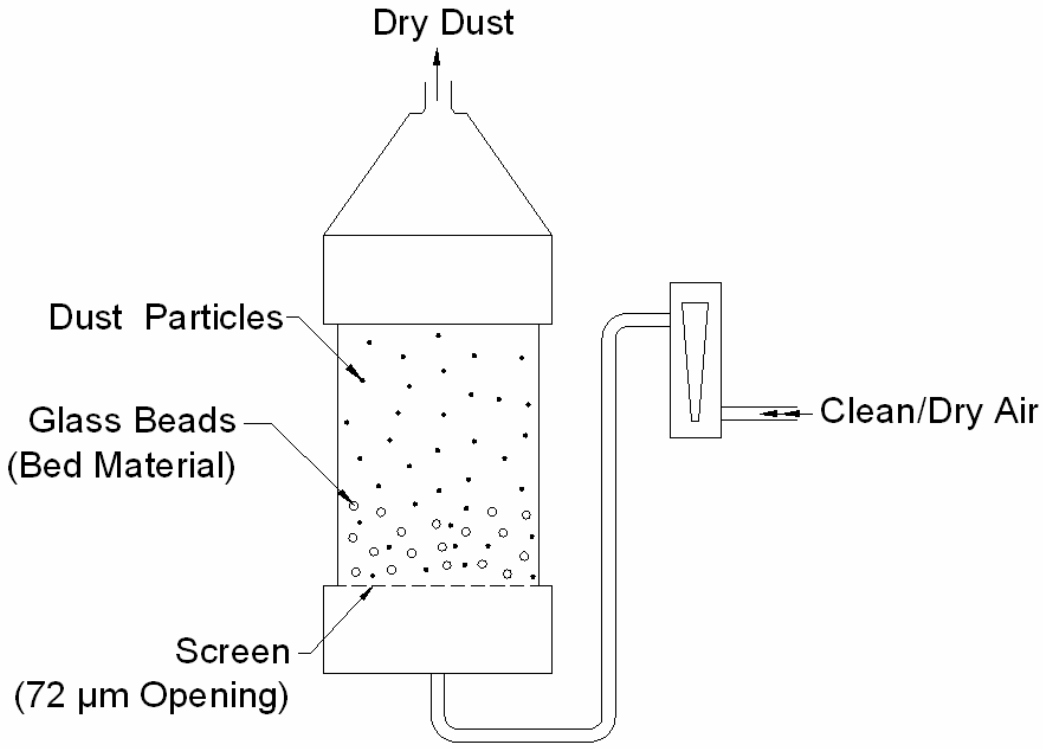

Figure 3.1. Schematic of the fluidized bed arrangement for dispersion of dry dust

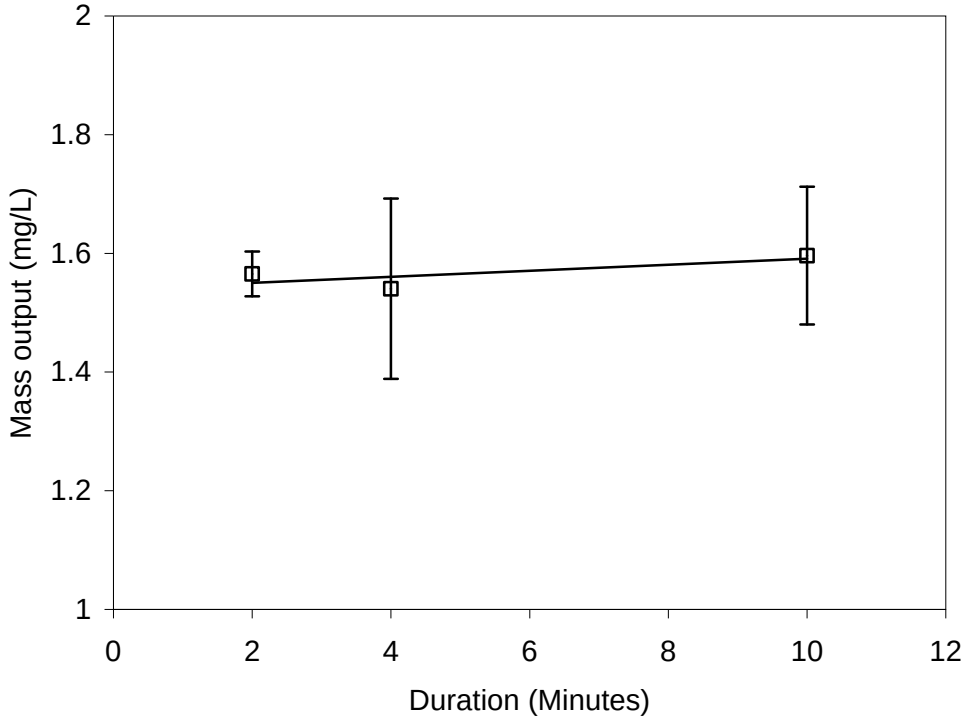

Figure 3.2. ARD mass output from the fluidized bed

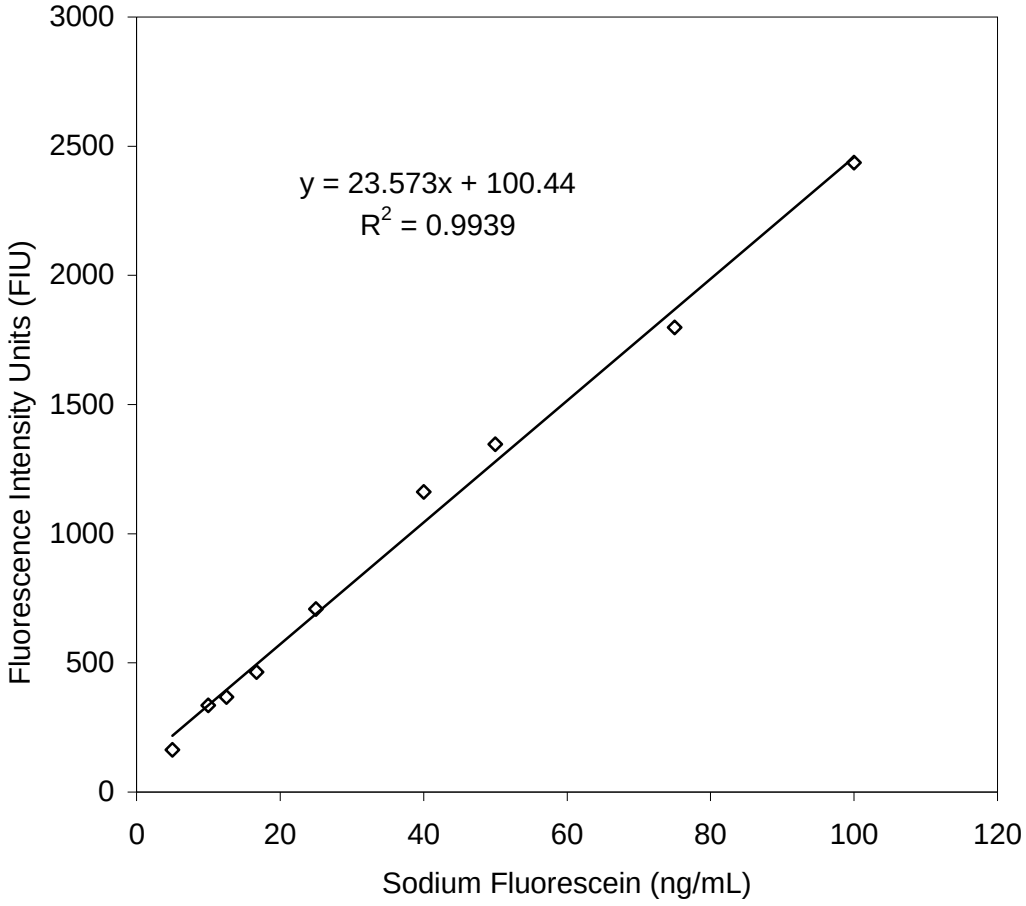

Figure 3.3. Calibration curve for the fluorometer (Gain = 13)

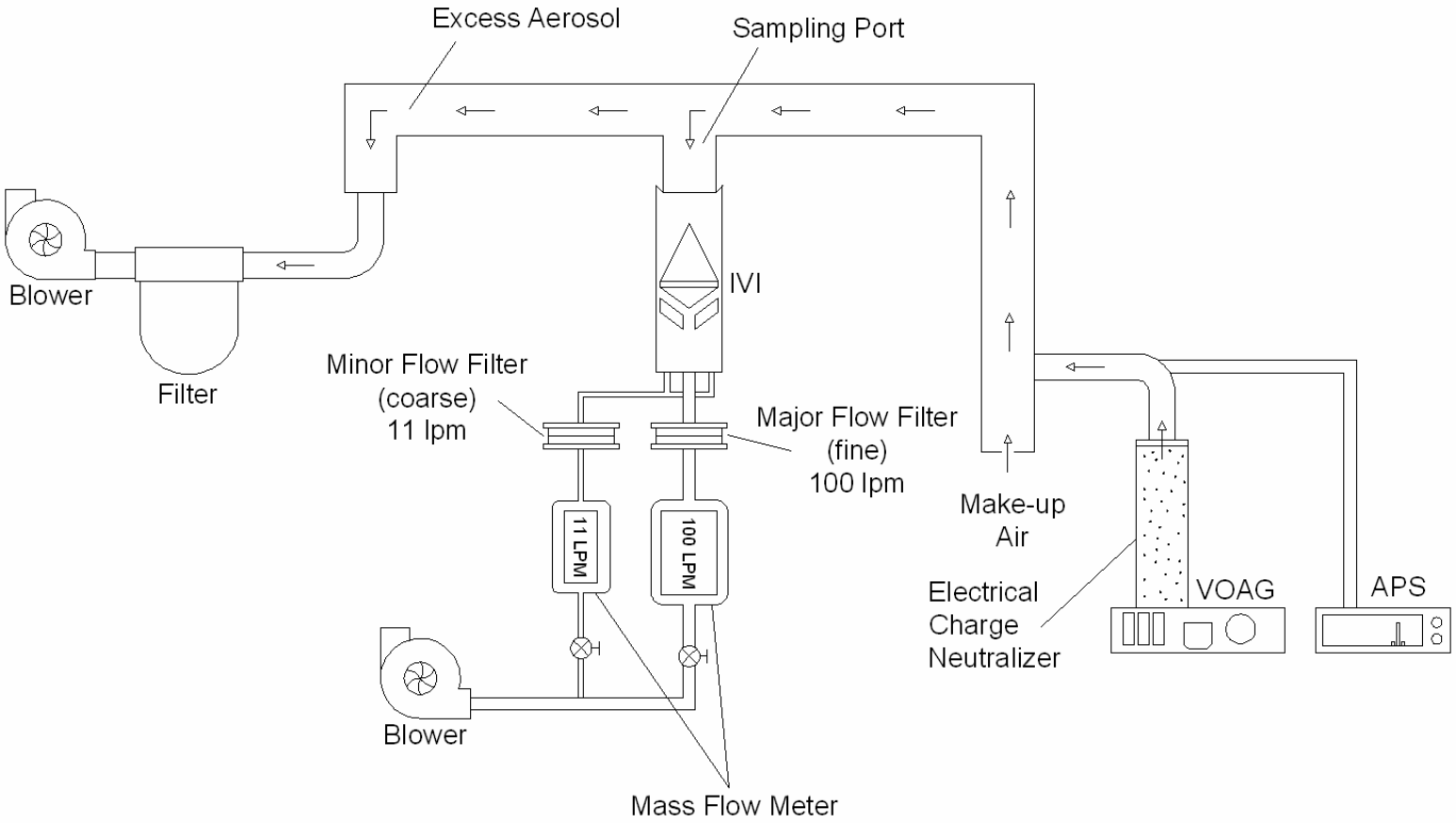

Figure 3.4. Schematic of the bench-top/standalone testing arrangement

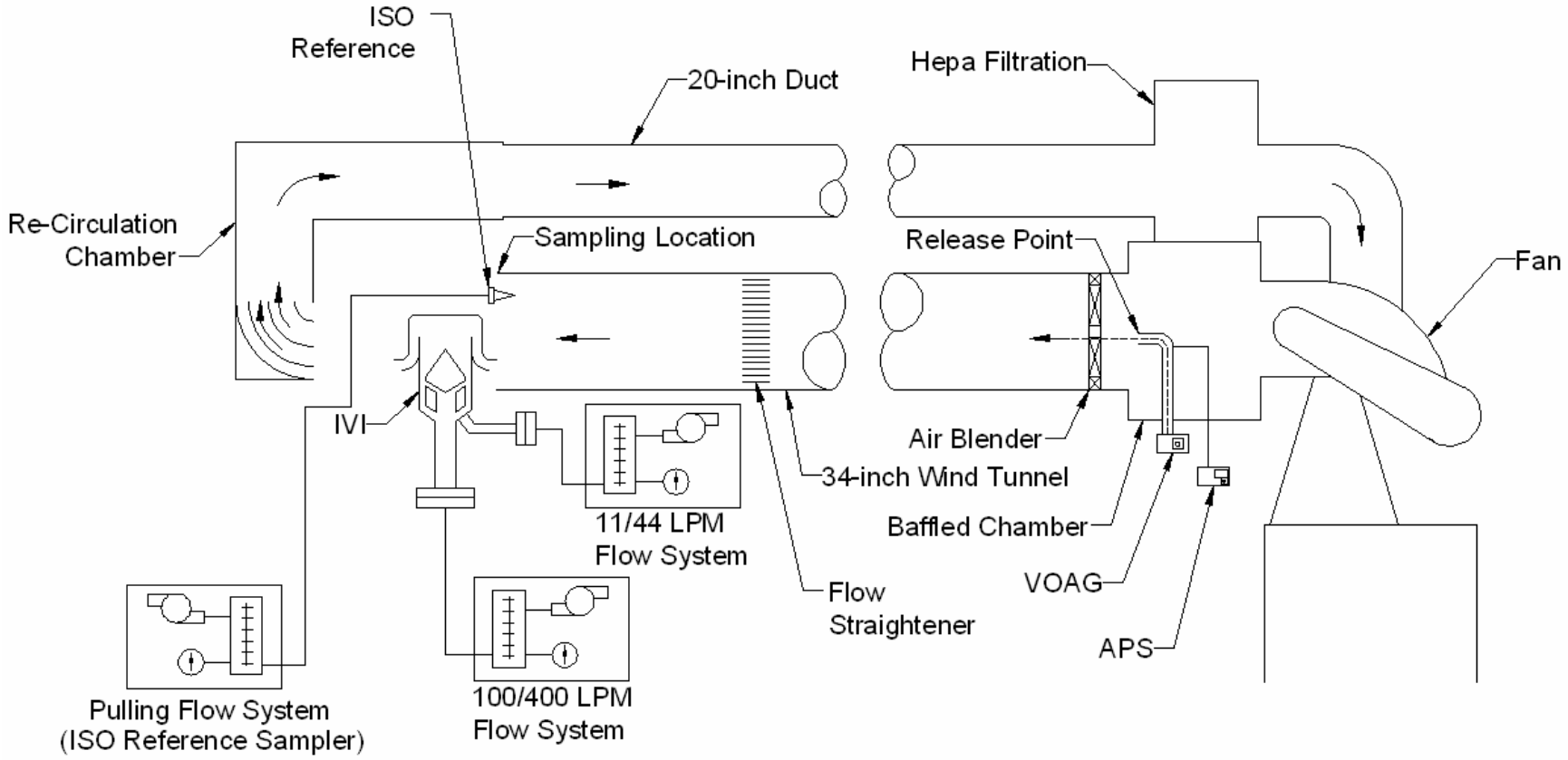

Figure 3.5. Schematic of the wind tunnel testing arrangement

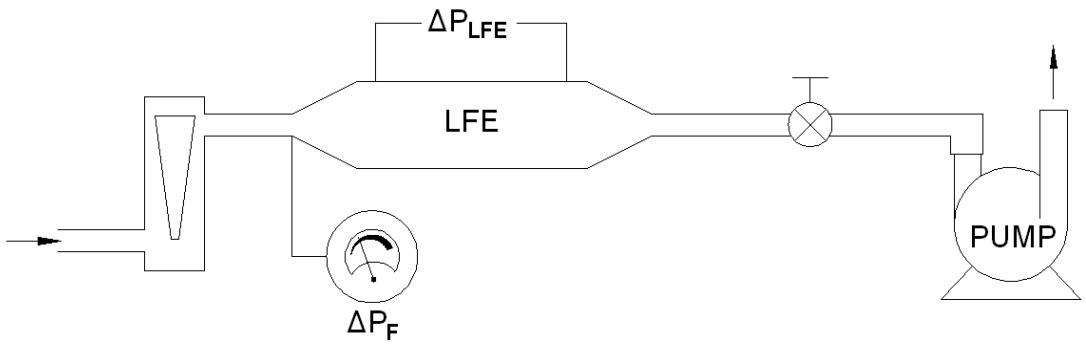

Figure 3.6. Schematic of arrangement used for calibration of the rotameters

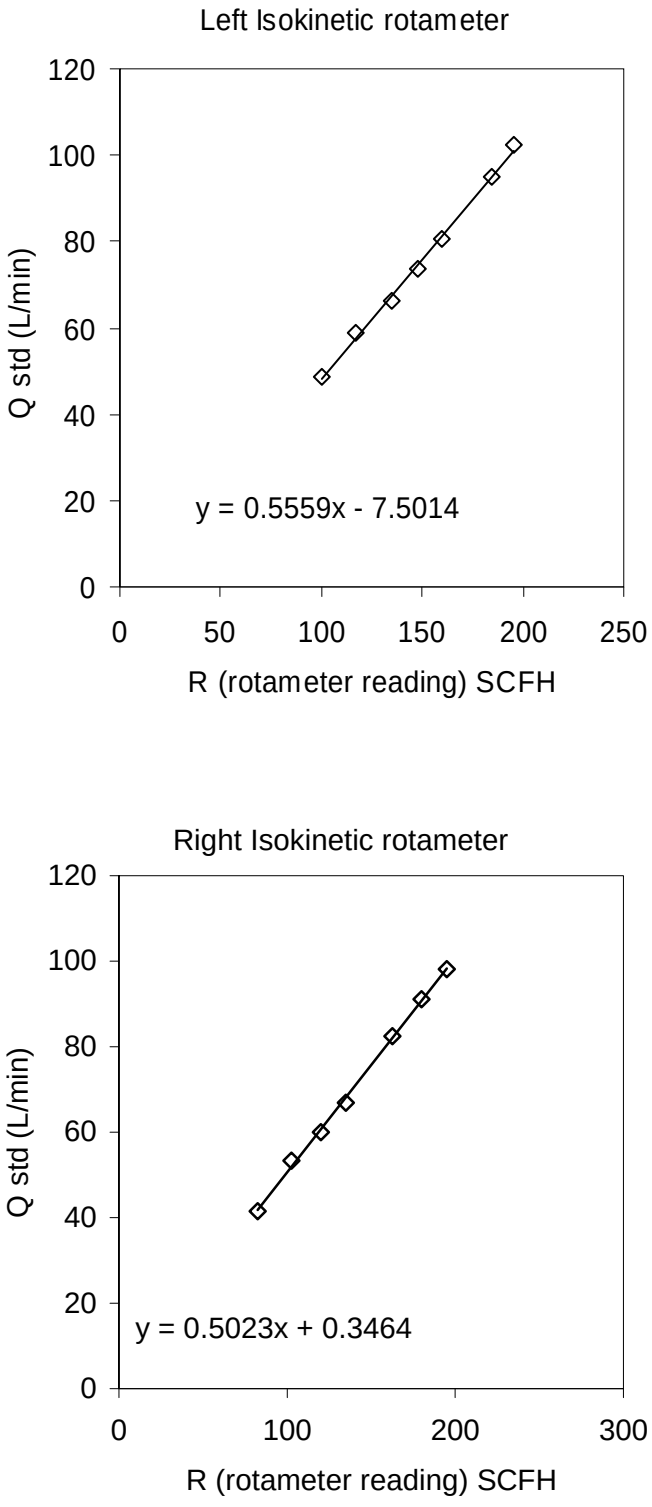

Figure 3.7. Rotameter calibration plots

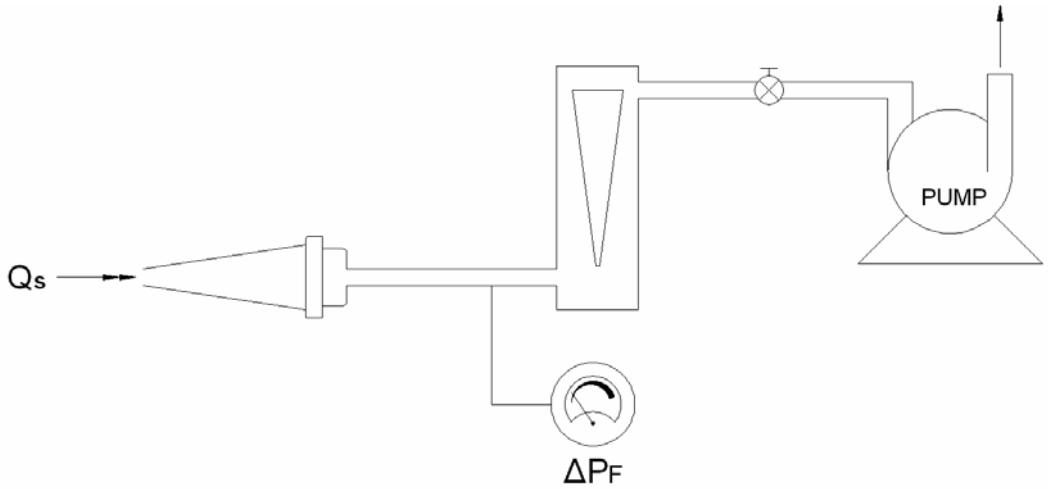

Figure 3.8. Schematic of the flow system controlling the flow through the isokinetic nozzles

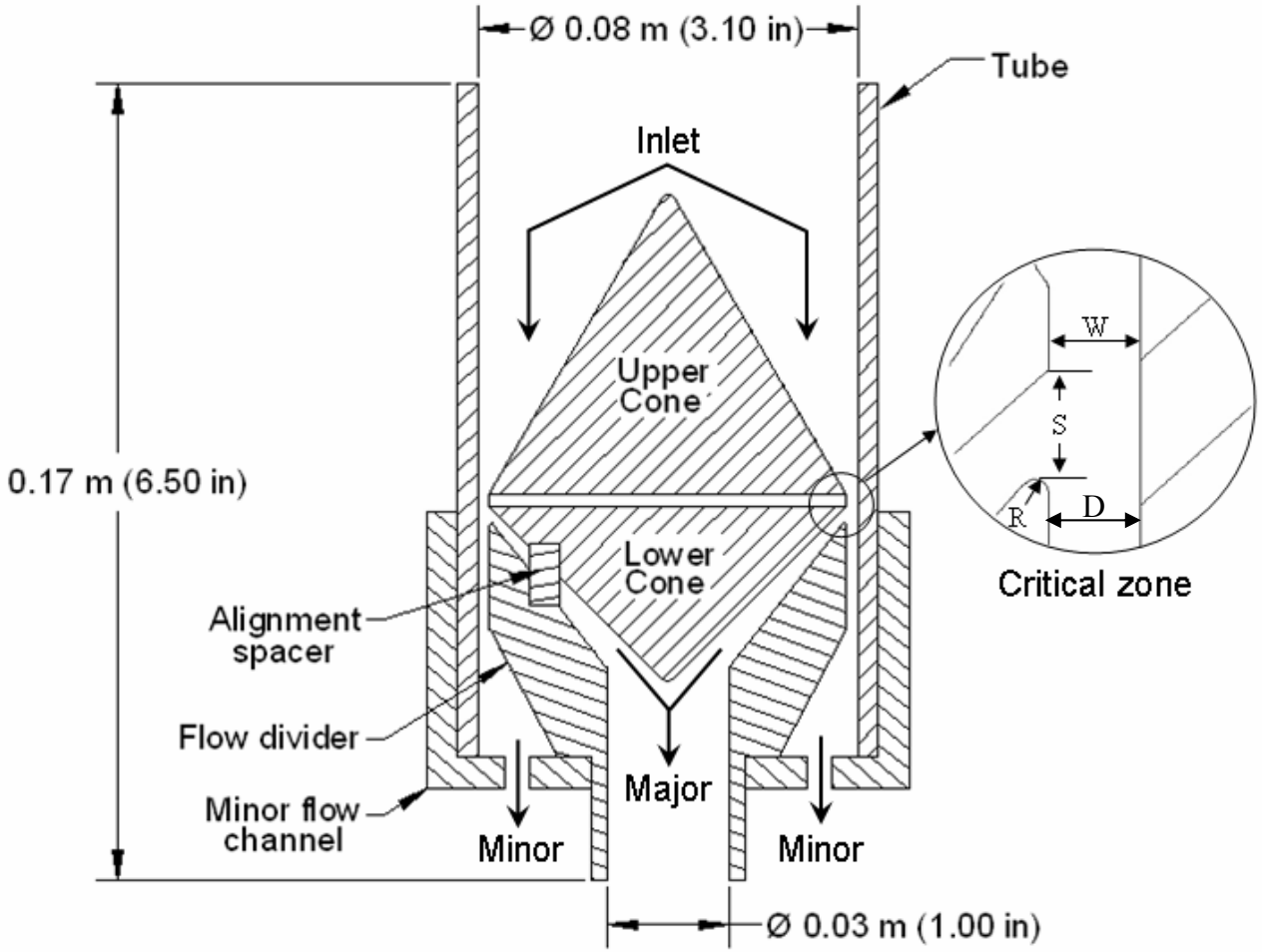

Figure 4.1. Schematic of the in-line virtual impactor prototype

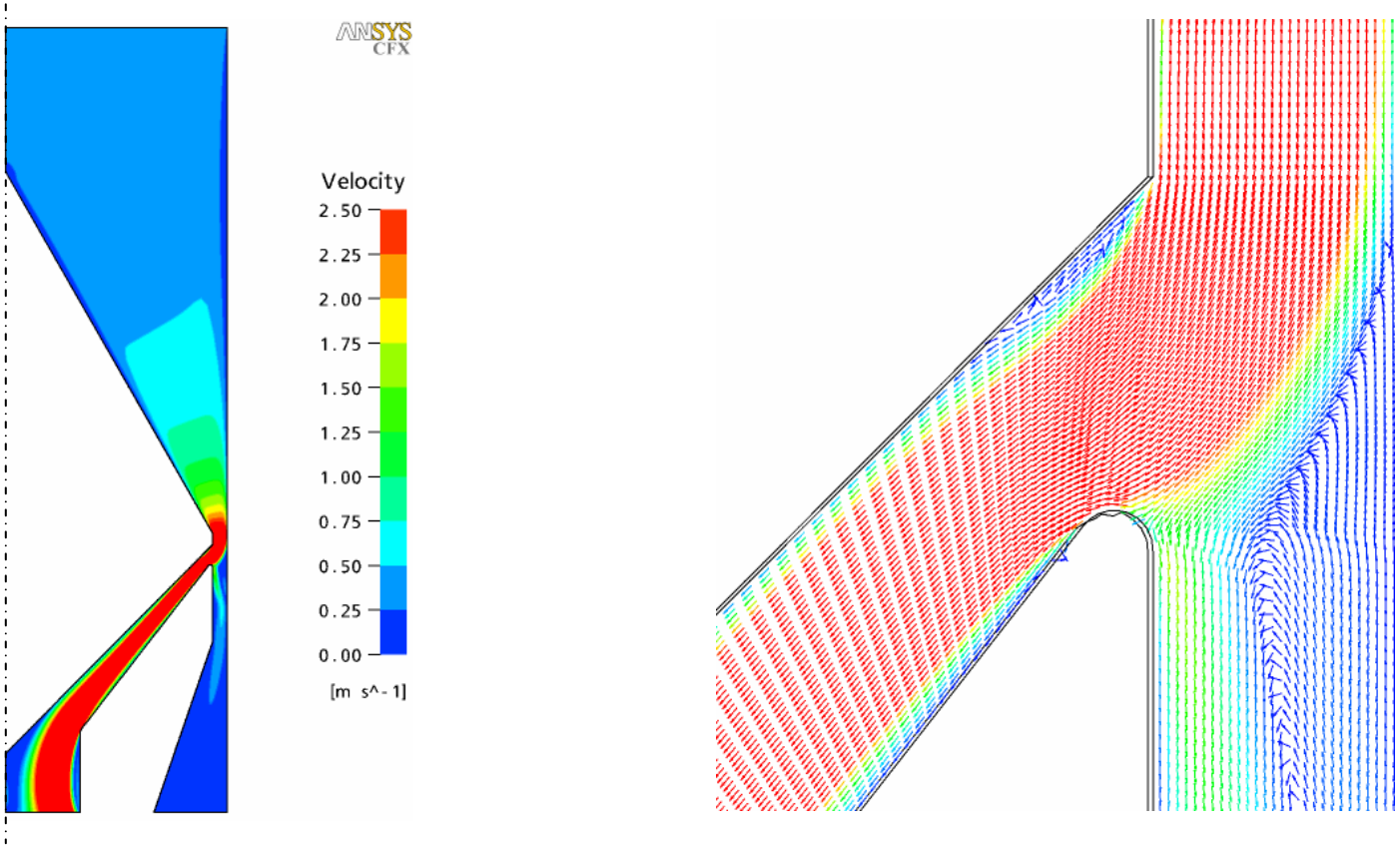

(a) (b)

Figure 4.2. (a) Velocity contours in the flow field (b) velocity vectors in the critical zone

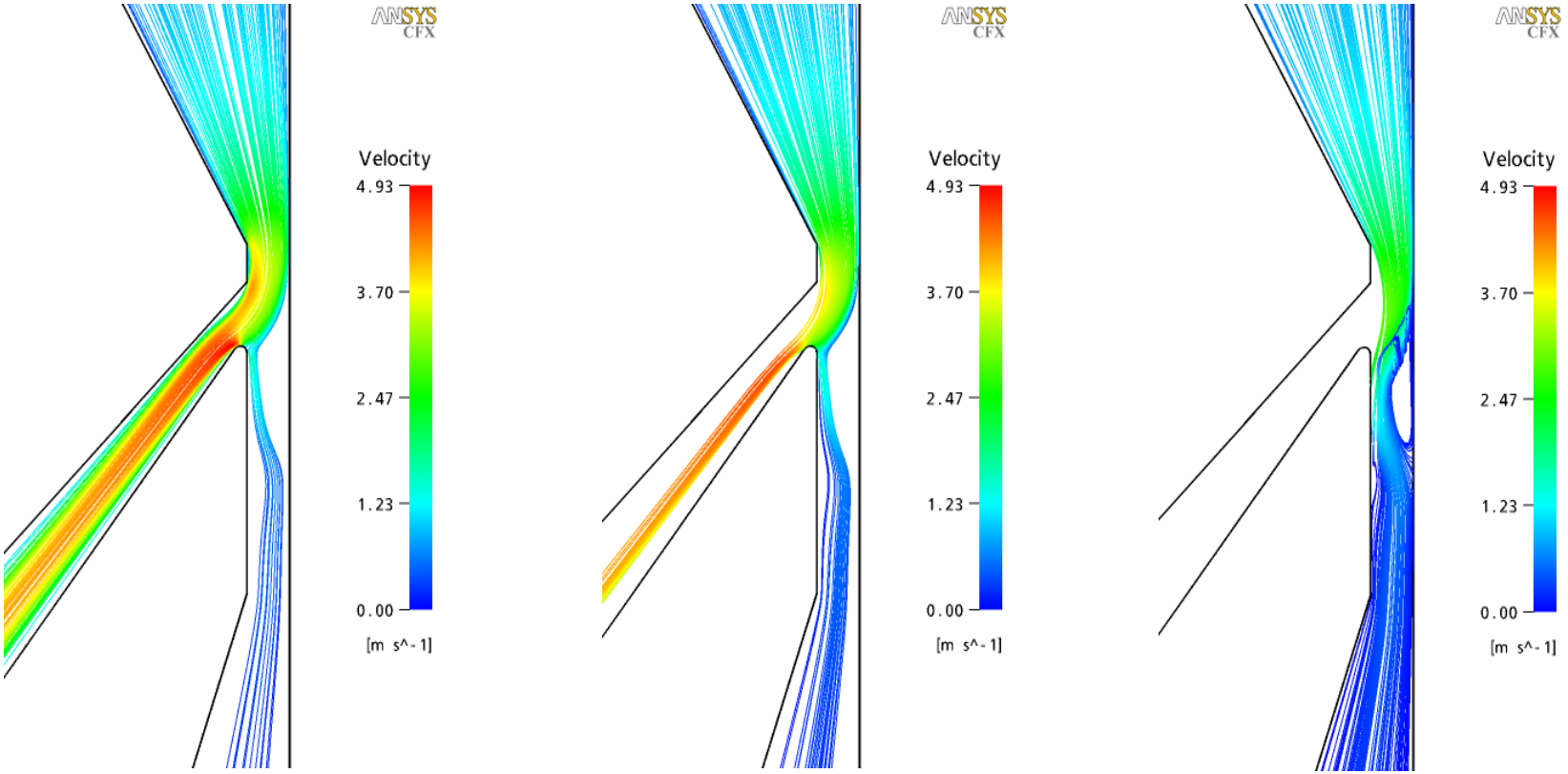

(a) (b) (c)

Figure 4.3. Aerosol particle trajectories with color coding to show local velocities. (a) 1 µm particles (b) 10 µm particles (c) 25 µm particles

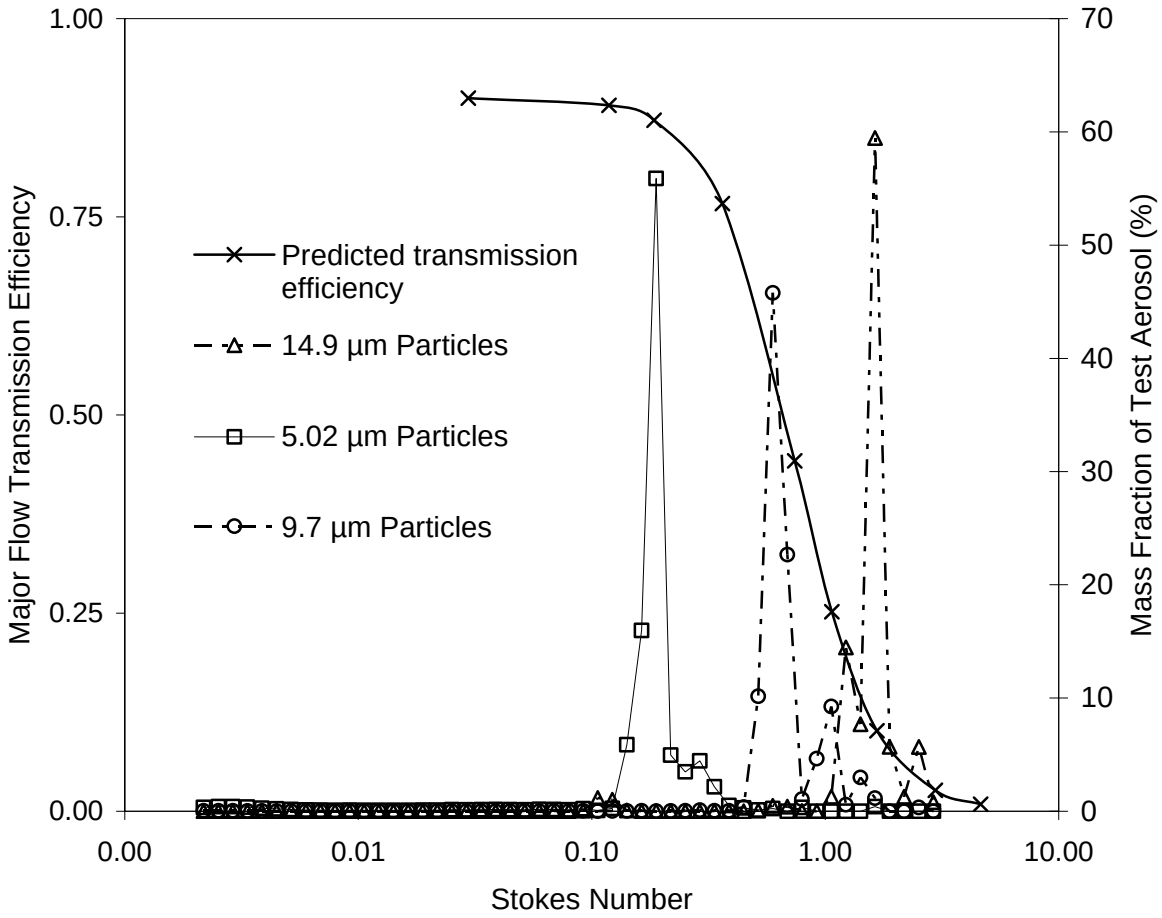

Figure 4.4. Predicted transmission efficiency curve with the size distribution of test aerosols superimposed

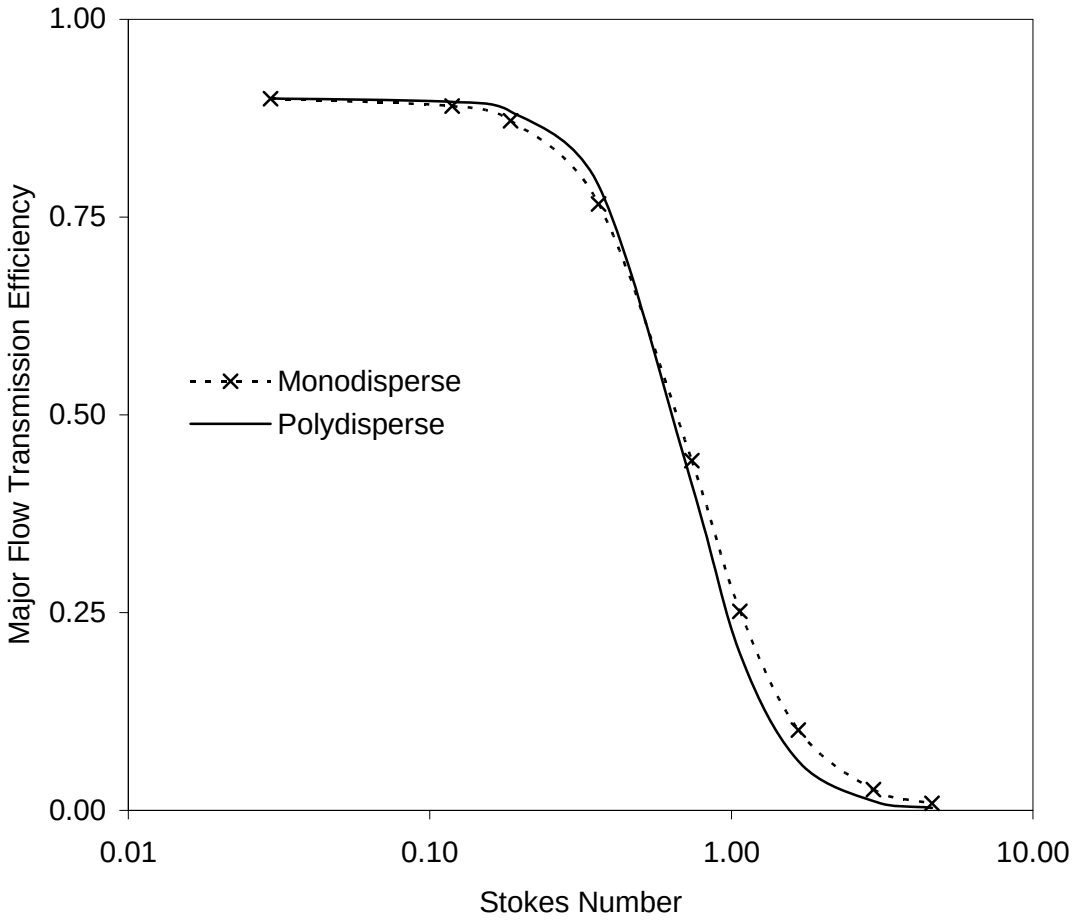

Figure 4.5. Comparison between the predicted transmission efficiency curves based on monodisperse and polydisperse nature of test particles

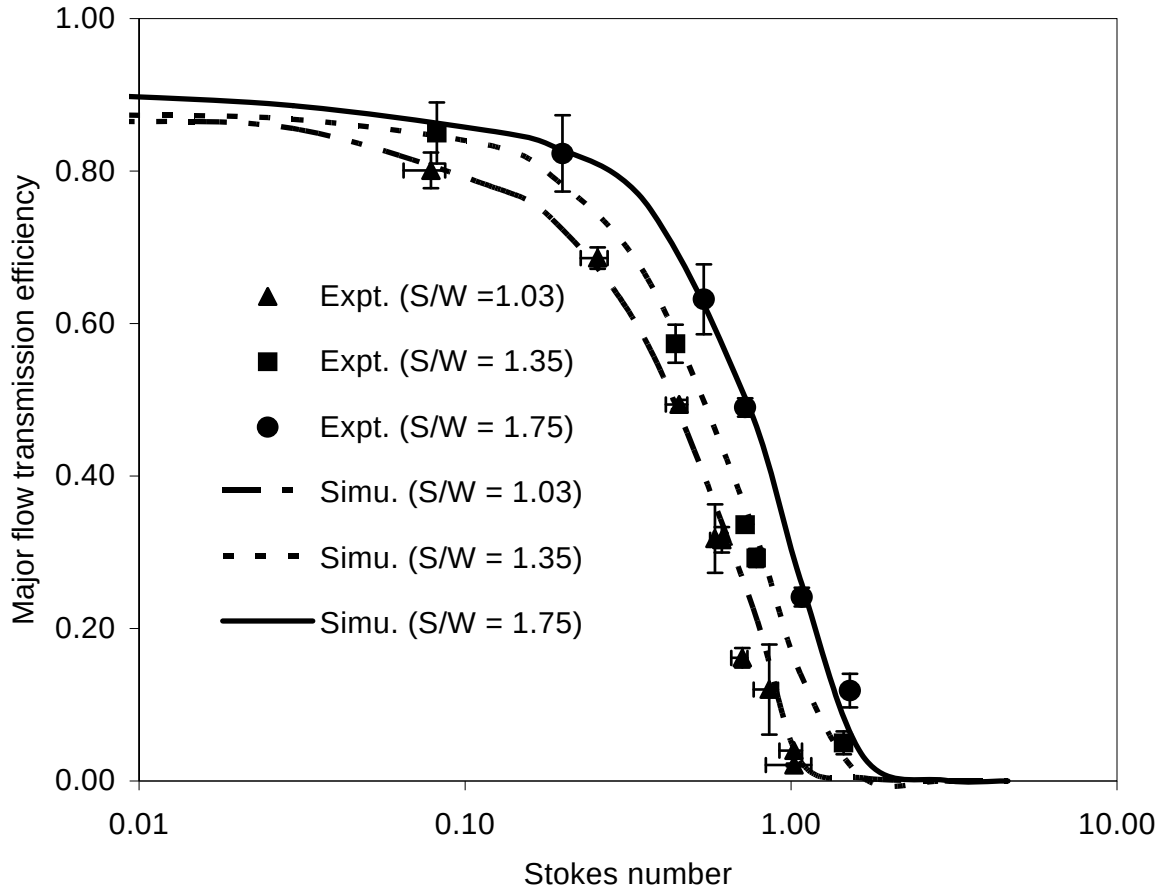

Figure 4.6. Major-flow transmission efficiency of IVI as a function of Stokes number

Note: Effect of aspect ratio is shown for *S/W* values of 1.03, 1.35 and 1.75. Error bars on experimental results are ± 1 standard deviation about the mean value

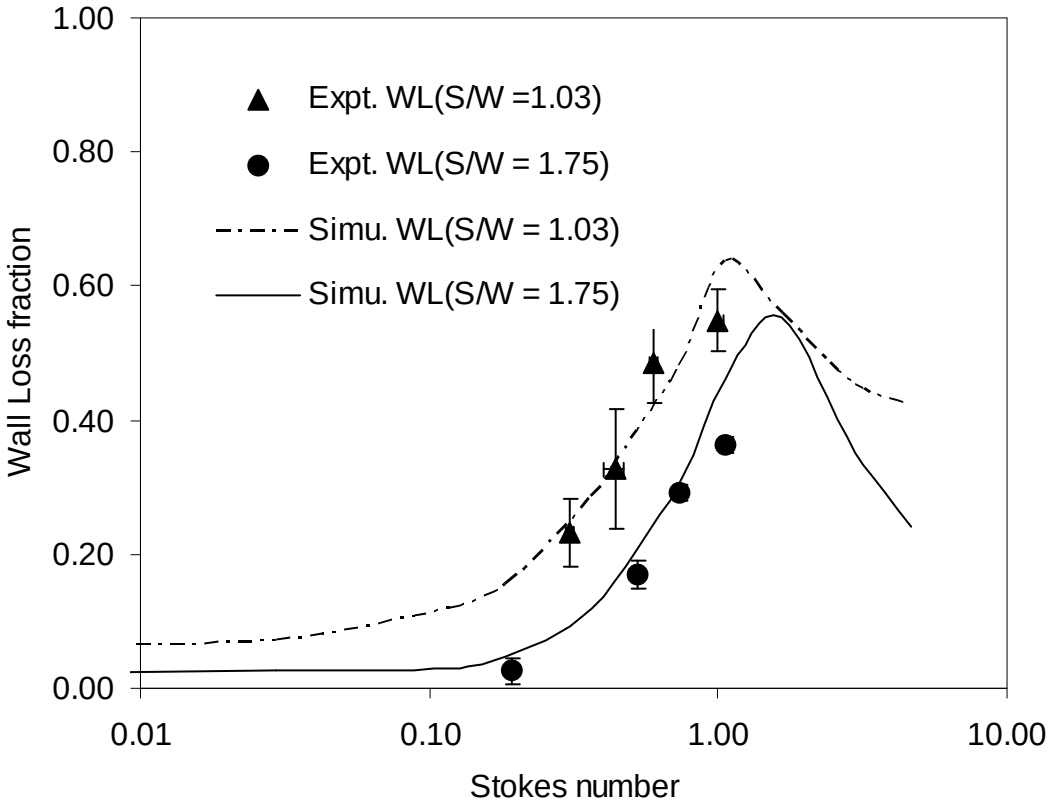

Figure 4.7. Internal wall loss characteristics of the IVI

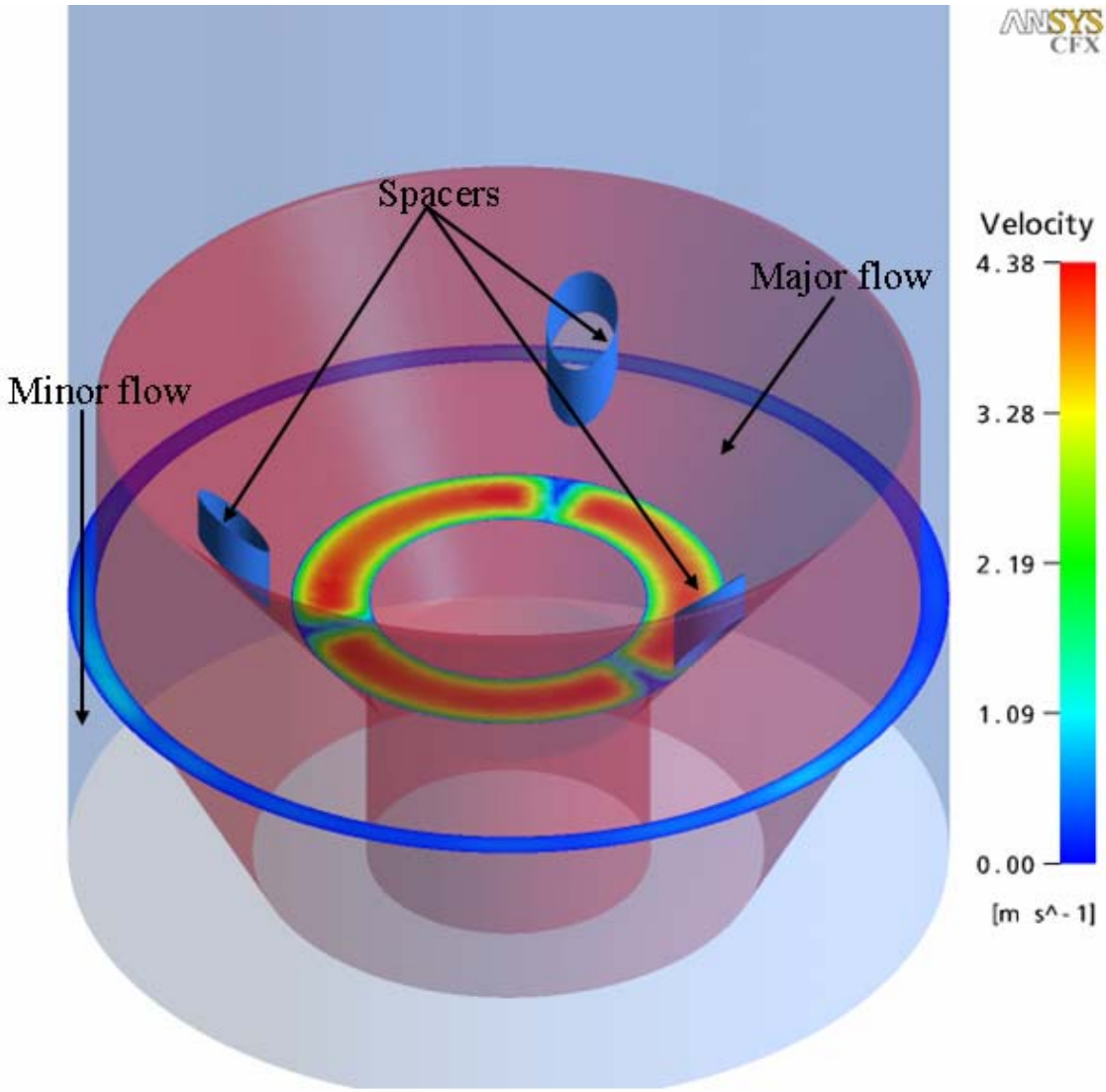

Figure 4.8. Three dimensional view showing velocity contours downstream of the alignment spacers

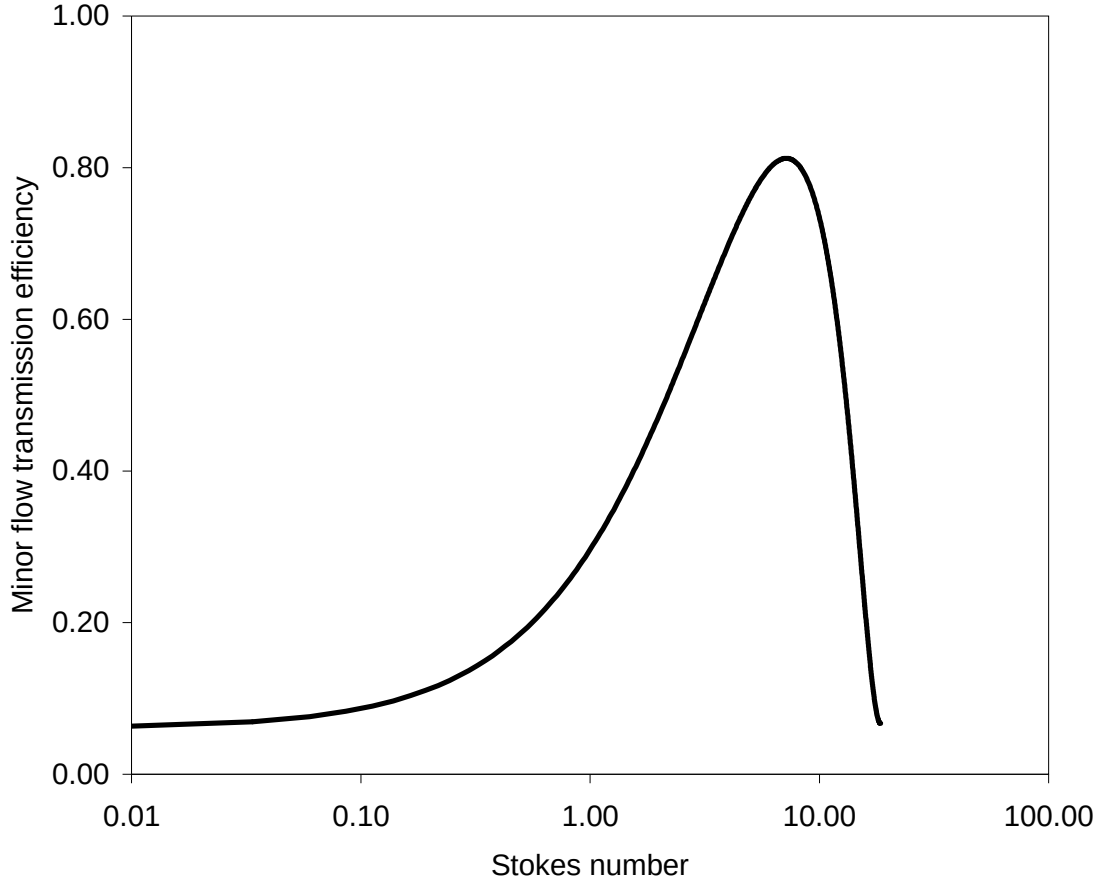

Figure 4.9. Minor flow transmission efficiency characteristics of the IVI

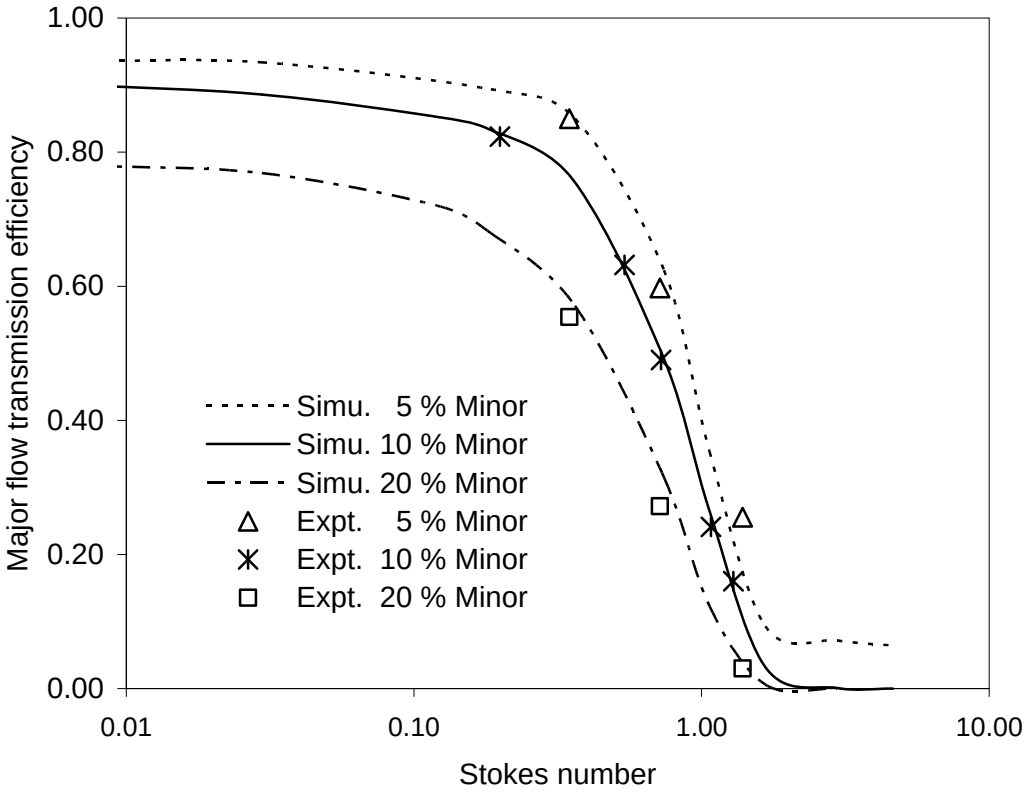

Figure 4.10. Major flow transmission efficiency as a function of Stokes number for different minor flow ratios

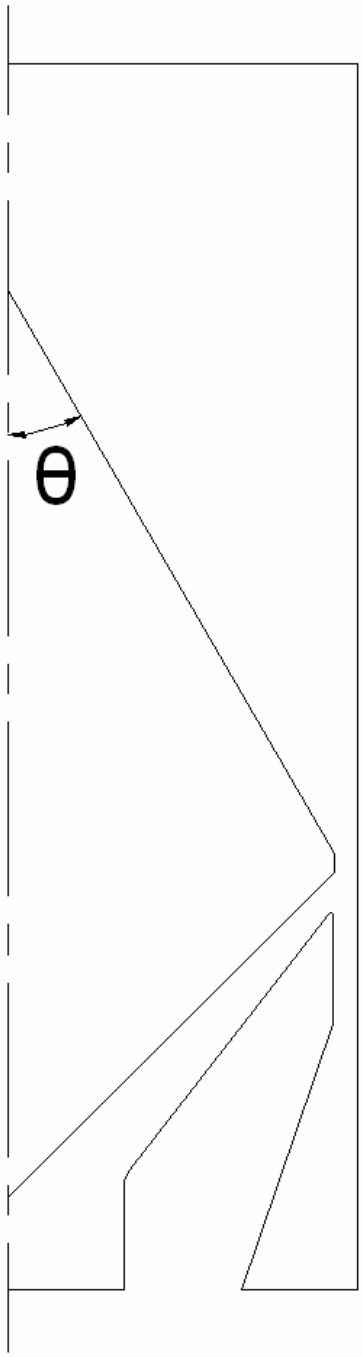

Figure 4.11. 2D domain that was evaluated for θ = 30, 45 and 60 degrees

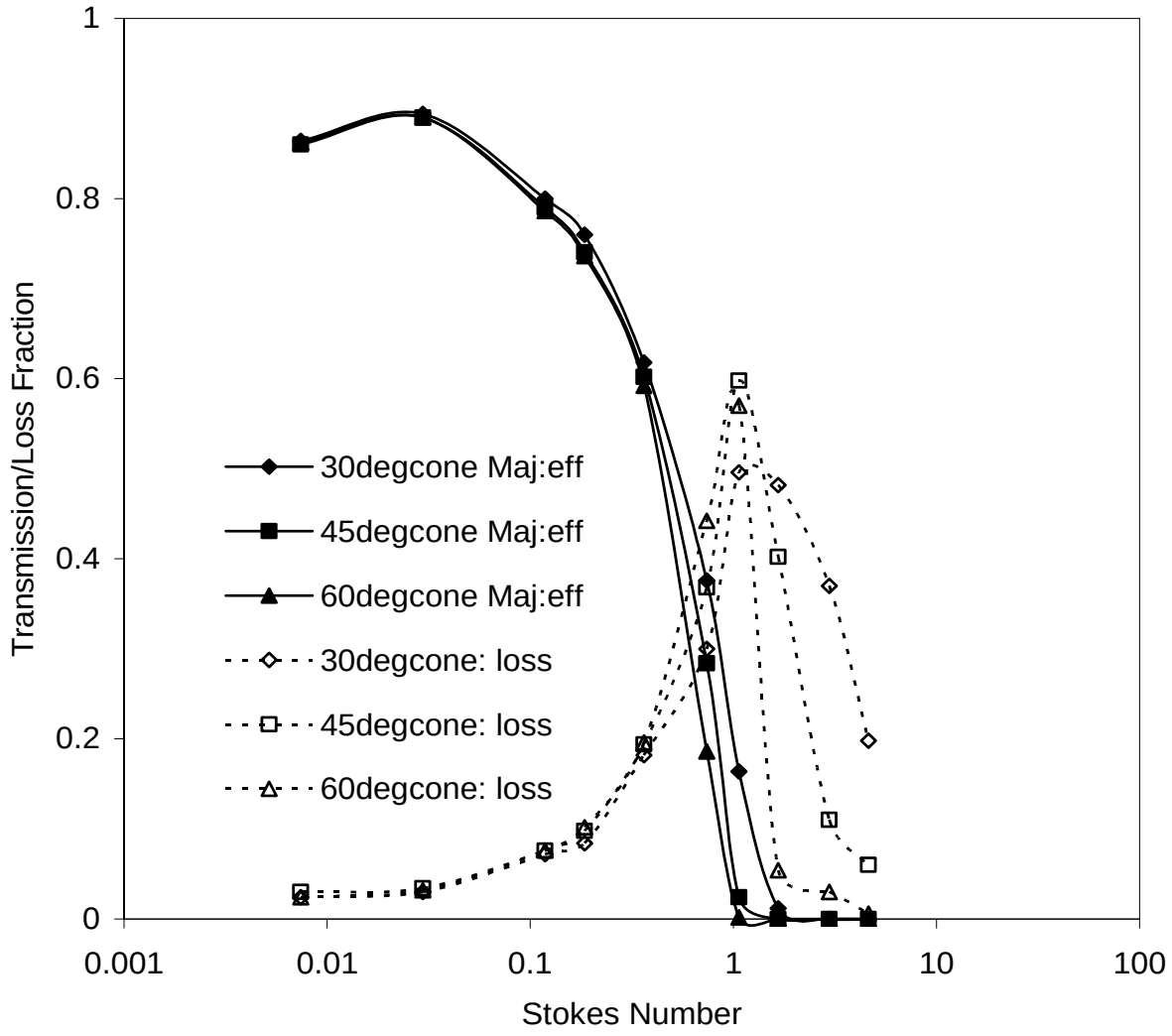

Figure 4.12. Major flow transmission efficiency and wall loss characteristics for different cone half angles

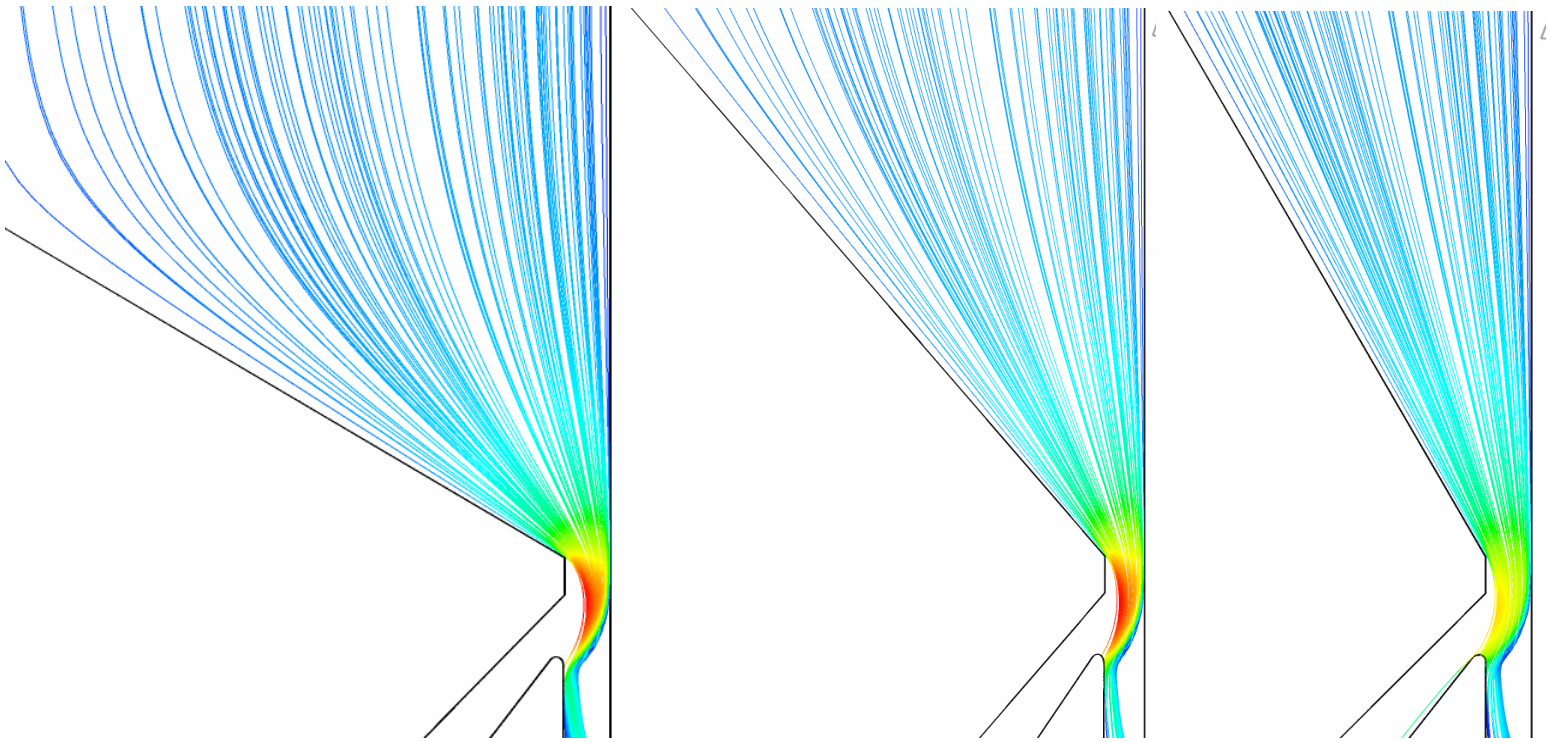

(a) (b) (c)

Figure 4.13. Particle trajectories of a 15 μm particles for different cone half angles, (a) 60º (b) 45º (c) 30º

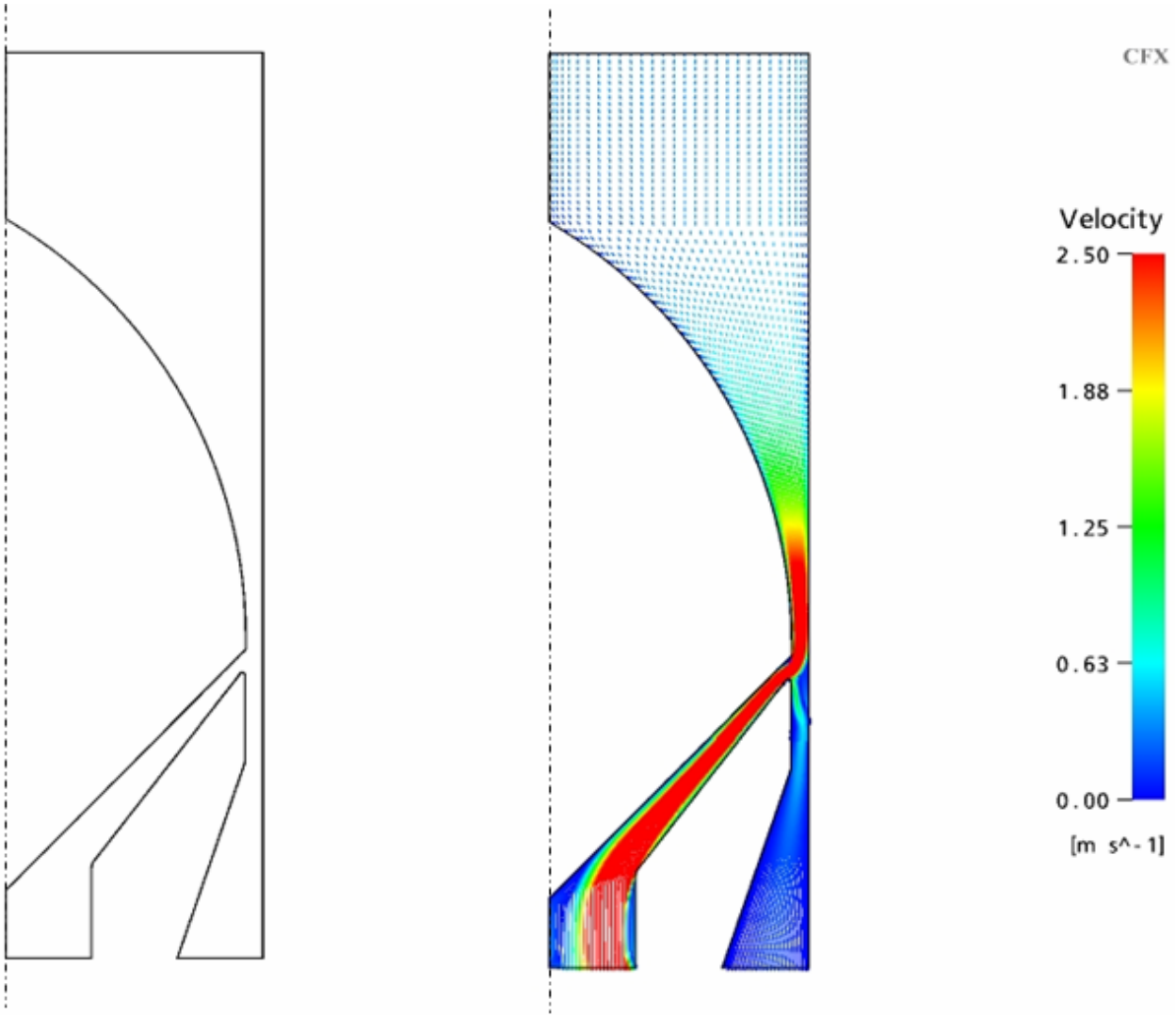

Figure 4.14. IVI elliptical inlet cone, simulation domain and velocity vector field

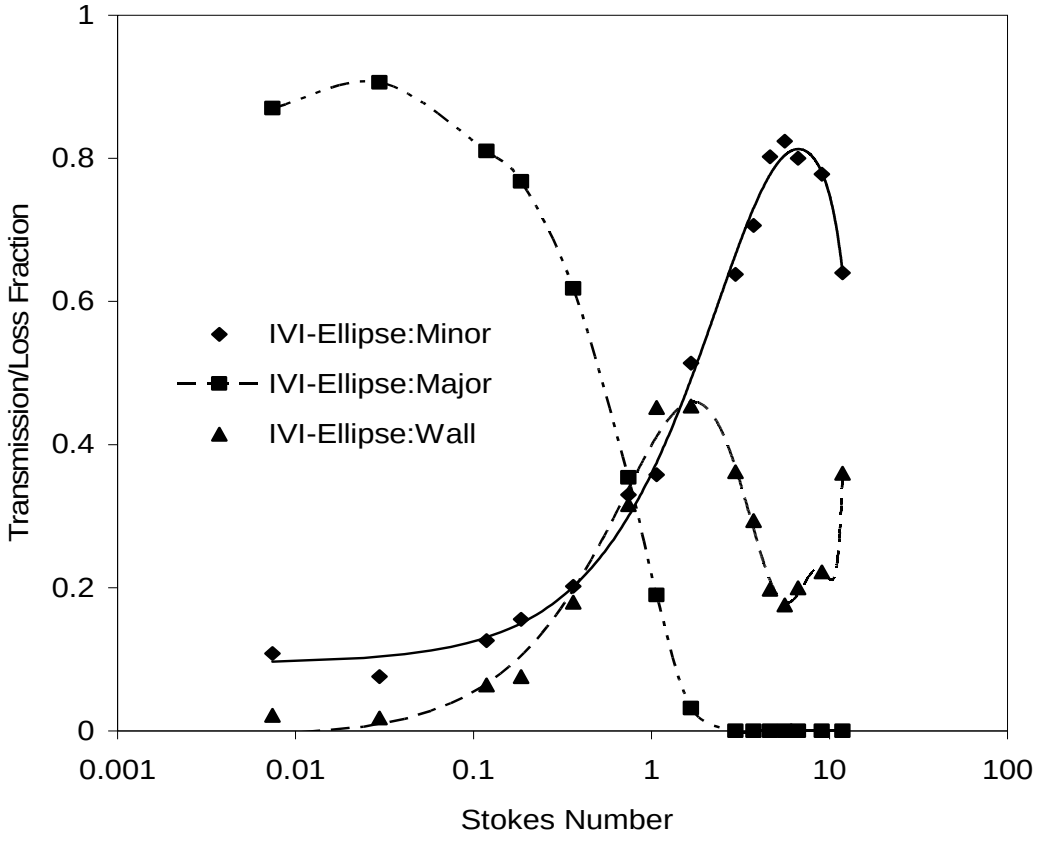

Figure 4.15. Aerosol penetration characteristics of IVI with elliptical inlet cone

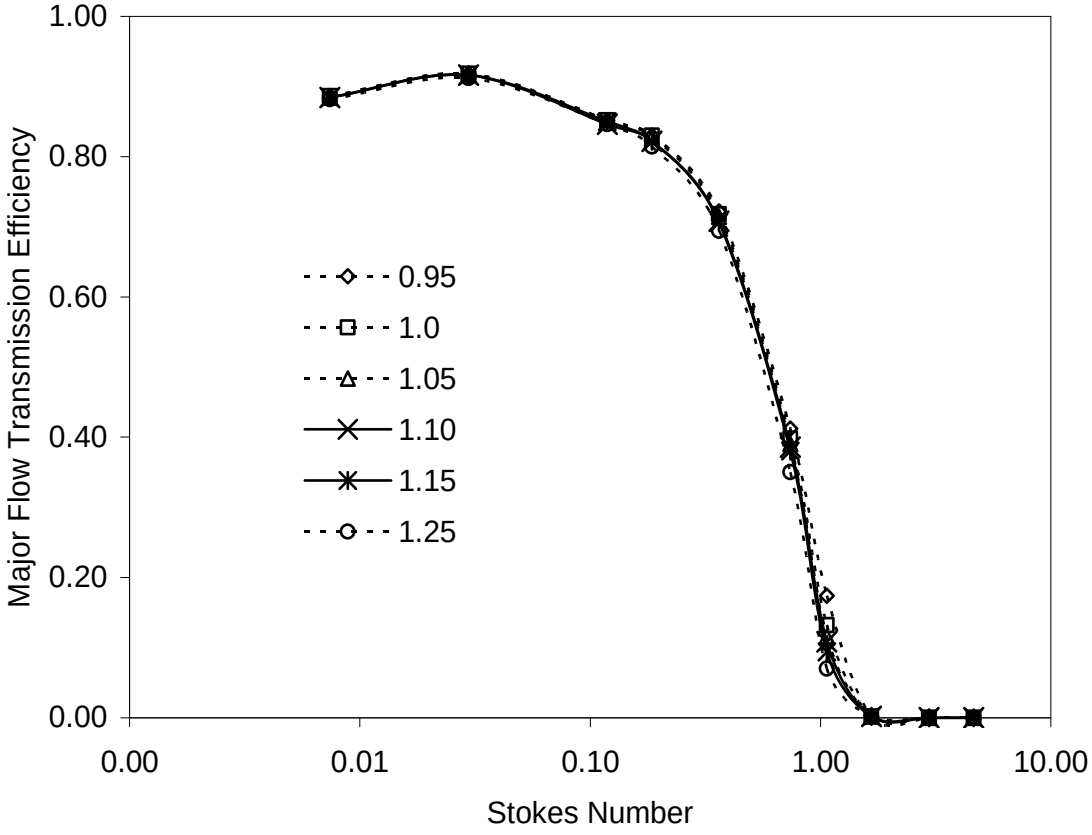

Figure 4.16. Major flow transmission efficiency plotted against Stokes number for different *D/W* ratios

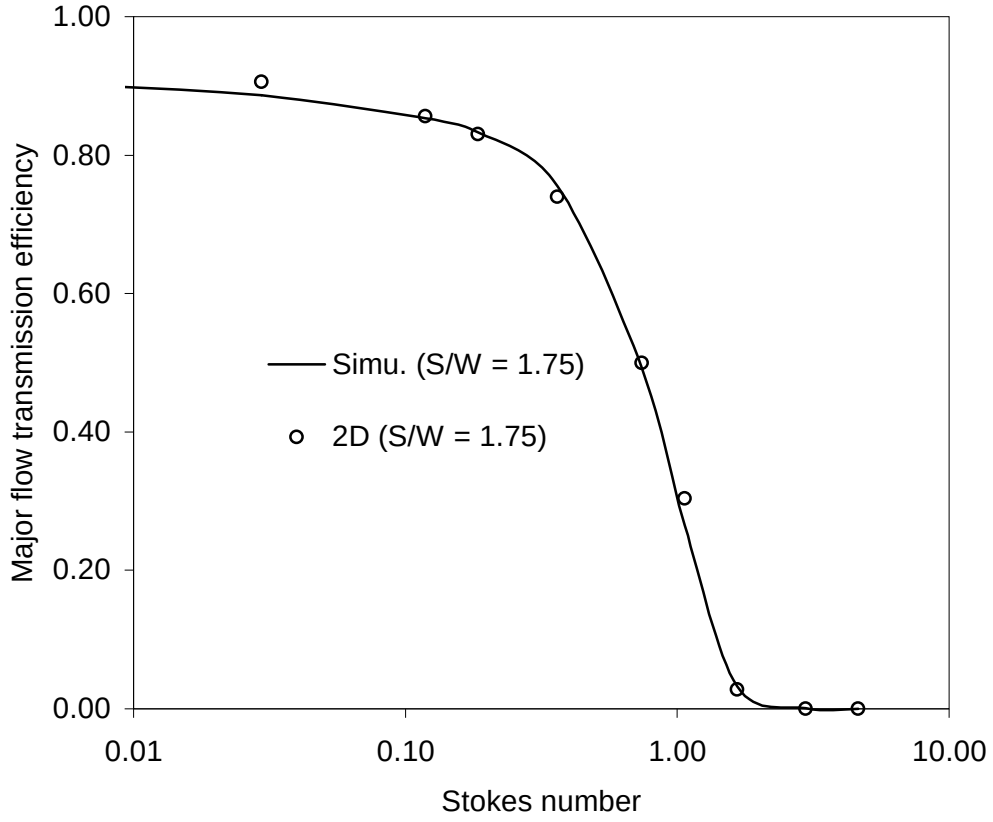

Figure 4.17. Comparison of 2D and 3D numerical simulation results

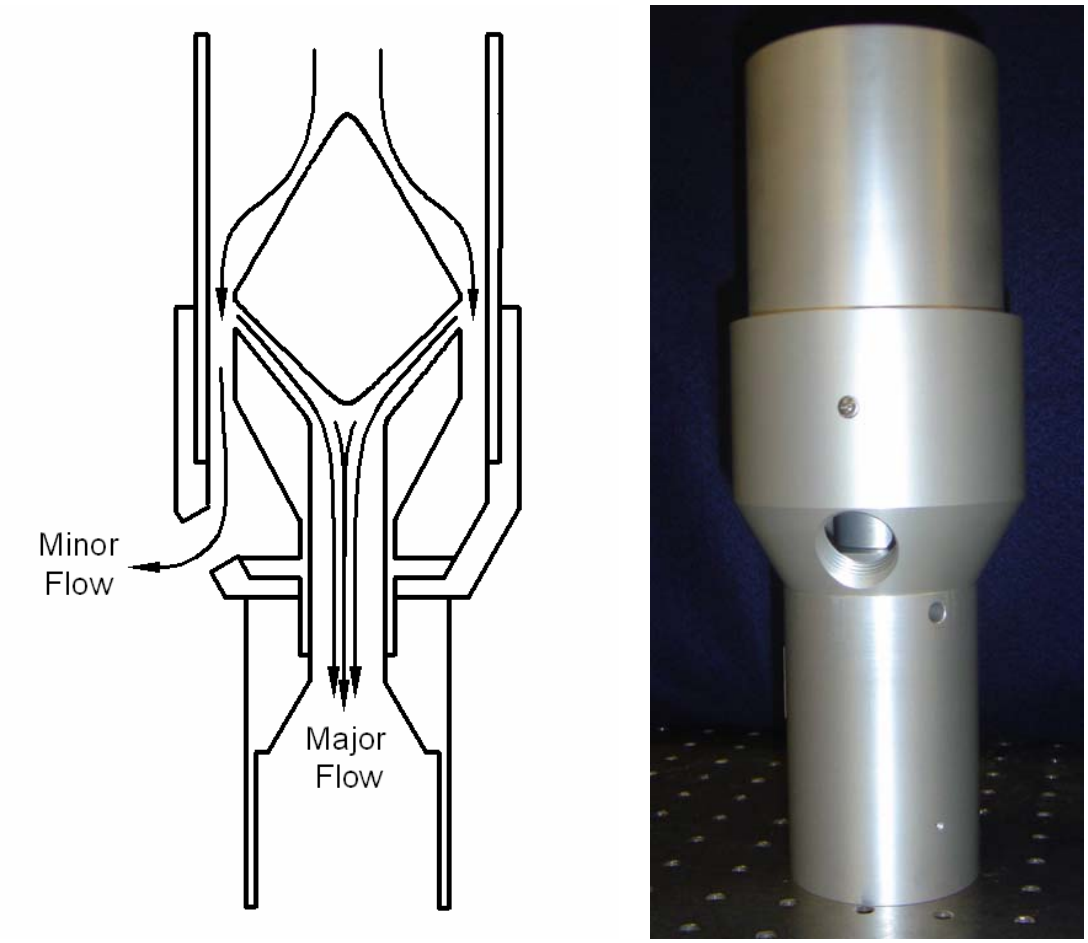

Figure 4.18. Schematic and a photograph of the upgraded prototype, IVI-100

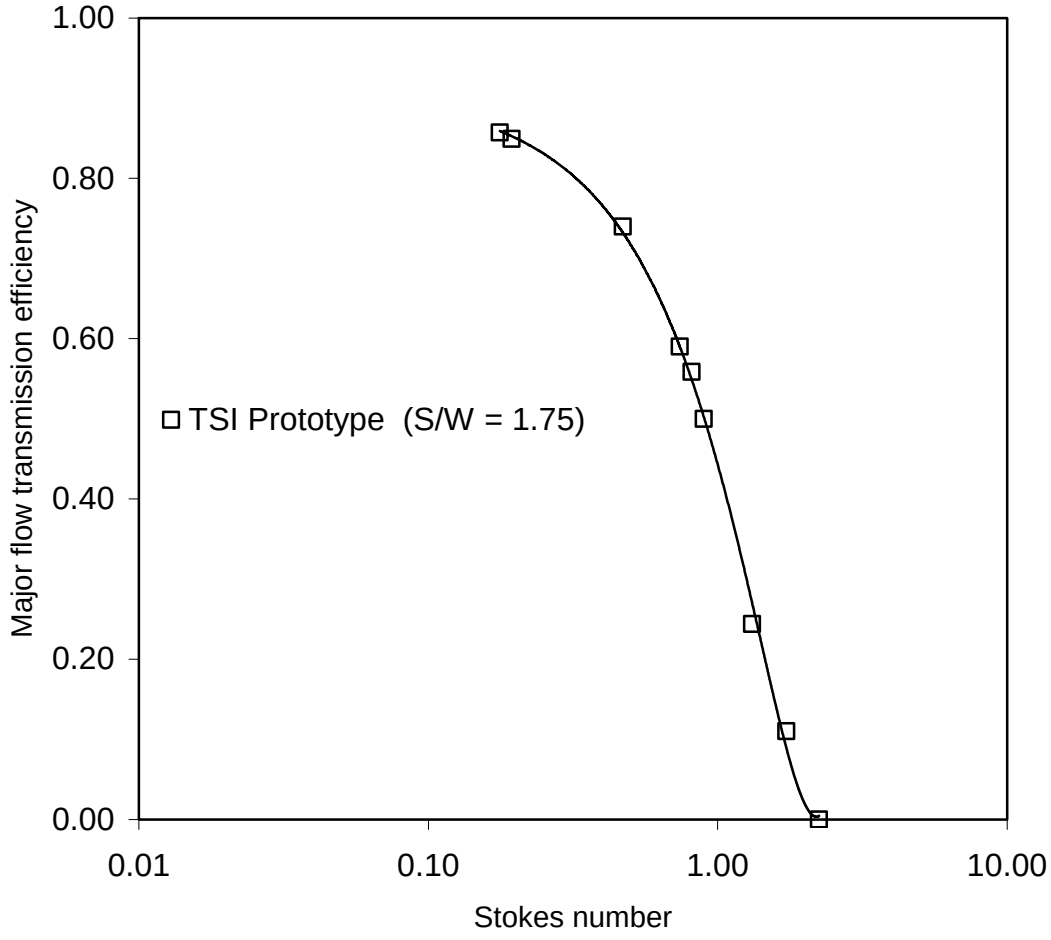

Figure 4.19. Performance characterization curve of the upgraded prototype

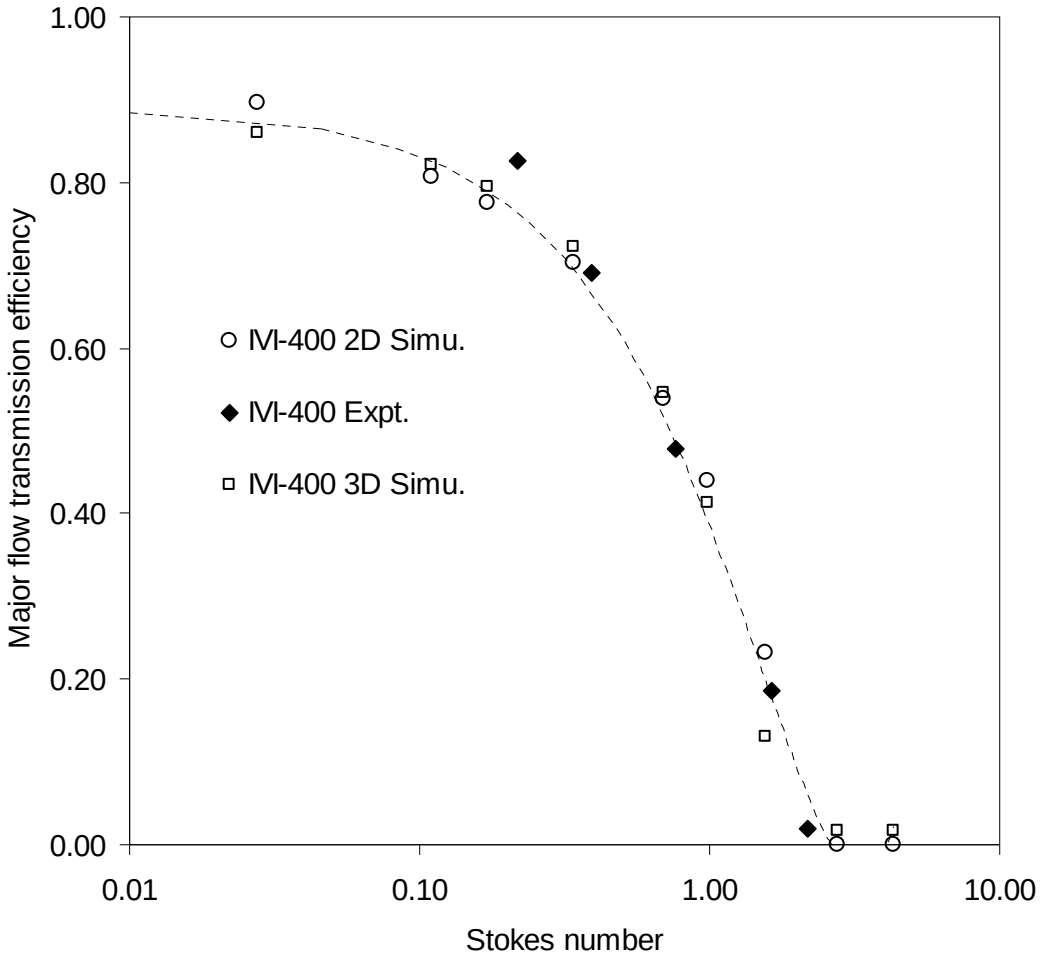

Figure 4.20. Numerical and experimental characterization curve of IVI-400

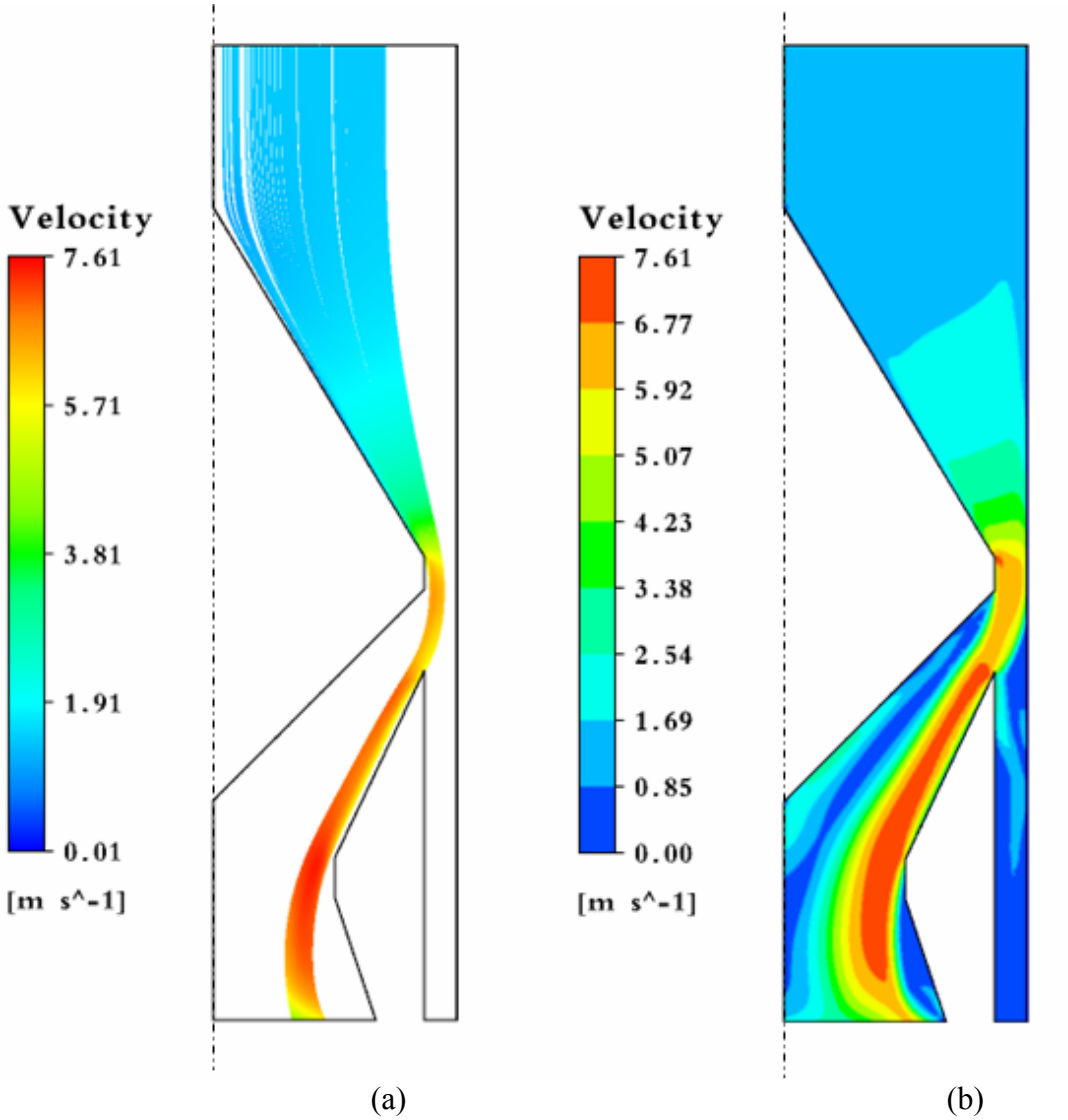

Figure 4.21. The new IVI-400-V2 design, (a) 12 µm particle trajectories, (b) Velocity contours

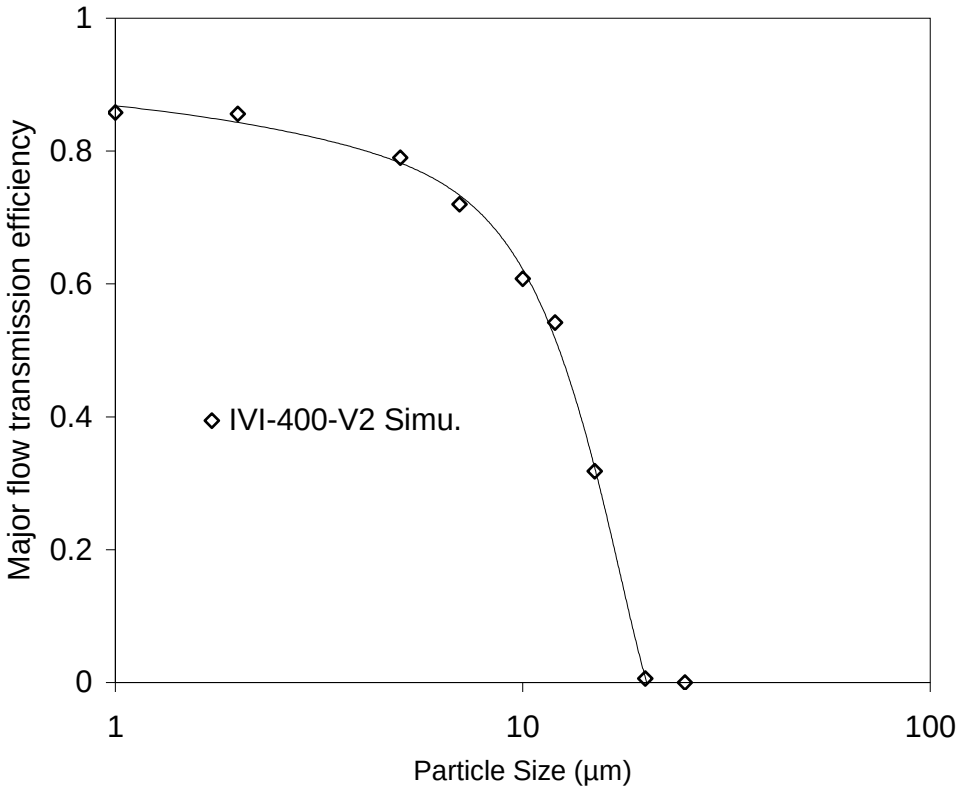

Figure 4.22. Numerical evaluation of IVI-400-V2, major flow transmission efficiency plotted against particle size

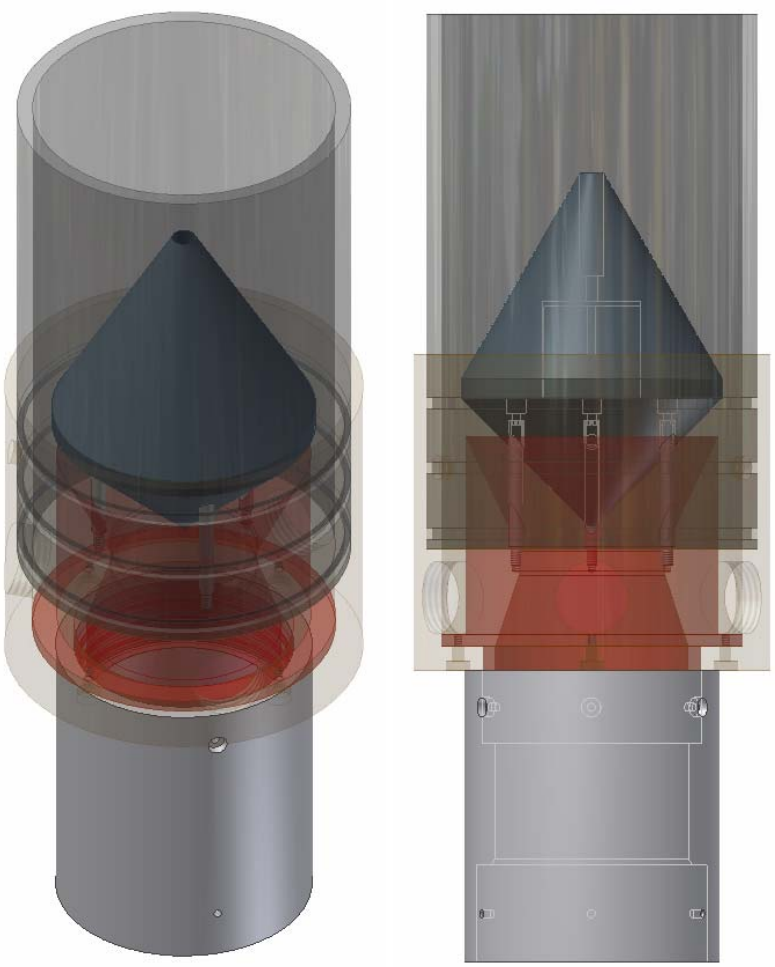

Figure 4.23. 3D model of IVI-V2 prototype

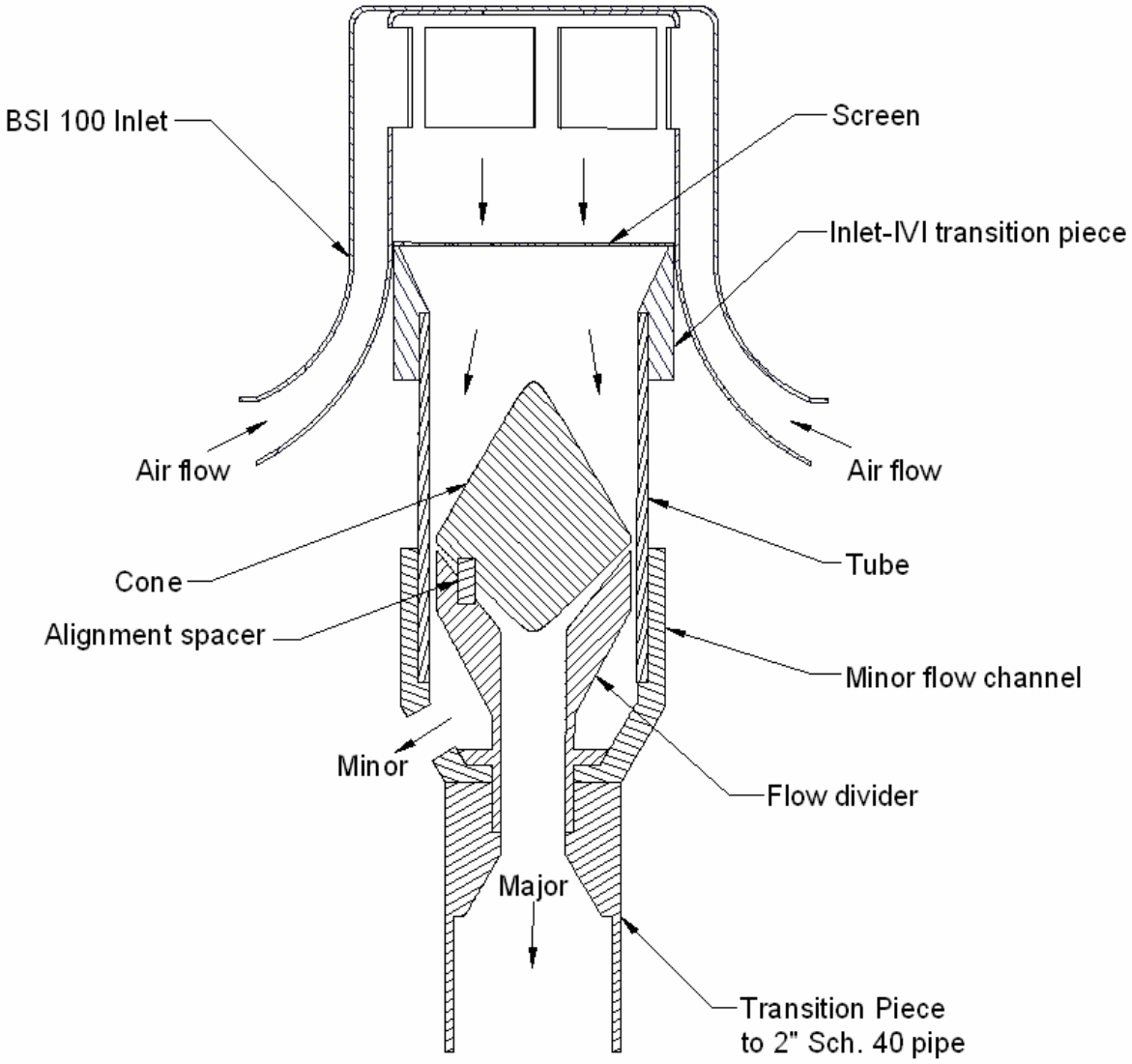

Figure 5.1. The BSI-IVI combined inlet system

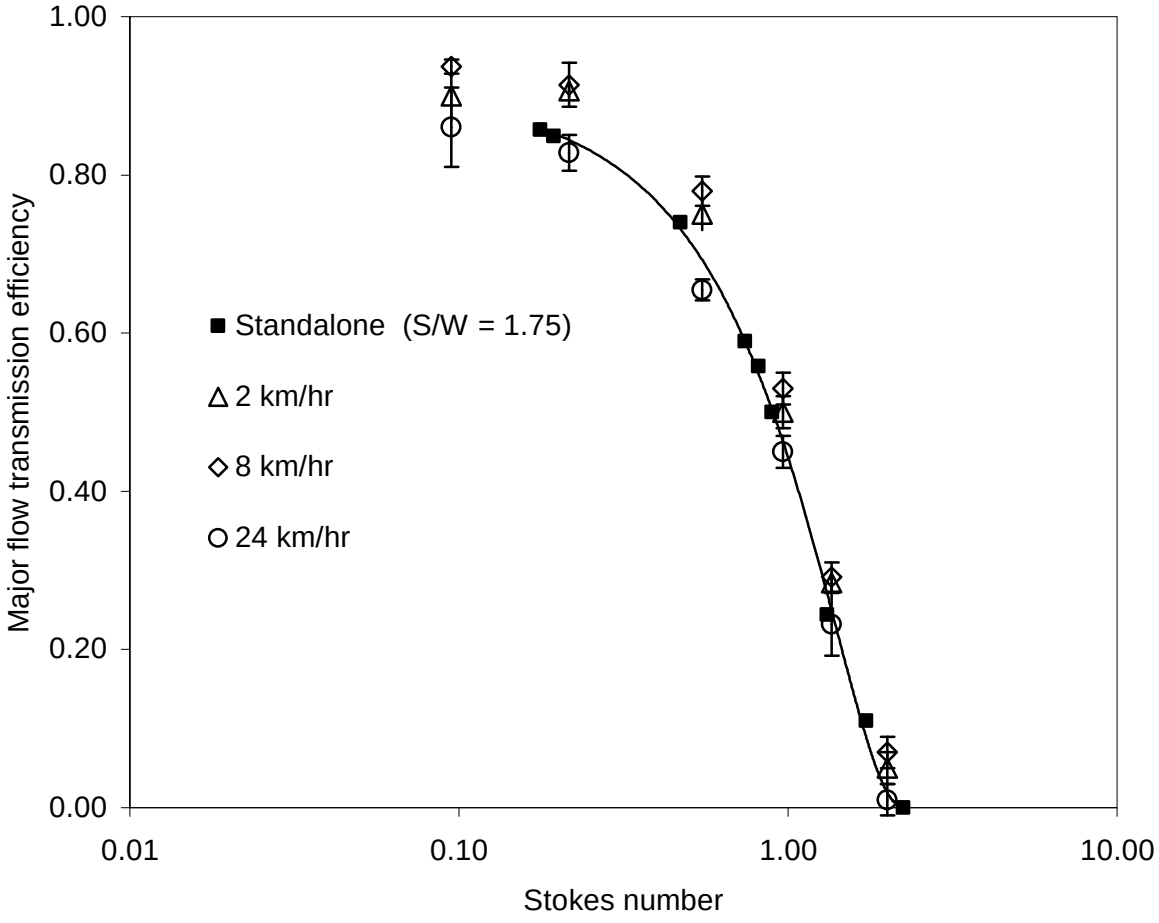

Figure 5.2. Aerosol sampling characteristics of BSI-IVI 100 inlet
Note: Error bars represent ± 1 standard deviation

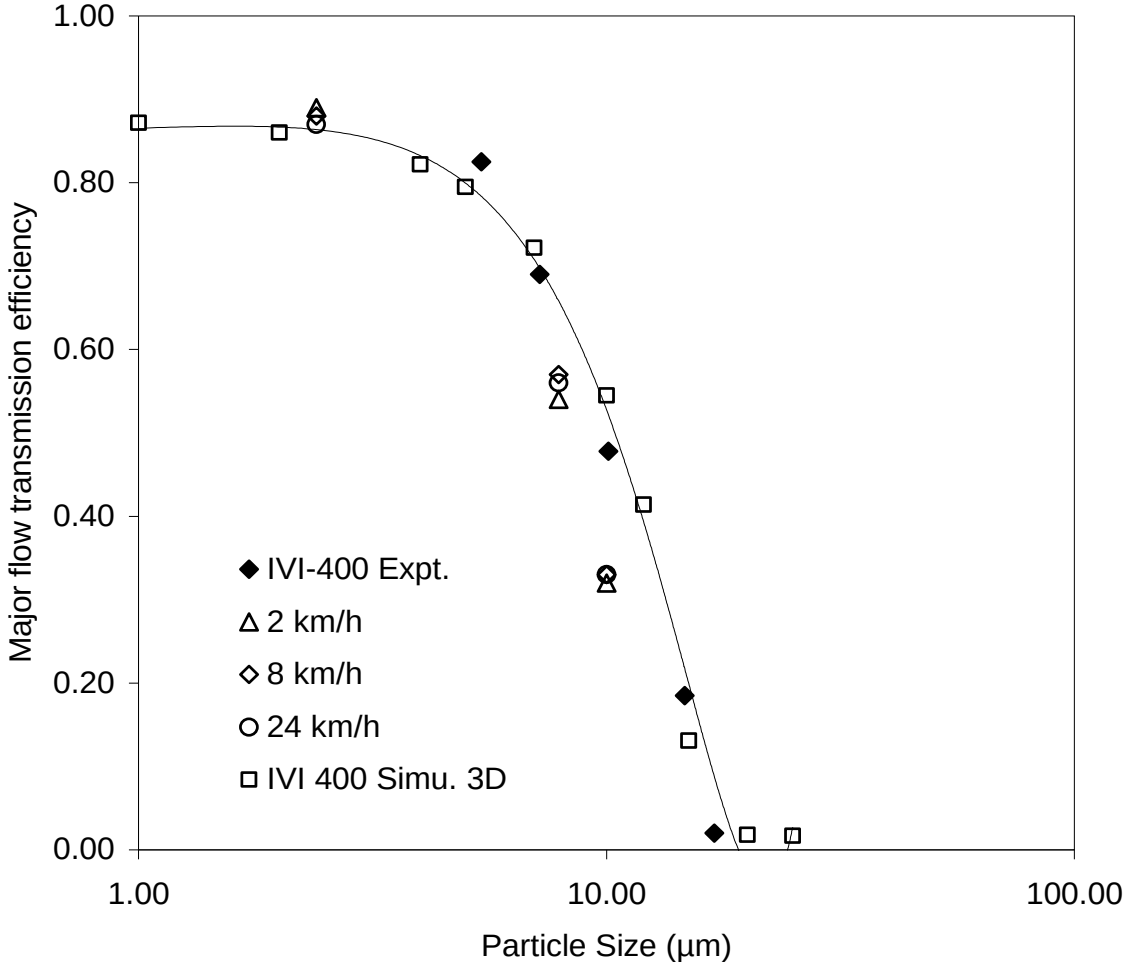

Figure 5.3. Aerosol sampling characteristics of BSI-IVI-400 inlet

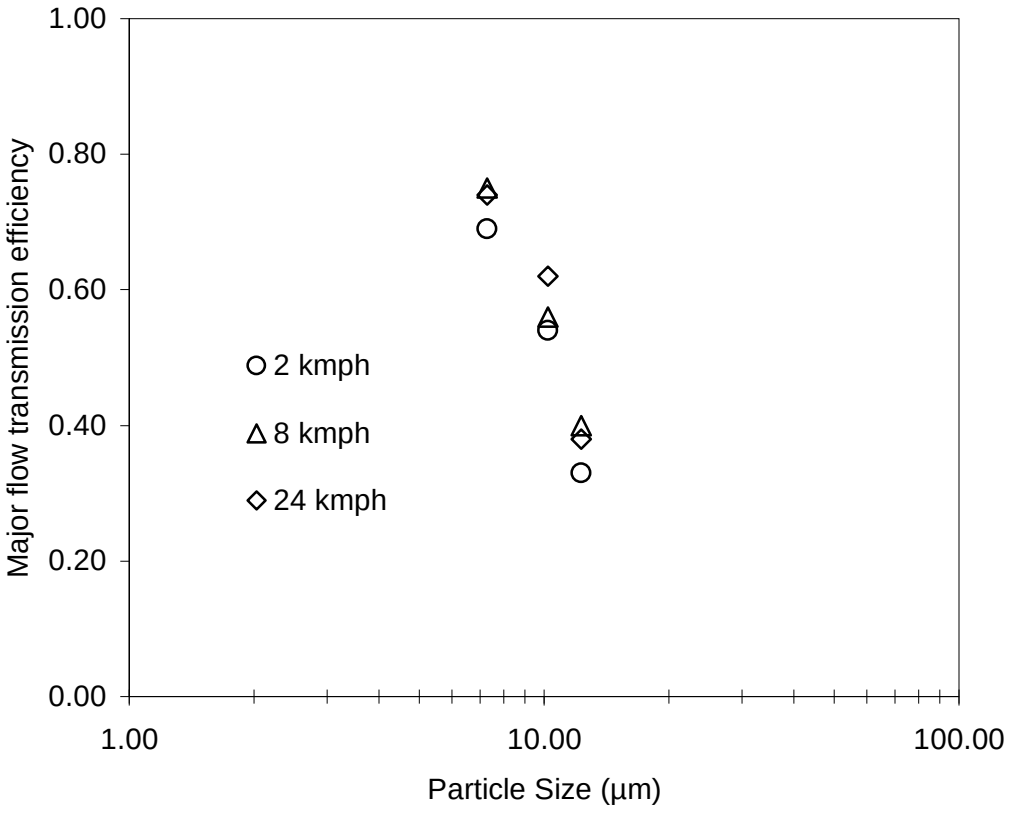

Figure 5.4. Aerosol sampling characteristics of BSI-IVI 300 inlet

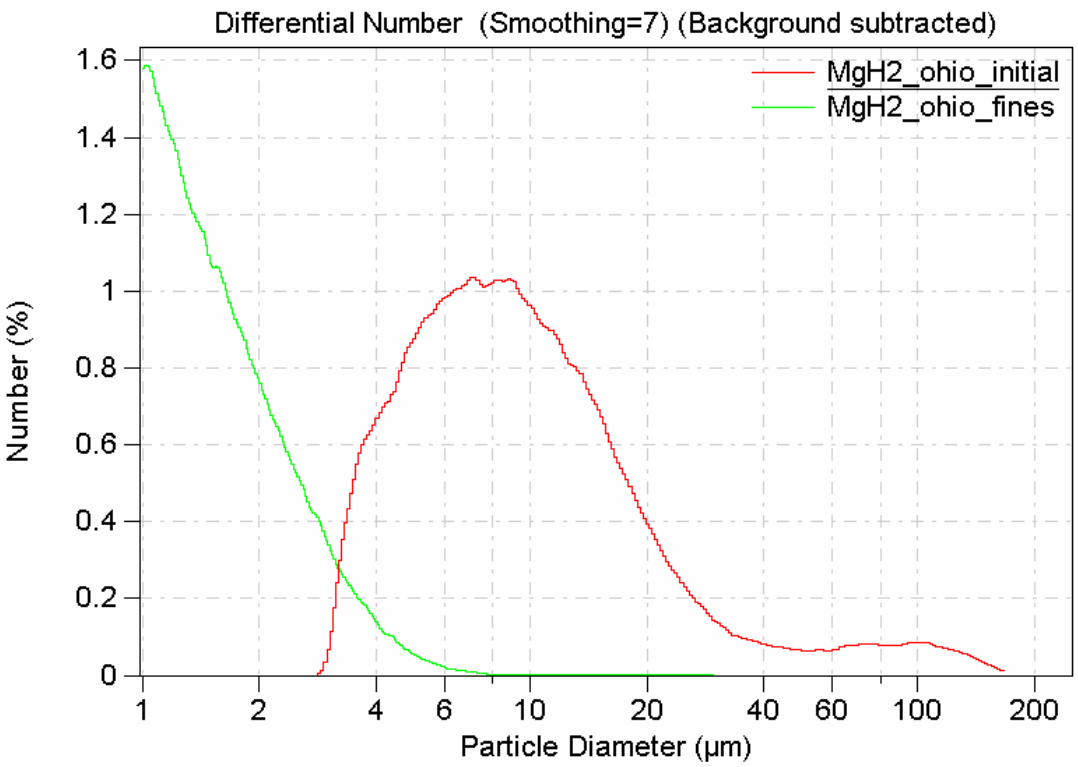

Figure 6.1. Powder separation characteristics of a LSVI
Note: Coulter counter data

Figure 6.2. Clogging of LSVI nozzles due to heavy mass loading

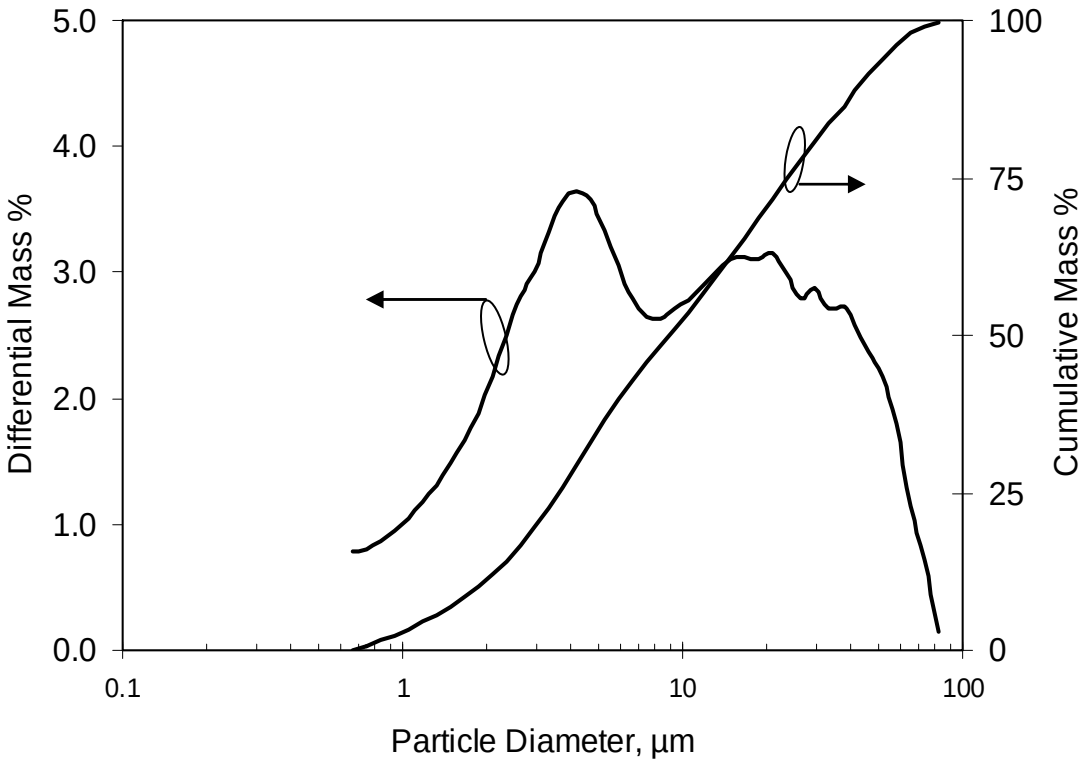

Figure 6.3. Particle size distribution of Arizona Road Dust (ARD) – fine, feed powder
Note: Coulter counter data

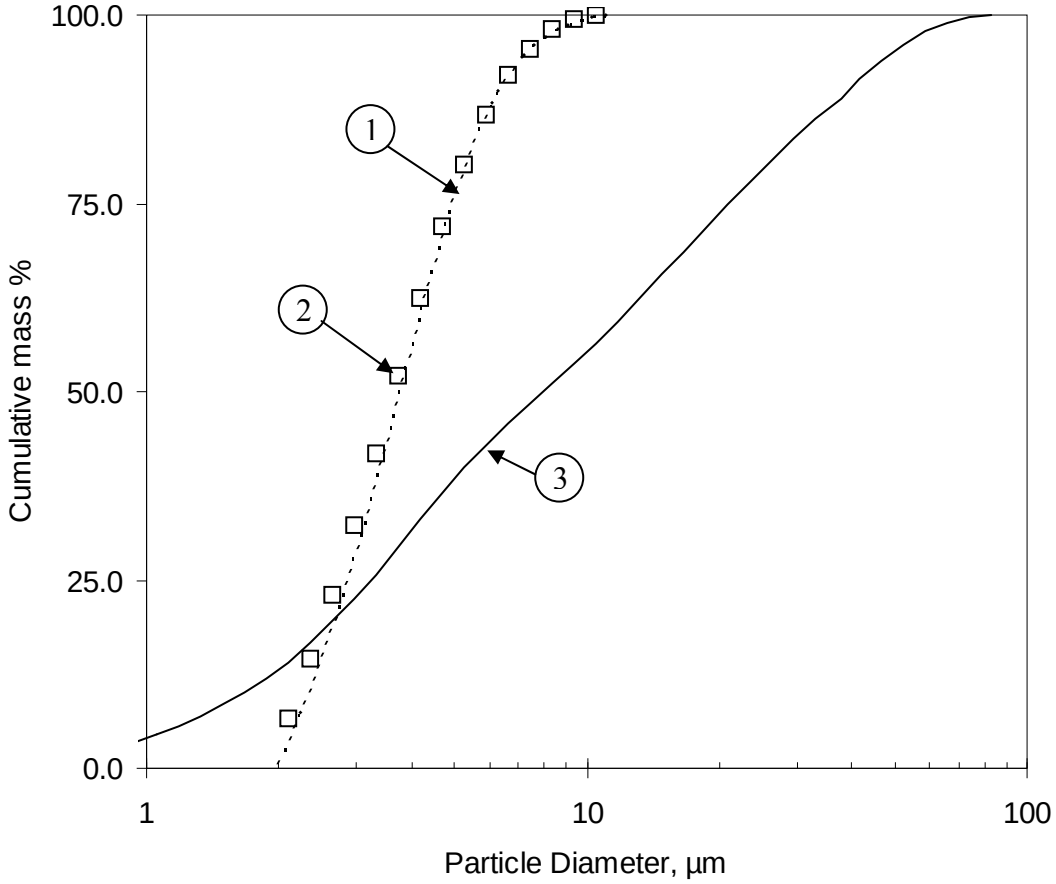

1. Cumulative mass of ARD collected in the major flow exhaust. Calculated using curve 3 and the major flow transmission efficiency of the IVI
2. Coulter counter analysis of sample filter from the major flow exhaust
3. Cumulative mass distribution of the feed powder

Figure 6.4. Particle size distribution of the processed powder

Figure 6.5. Inlet manifold used for distribution of aerosol to four IVI-350 units

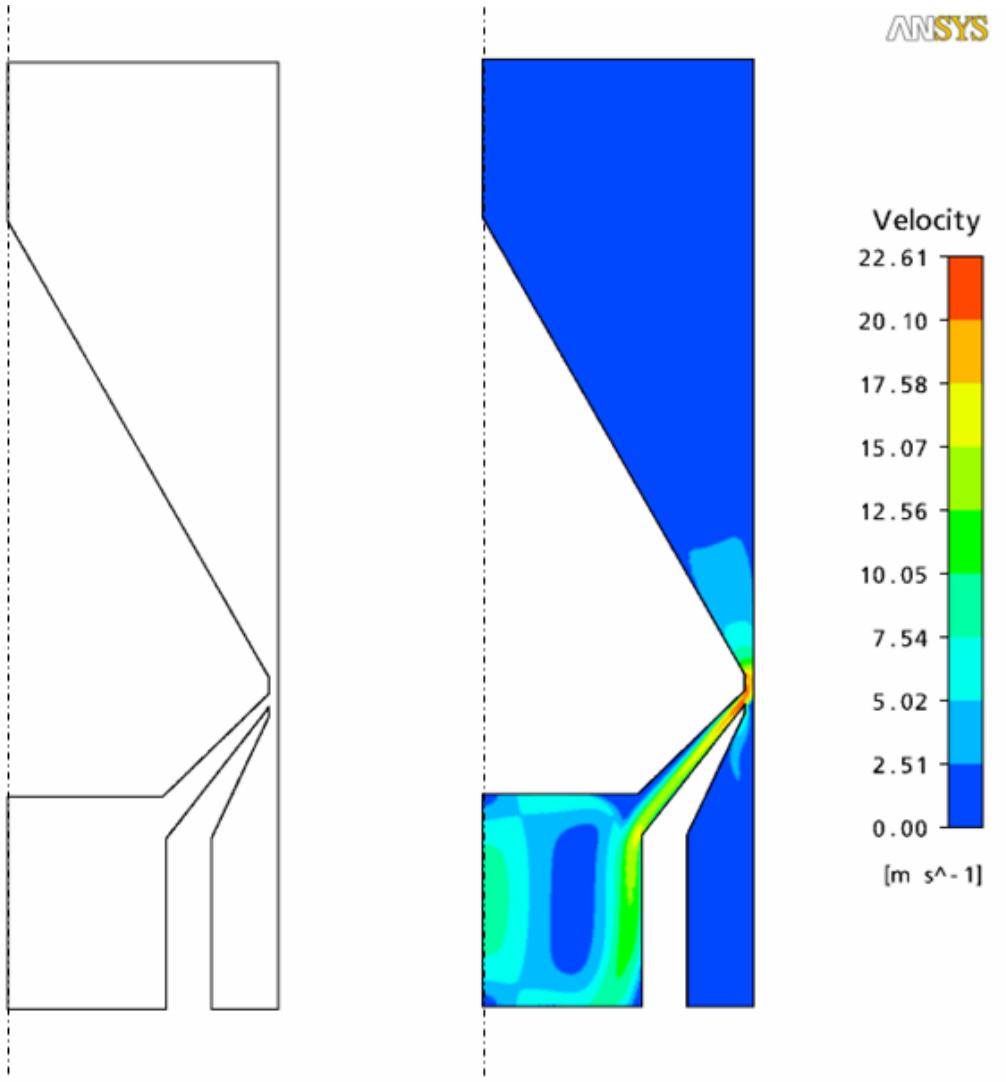

(a) (b)

Figure 6.6. IVI-350, (a) Geometry, (b) Velocity contours

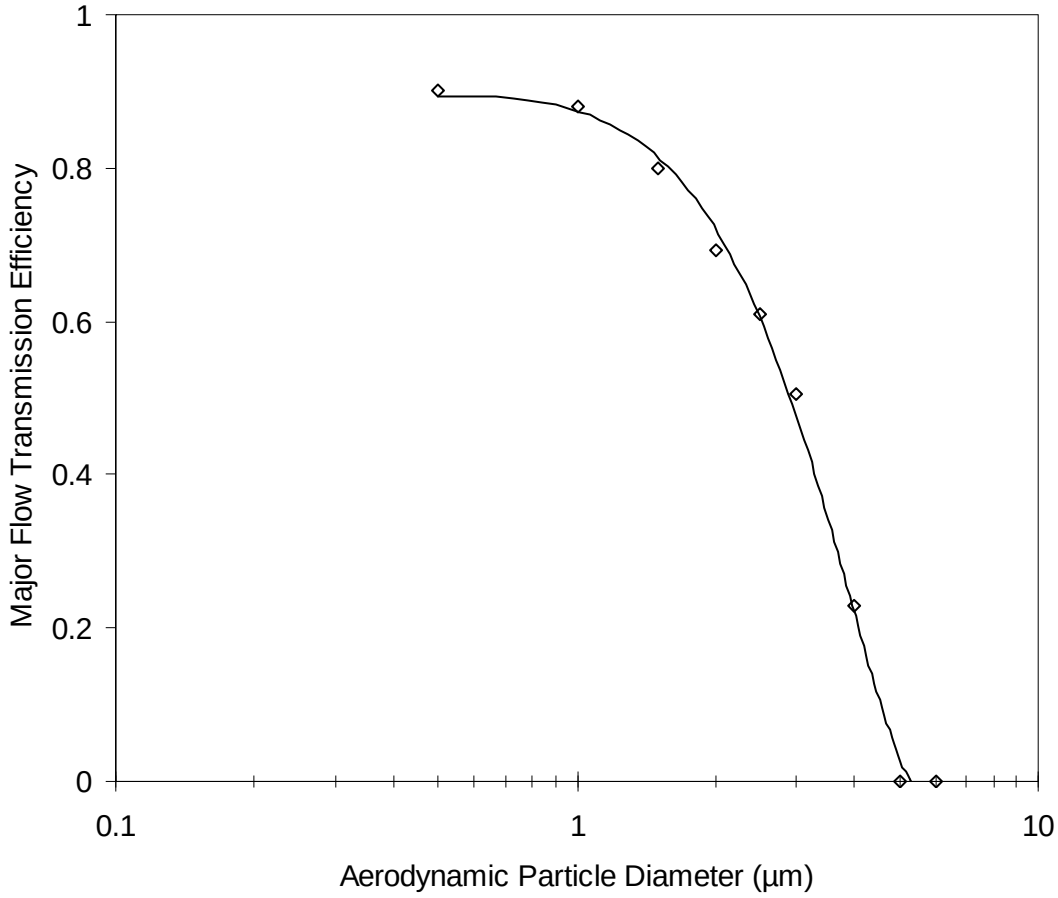

Figure 6.7. Major flow transmission efficiency curve of IVI-350, computational result

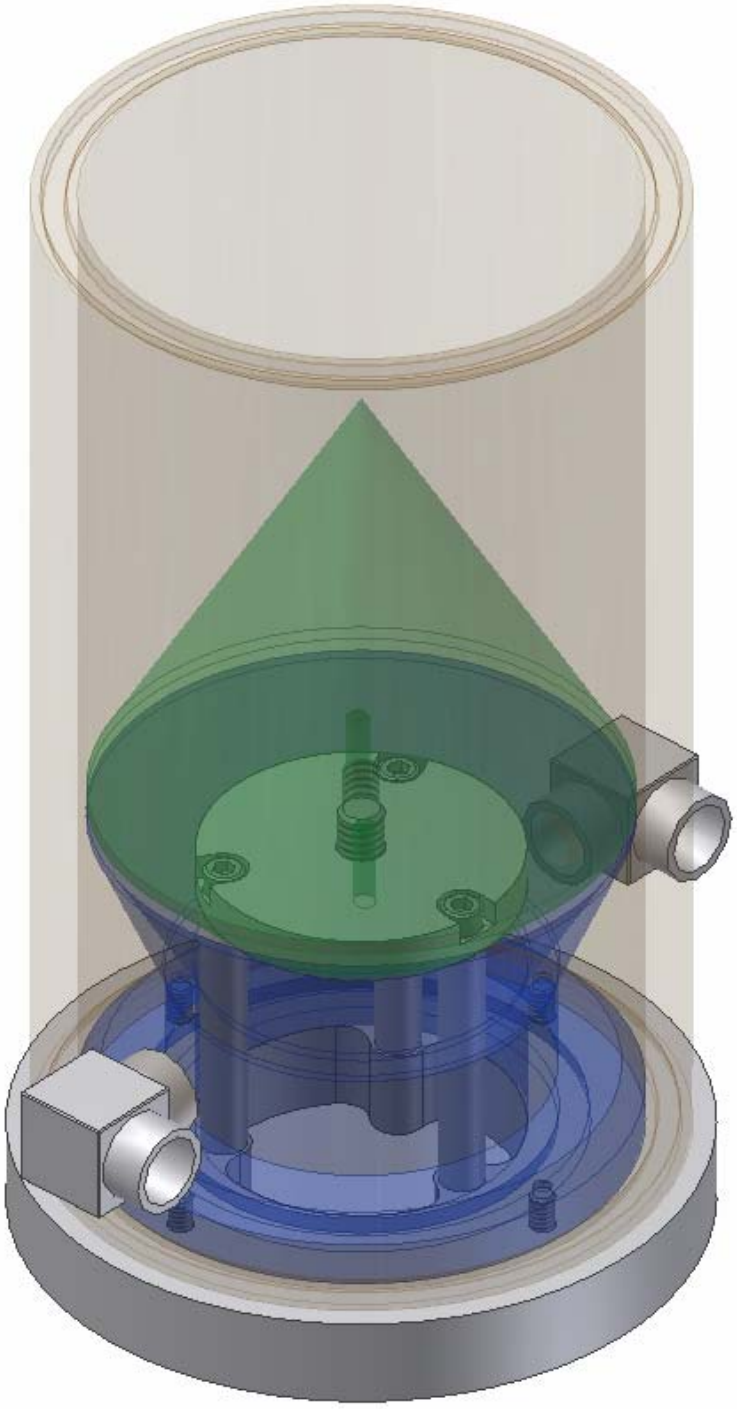

Figure 6.8. 3D model view of the IVI-350 prototype

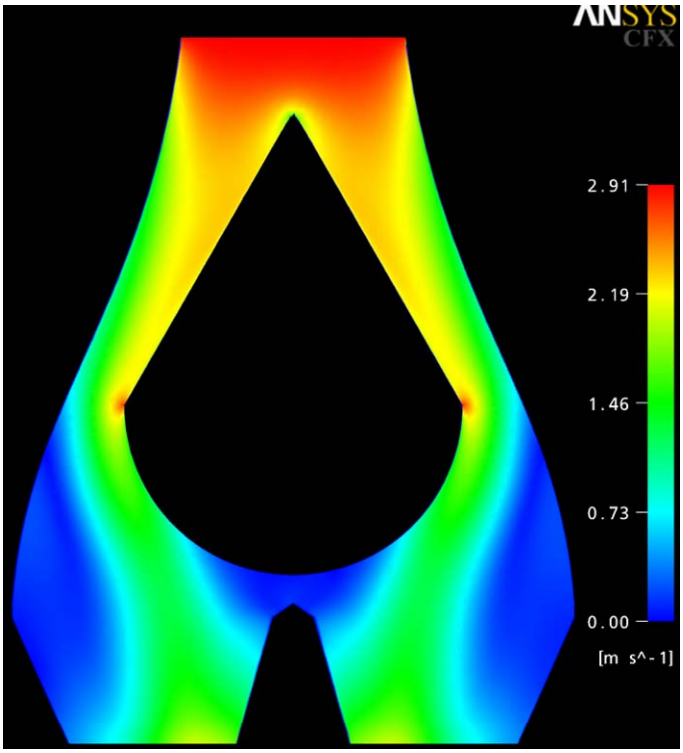

(a)

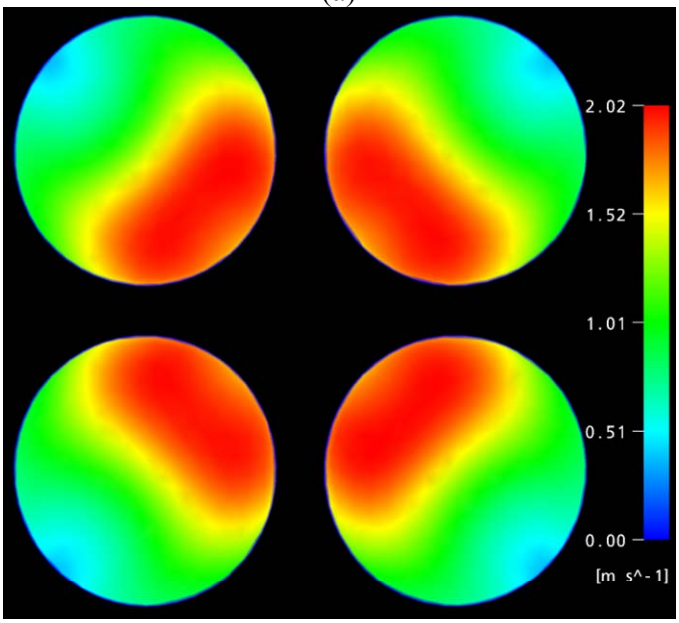

(b)

Figure 6.9. (a) Velocity contours in a planar section in the base case (b) Velocity contours at the exit plane for the base case

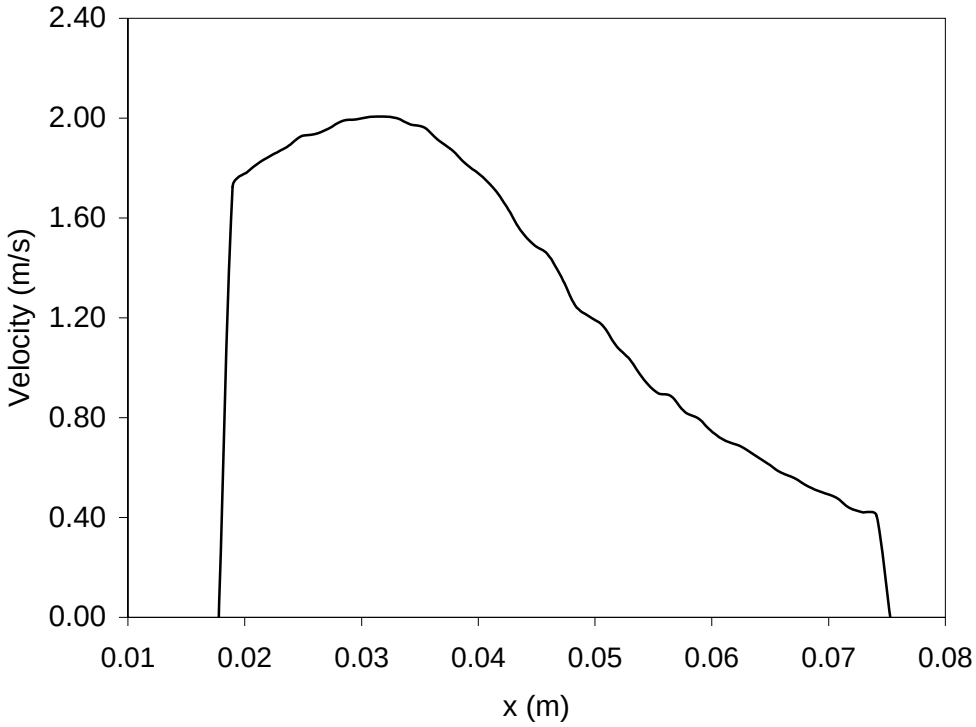

Figure 6.10. Velocity profile across the exit planes for the base case

Figure 6.11. Computational model of the optimized inlet

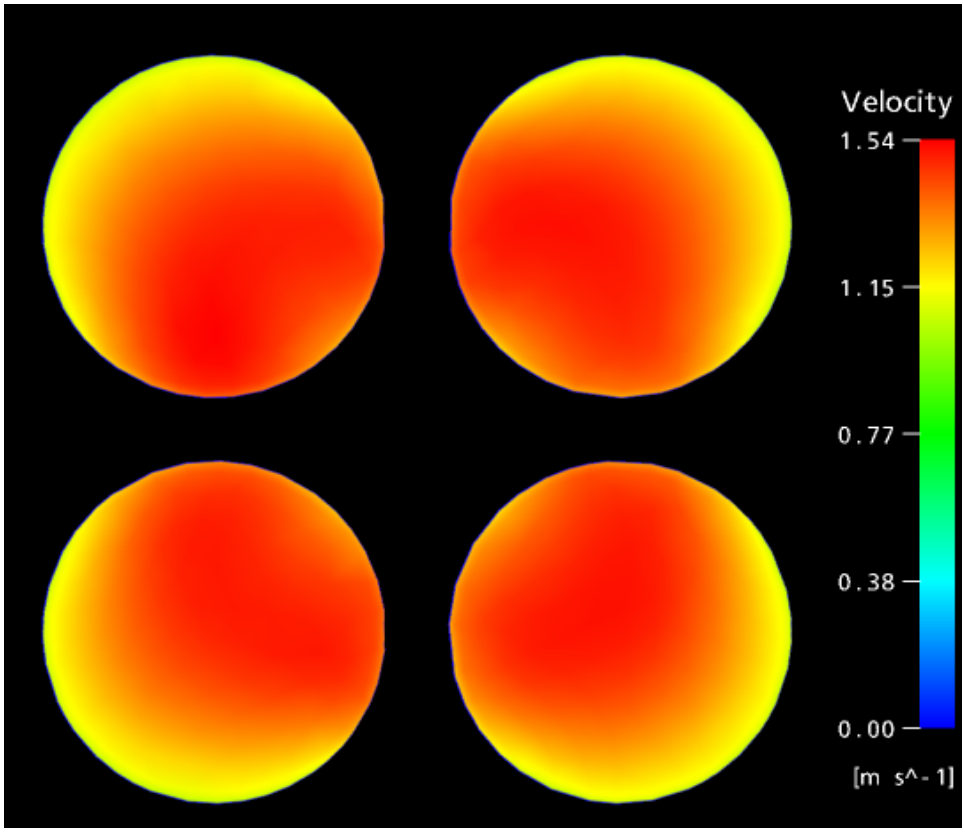

Figure 6.12. Velocity contours at the exit plane for the optimized inlet

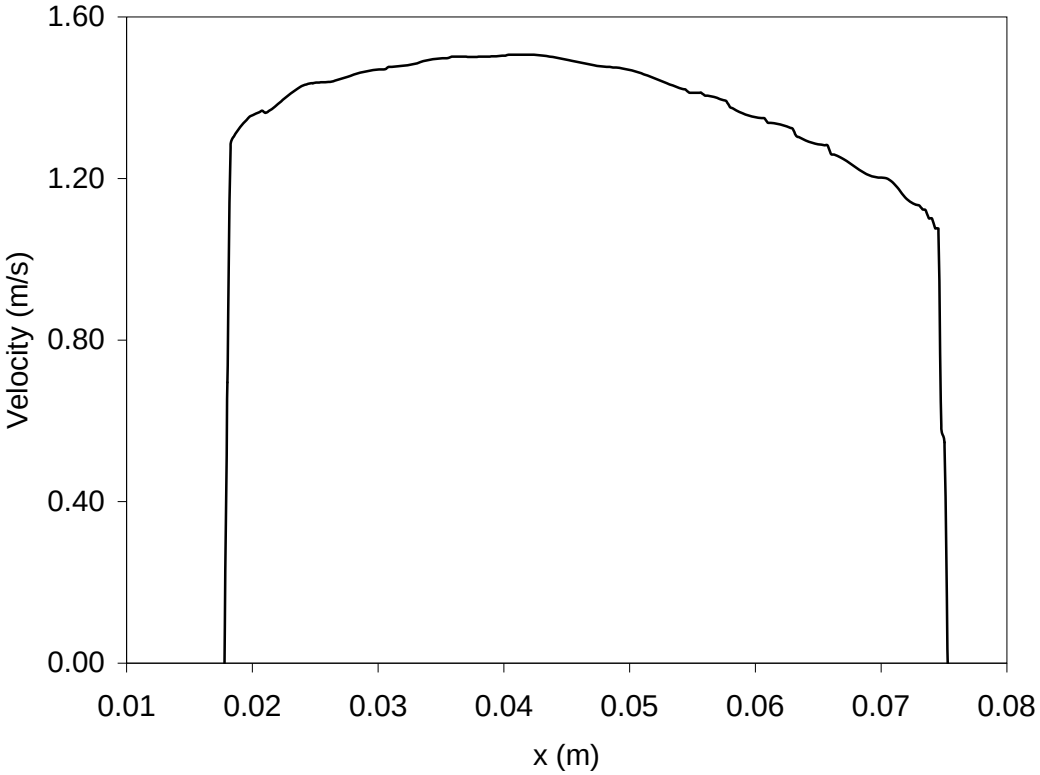

Figure 6.13. Velocity profile across the exit planes for the optimized inlet

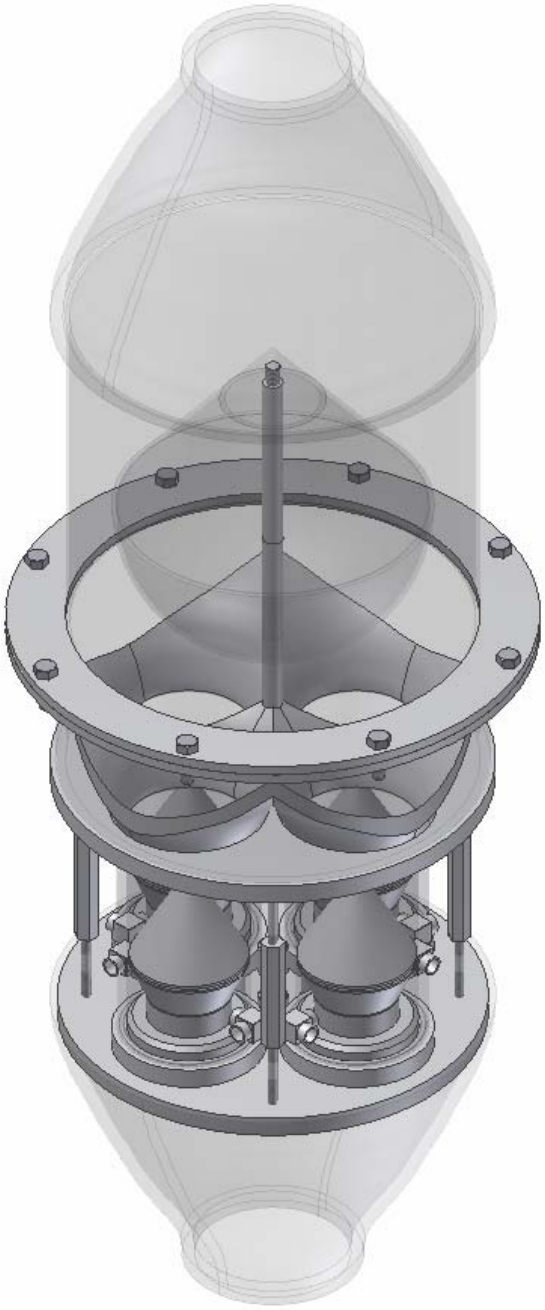

Figure 6.14. A 3D model view of the complete IVI powder separation system

VITA

Name Satyanarayanan Seshadri

Address Aerosol Technology Lab

Department of Mechanical Engineering

Texas A&M University, College Station, TX 77843-3123

Email: satya.seshadri@gmail.com

Education B.E., University of Madras, Chennai, India (2002)

Major: Mechanical engineering

M.S., Texas A&M University, College Station, TX 77843, USA (2004)

Major: Mechanical engineering

Ph.D., Texas A&M University, College Station, TX 77843, USA (2007)

Major: Mechanical engineering